저작자표시-비영리-변경금지 2.0 대한민국

이용자는 아래의 조건을 따르는 경우에 한하여 자유롭게

- 이 저작물을 복제, 배포, 전송, 전시, 공연 및 방송할 수 있습니다.

다음과 같은 조건을 따라야 합니다:

저작자표시. 귀하는 원저작자를 표시하여야 합니다.

비영리. 귀하는 이 저작물을 영리 목적으로 이용할 수 없습니다.

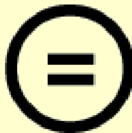

변경금지. 귀하는 이 저작물을 개작, 변형 또는 가공할 수 없습니다.

- 귀하는, 이 저작물의 재이용이나 배포의 경우, 이 저작물에 적용된 이용허락조건을 명확하게 나타내어야 합니다.
- 저작권자로부터 별도의 허가를 받으면 이러한 조건들은 적용되지 않습니다.

저작권법에 따른 이용자의 권리는 위의 내용에 의하여 영향을 받지 않습니다.

이것은 이용허락규약(Legal Code)을 이해하기 쉽게 요약한 것입니다.

Disclaimer

dCollection

공학박사학위논문

Design of Adaptive Model Predictive Controller for Plasma Etching Reactor

플라즈마 식각 장치를 위한 적응모델예측제어기의 설계

2019 년 2 월

서울대학교 대학원

화학생물공학부

구 준 모

Abstract

Design of Adaptive Model Predictive Controller for Plasma Etching Reactor

Junmo Koo
School of Chemical & Biological Engineering
The Graduate School
Seoul National University

The semiconductor etching process, which is one of the most critical processes in the manufacturing of semiconductors and one that comprises numerous steps, requires higher sophistication as 10 nm semiconductors are mass produced. Currently, the semiconductor etching process is mostly done by physical and/or chemical etching with plasma. In addition, the plasma etching is getting increasingly popular with the miniaturization of the process to a scale of less than 10 nm. The result of a plasma etching process is represented in the form of an etch profile which is determined by the plasma variables. Therefore, the performance of the process depends on these variables, and it is essential to measure and control them in real time. Although research on the control of plasma etching processes has been actively carried out, the plasma etching process strongly relies on the experience and skill level of seasoned engineers at the industry level. This is because a plasma-based system is very complicated

and sensitive, and has a time-varying characteristics. However, even though previous studies show excellent results, they employed invasive diagnostic tools, and have single variable control schemes where a counter change of another plasma variable during control actions for other variables might occur due to the highly interactive plasma characteristics. Moreover, they did not consider the time-varying characteristics of plasma-based systems. Therefore, this thesis proposes a multivariable control strategy which can cope with interaction effects and a design of an adaptive model predictive controller which maintains its performance wherein systems vary with time.

At first, the plasma variables which are considered as controlled variables were selected as the electron density and the electron temperature. This is because one of the etch profile, especially etch rate, can be expressed as functions of those plasma variables and the variables can be measured by the optical emission spectroscopy which is a non-invasive diagnostic tool. The plasma variables were paired with instrumental variables through singular value decomposition and relative gain array for constructing the optimal multivariable system model. Two parallel proportional integral derivative (PID) controllers were designed based on the output errors then conducted plasma variable control simulations. Through the simulations, the exist of interaction between the variables was obviously verified. For resolving the interaction effectively, decoupler controllers were applied to the PID controllers. As it performed the control experiment of the Ar plasma electron density and

electron temperature excellently, the possibility of multivariable control of plasma-based system is demonstrated.

In spite of the meaningful control results using the PID controllers, there are obvious limitations in relation to the exquisiteness and to the characteristics of decoupler controllers as it highly dependent to the accuracy of the system model. In order to maintain performance even in the case of a system change, an advanced control strategy is required and model predictive control can be an alternative. Therefore, a model predictive controller was designed where the Bayesian optimization is used as tuning method for the maximization of the exquisiteness. The controller verified its capability as it conducted Ar plasma electron density control in a drift-free system. However, the performance of it deteriorated in control simulations of time-varying systems and in a control experiment performed in a system where O_2 plasma was injected into an Ar plasma system inducing the high nonlinearity. Therefore, a more advanced control strategy which can overcome the difficulty was required.

In an adaptive control method, once the information from the system is entered into the adjustment mechanism part, the part makes a decision to deliver it to the controller. Then the controller is modified in accordance with the decision and releases the optimal control action. The typical adaptive control algorithm, which is the recursive least squares algorithm, was used in this thesis. Using the algorithm with Kalman filter interpretation, the time-delay effect which comes from the plasma etching reactor can be considered. The recursive model parameter estimator utilizing this algorithm was tuned by Bayesian

optimization. When the recursive model parameter estimator detects changes of the system model parameters in real time and transmits it to the model predictive controller, the controller calculates the optimal manipulated variable based on the modified model. The adaptive model predictive controller performed the same simulations and experiment as those performed by the model predictive controller. Unlike the model predictive controller, the proposed controller performed control excellently even when the system changes over time. Numerically, it showed the improved control ability by 24.7% and 30.4% in terms of the mean absolute percentage error and the number of deviated sample, respectively compared to the conventional model predictive controller. These results demonstrate that the adaptive model predictive controller designed in this theses is invaluable for plasma-based system control and is the effective controller for the plasma etching reactor. It is expected to make a significant contribution to plasma-based processes that require high sophistication and flexibility.

Keywords: Plasma Variable Control; Real Time Control; Multi-Input Multi-Output PID Control; Disturbance Rejection Control; Adaptive Model Predictive Control; Recursive Model Parameter Estimation

Student Number: 2014-21587

Contents

Abstract i

Contents..... v

List of Figures viii

List of Tables xii

CHAPTER 1. Introduction 1

1.1. Research motivation 1

1.2. Research objectives 4

1.3. Description of the equipment used in this thesis 5

1.4. Outline of the thesis 9

CHAPTER 2. Design of Multi-Input Multi-Output Controller for Plasma-based System 10

2.1. Introduction 10

2.2. Theoretical backgrounds 13

2.2.1. Estimation of plasma variables from optical emission spectroscopy 13

2.2.2. The influence of oxygen in plasma etching reactor 16

2.2.3. Singular value decomposition and condition number 18

2.2.4. Relative gain array method 21

2.2.5. Multi-loop control system 23

2.3. MIMO control results in the Ar plasma system 31

2.3.1. Variable selection and pairing 31

2.3.2. Disturbance rejection control results for SISO systems 37

2.3.3. Simulation of multi-loop control scheme and decoupling control scheme 41

2.3.4. Set-point tracking control experiment of multi-loop controller with decoupler controllers 58

2.4. Concluding remarks 62

CHAPTER 3. Disturbance Rejection Control of Plasma Electron Density by Model Predictive Controller.. 64

3.1. Introduction 64

3.2. Model predictive control 68

3.2.1. Concept of model predictive control 68

3.2.2. Description of model predictive control algorithm 71

3.2.2.1. State estimation algorithm.................................... 71

3.2.2.2. Optimization algorithm 76

3.3. Design of model predictive controller for Ar plasma system.......78

3.3.1. System identification of Ar plasma system 78

3.3.2. Optimal MPC weight parameters from integral squared error based Bayesian optimization 80

3.3.3. Experimental results of Ar plasma electron density control 84

3.4. Disturbance rejection control using model predictive controller .86

3.4.1. Development of time-varying system model for control simulation 86

3.4.2. Design of model predictive controller for disturbance rejection control... 91

3.4.3. Experimental result of disturbance rejection control in Ar/O_2 plasma system 101

3.5. Concluding remarks 104

CHAPTER 4. Design of Adaptive Model Predictive Controller for Plasma Etching Reactor 106

4.1. Introduction 106

4.2. Recursive model parameter estimation 112

4.2.1. Recursive least squares algorithm with forgetting factor 113

4.2.2. Recursive least squares algorithm with Kalman filter interpretation 116

4.3. Adaptive model predictive control algorithm............................ 119

4.4. Time-varying system control using adaptive model predictive controller 123

4.4.1. Initial system identification (Scaling method) 123

4.4.2. Design of adaptive model predictive controller for time-varying system 125

4.4.3. Set-point tracking control results in drifted system........ 143

4.5. Concluding remarks 152

CHAPTER 5. Conclusion 154

5.1. Summary of contributions.. 154

5.2. Future work 157

Nomenclature 159

References 167

Abstract in Korean (국문초록).. 174

List of Figures

Figure 1-1 CCP etching reactor used for this thesis 7

Figure 1-2 Schematic of CCP etching reactor employed in this thesis. 8

Figure 2-1 Standard block diagram of feedback control system. 24

Figure 2-2 Block diagram of multi-loop control system. 27

Figure 2-3 Block diagram of decoupling multi-loop control system. 29

Figure 2-4 Results of SISO disturbance rejection control of (a) the electron density and (b) electron temperature. 38

Figure 2-5 Undesirable movement of electron density when electron temperature is controlled. 40

Figure 2-6 Multi-loop control simulation results of (a) electron density (CV_1) movement and (b) electron temperature (CV_2) (without decoupler). 43

Figure 2-7 (a) 60 MHz RF Power (MV_1) movement and (b) pressure (MV_2) movement during multi-loop control simulation (without decoupler). 44

Figure 2-8 Multi-loop control simulation results of (a) electron density (CV_1) and (b) electron temperature (CV_2) (without decoupler). 46

Figure 2-9 (a) 60 MHz RF Power (MV_1) movement and (b) pressure (MV_2) movement during multi-loop control simulation (without decoupler). 47

Figure 2-10 The control simulation results of electron density (CV_1) set-point tracking test conducted by the SISO controller (red line) and the MIMO controller with decoupler controllers (blue line). 50

Figure 2-11 (a) 60 MHz RF Power (MV_1) movements and (b) pressure (MV_2) movements during electron density set-point tracking control simulation conducted by the SISO controller (dash dot) and the MIMO controller with decoupler controllers (gray line). 51

Figure 2-12 The control simulation results of electron temperature (CV_2) set-point tracking test conducted by the SISO controller (red line) and the MIMO controller with decoupler controllers (blue line). 53

Figure 2-13 (a) 60 MHz RF Power (MV_1) movements and (b) pressure (MV_2) movements during electron density set-point tracking control simulation conducted by the SISO controller (dash dot) and the MIMO controller with decoupler controllers (gray line). 54

Figure 2-14 Multi-loop control simulation results of (a) electron density (CV_1) movement and (b) electron temperature (CV_2) conducted by the MIMO controller with decoupler controllers (blue line) are compared to the results come from the MIMO controller without decoupler controllers (red line). 56

Figure 2-15 (a) 60 MHz RF Power (MV_1) movement and (b) pressure (MV_2) movement during multi-loop control simulation conducted by the MIMO controller with decoupler controllers (gray line) are compared to the MV movements released from the MIMO controller without decoupler controllers (dash dot)... 57

Figure 2-16 Set-point tracking control results of (a) electron density (CV_1) and (b) electron temperature(CV_2))... 60

Figure 2-17 The movement of 60 MHz RF power (MV_1) and (b) pressure (MV_2) during the set-point tracking control experiment................... 61

Figure 3-1 Block diagram of MPC... 69

Figure 3-2 Basic concept of MPC. 70

Figure 3-3 Diagram of MPC system based on state space models............. 72

Figure 3-4 Concept of Bayesian optimization algorithm. 81

Figure 3-5 Result of set-point tracking control of a drift-free Ar plasma system conducted by the Model predictive controller. (a) The CV, which is the electron density, tracks the set-point of it when (b) the MV, which is the RF power, changes to achieve the control............. 85

Figure 3-6 Block diagram of time-varying system model affected by the system gain drift and the offset drift. 87

Figure 3-7 Offset drift effect as a result of long time exposure of OES (about 40 min.). 89

Figure 3-8 Simulation results of set-point tracking control of a gain increasing system conducted by the model predictive controller. (a) The CV, which is the electron density, tracks the set-point of it when (b) the MV, which is the RF power, changes to achieve the control.. 93

Figure 3-9 Simulation results of set-point tracking control of a gain decreasing system conducted by the model predictive controller. (a) The CV, which is the electron density, tracks the set-point of it when (b) the MV, which is the RF power, changes to achieve the control. . 95

Figure 3-10 Simulation results of set-point tracking control of an offset drift system conducted by the model predictive controller. (a) The CV, which is the electron density, tracks the set-point of it when (b) the MV, which is the RF power, changes to achieve the control............. 97

Figure 3-11 Simulation results of set-point tracking control of a gain increasing system with an offset drift conducted by the model predictive controller. (a) The CV, which is the electron density, tracks the set-point of it when (b) the MV, which is the RF power, changes to achieve the control. 99

Figure 3-12 Experiment result of set-point tracking control of an Ar/O_2 plasma system with an artificial drift induced by O_2 plasma, conducted by the model predictive controller. (a) The CV, which is the electron density, tracks the set-point of it when (b) the MV, which is the RF power, changes to achieve the control. 103

Figure 4-1 Standard block diagram of adaptive control methods. 109

Figure 4-2 Block diagram of adaptive model predictive control. 120

Figure 4-3 Flowchart of the proposed AMPC. 122

Figure 4-4 Simulation results of set-point tracking control of a gain increasing system conducted by the model predictive controller (red line) and the adaptive model predictive controller (blue line). The CV, which is the electron density, tracks the set-point of it.................... 128

Figure 4-5 The MV (RF power) movements released from the model predictive controller (black dot) and the adaptive model predictive controller (gray line) in simulation 1... 129

Figure 4-6 The model parameters estimated by the recursive model parameter estimator in simulation 1. 130

Figure 4-7 Simulation results of set-point tracking control of a gain decreasing system conducted by the model predictive controller (red line) and the adaptive model predictive controller (blue line). The CV, which is the electron density, tracks the set-point of it.................... 132

Figure 4-8 The MV (RF power) movements released from the model predictive controller (black dot) and the adaptive model predictive controller (gray line) in simulation 2... 133

Figure 4-9 The model parameters estimated by the recursive model parameter estimator in simulation 2. 134

Figure 4-10 Simulation results of set-point tracking control of an offset drift system conducted by the model predictive controller (red line) and the adaptive model predictive controller (blue line). The CV, which is the electron density, tracks the set-point of it.................... 136

Figure 4-11 The MV (RF power) movements released from the model predictive controller (black dot) and the adaptive model predictive controller (gray line) in simulation 3... 137

Figure 4-12 The model parameters estimated by the recursive model parameter estimator in simulation 3. 138

Figure 4-13 Simulation results of set-point tracking control of a gain increasing with an offset drift system conducted by the model predictive controller (red line) and the adaptive model predictive controller (blue line). The CV, which is the electron density, tracks the set-point of it. 140

Figure 4-14 The MV (RF power) movements released from the model predictive controller (black dot) and the adaptive model predictive controller (gray line) in simulation 4... 141

Figure 4-15 The model parameters estimated by the recursive model parameter estimator in simulation 4. 142

Figure 4-16 Experiment result of set-point tracking control of an Ar plasma system with an artificial drift induced by O_2 plasma (light gray, right axis), conducted by the model predictive controller (red line, left axis) and the adaptive model predictive controller (blue line, left axis). The CV, which is the electron density, tracks the set-point of it. 145

Figure 4-17 The MV (RF power) movements released from the model predictive controller (black dot) and the adaptive model predictive controller (gray line) in the experiment.. 146

Figure 4-18 The model parameters estimated by the recursive model parameter estimator in the experiment. 147

List of Tables

Table 1 Steady state gain matrix obtained from PRBS tests. 32

Table 2 Minimized condition numbers and relative gains for every 2×2 system.. 34

Table 3 The selected 2×2 first order transfer function system model........ 36

Table 4 The overview of MPC and AMPC results in set-point tracking tests based on MAPE (%) and $\gamma MAPE$ (%).. 149

Table 5 The overview of MPC and AMPC results in set-point tracking tests based on nyd and γn (%). 150

CHAPTER 1. Introduction

1.1. Research motivation

The semiconductor etching process, which is one of the most critical processes in the manufacturing of semiconductors and one that comprises numerous steps, requires higher sophistication as 10 nm semiconductors are mass produced. Currently, the semiconductor etching process is mostly done by physical and/or chemical etching with plasma, which is a very sensitive material. In a plasma etching process, an electric power is first applied to the electrodes in a vacuum reactor, which is called a chamber, and plasma is generated by dissociating the etchant gas into electrons, ions, photons, and radicals. Subsequently, electric and magnetic fields are applied to transfer the kinetic energy to the charged particles, which help etch the wafer surface via physical and/or chemical reactions (Manos & Flamm, 1989; Yeom, 2006). Plasma etching is getting increasingly popular with the miniaturization of the process to a scale of less than 10 nm, as the lithograph pattern can be transferred accurately owing to the relatively high anisotropy. In addition, plasma etching is eco-friendly, has low process pollution, and is advantageous for process automation, as engineers can trace the progress of the process.

The result of a plasma etching process is represented in the form of an etch profile, which typically contains the etch rate, anisotropy, uniformity, and selectivity (May & Spanos, 2006). These factors are determined by the plasma

variables such as the electron density, ion density, electron temperature, ion flux, plasma potential, and electron energy distribution function (Chung, 2013). Therefore, the performance of the process depends on these variables, and it is essential to measure and control them in real time. However, as a plasma-based system is highly sensitive, plasma reacts with the intrusive sensor tip as well as with the inner walls of the chamber (Cunge et al., 2005; Kim & Aydil, 2003; Miwa et al., 2009). In addition, as polyatomic molecules, such as CF_4 and SF_6, dissociate to produce numerous chemical species, more than 50 physiochemical mechanisms are involved even in the case of a binary composition gas system (Hamaoka et al., 2009; Kokkoris et al., 2009). Therefore, unlike general chemical processes, the plasma etching process has two major characteristics. First, as the process is influenced by so many factors, it is fundamentally difficult to model the entire process based on the first principle, and even if such modeling is realized, it is difficult to control the plasma variables precisely in real time. Therefore, it is effective to use an empirical model through an approximate formulation. Second, a non-intrusive sensor should be used to avoid the sensor being a disturbance in a plasma-based system. In fact, in the production line, end-point detection is performed using an optical emission spectrometer (OES), which is used to measure the concentrations of the chemicals generated from the emission of excited chemicals. As an OES uses light, it is non-intrusive, and it is possible to carry out measurements in the order of microseconds, enabling engineers to control the variables in real time (Donnelly & Kornblit, 2013).

Although research on the control of plasma etching process has been actively carried out, the plasma etching process strongly relies on the experience and skill level of seasoned engineers at the industry level. This is because a plasma-based system is fundamentally very complicated and sensitive, and although the above studies have obtained excellent results, they have not considered the specificity of a plasma-based system, particularly the time-varying characteristics. Because a plasma-based system is very sensitive to the chamber environment, if a sensor that measures the plasma variables is invasive, it easily affects the performance of the control. Also, although plasma variables and instrumental variables are intertwined with each other, most studies proposed single-input single-output (SISO) control strategies which cannot consider the interaction effect. Moreover, a plasma-based system varies with time continuously because of various factors such as system drift and inconsistency in the initial point for each batch. This leads to model–plant mismatches (MPMs) within a batch and/or between batches. Therefore, a control strategy considering the characteristics of the plasma-based system and designing a real-time advanced controller is expected to contribute to the development of the semiconductor manufacturing process.

1.2. Research objectives

As described in the research motivation section, Section 1.1, designing a controller that reflects the characteristics of the process is critical to achieving effective control. Therefore, the objective of this thesis is to design a multi-input multi-output (MIMO) controller that can handle the interaction effect and to design a advanced controller with thorough consideration of plasma-based system characteristics to effectively control the plasma variable in real time. First of all, the interaction between manipulated variables (MVs) and controlled variables (CVs) in an Ar plasma system is identified. Then, the possibility of MIMO control is demonstrated through the design of MIMO proportional integral derivative (PID) controllers with decoupler controllers. Afterward, an advanced controller that effectively controls the Ar plasma electron density considering system drift is proposed. The advanced controller comes in the form of an adaptive model predictive controller where a recursive model parameter estimator is applied. This controller is aimed at performing excellent control despite the fact that the Ar/O_2 plasma system shows time-varying characteristics.

1.3. Description of the equipment used in this thesis

Figure 1-1 shows the capacitively coupled plasma (CCP) etching reactor used for this thesis and Figure 1-2 shows a schematic of the reactor. Our equipment consists of an etch equipment and a system control device. The etch equipment is composed of an etch tool and a regulator system. In the chamber in the etch tool, plasma is generated by a CCP equipment that can carry 300 mm wafers. The gap size between the top and bottom electrodes is 25 mm, and the area ratio between the top showerhead and the bottom electrode is 1.33. A 60 MHz radio frequency (RF) source power generator is used for the bottom electrode. It generates RF source power which directly affects the electron density, a CV, based on the power regulator in the regulator system. The throttle valve of the vacuum pump is controlled by the pressure regulator, manipulating the pressure of the chamber. Also, various gas valves are connected to the chamber, and the flowrates of gases are determined according to the command from the flow regulator. All of the signals from these regulators are decided by the regulator controller. The employed OES, AvaSpec-ULS2048L from Avantes, can be used to measure light of wavelengths ranging from 200 nm to 1100 nm with a spectral resolution of 0.2 nm. To obtain higher spectral resolution and emission sensitivity, two OES systems are employed as a dual-channel system. Thus, light with a low wavelength range (255–523 nm) and a high wavelength range (492–1030 nm) can be measured separately. This helps increase the signal-to-noise ratio even for a sampling time of 50 ms for in-situ control. CVs are measured from a raw OES signal through LabVIEW®. From this, the

optimal control action is evaluated at each sampling time of 50 ms using the controller designed by using Simulink® and is fed to the regulator controller. The OES signals measured by LabVIEW® and the optimal control actions calculated from Simulink® are transmitted over the UDP. Finally, the regulator uses these values as set-points for its own controller.

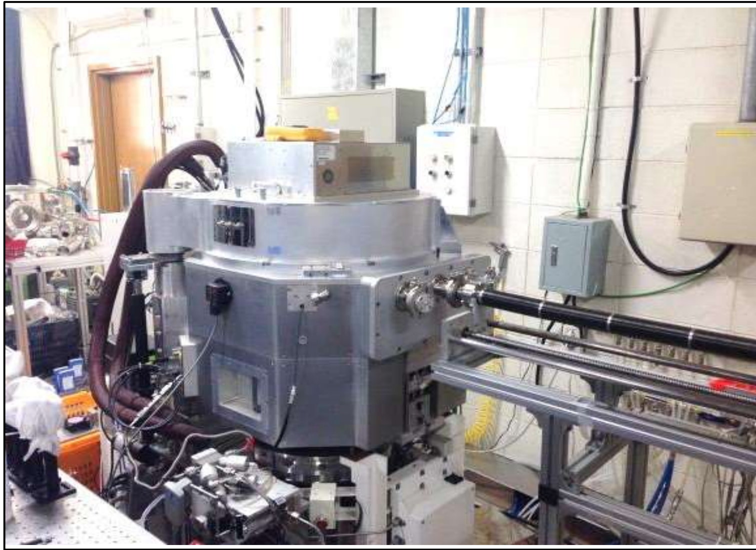

Figure 1-1 CCP etching reactor used for this thesis

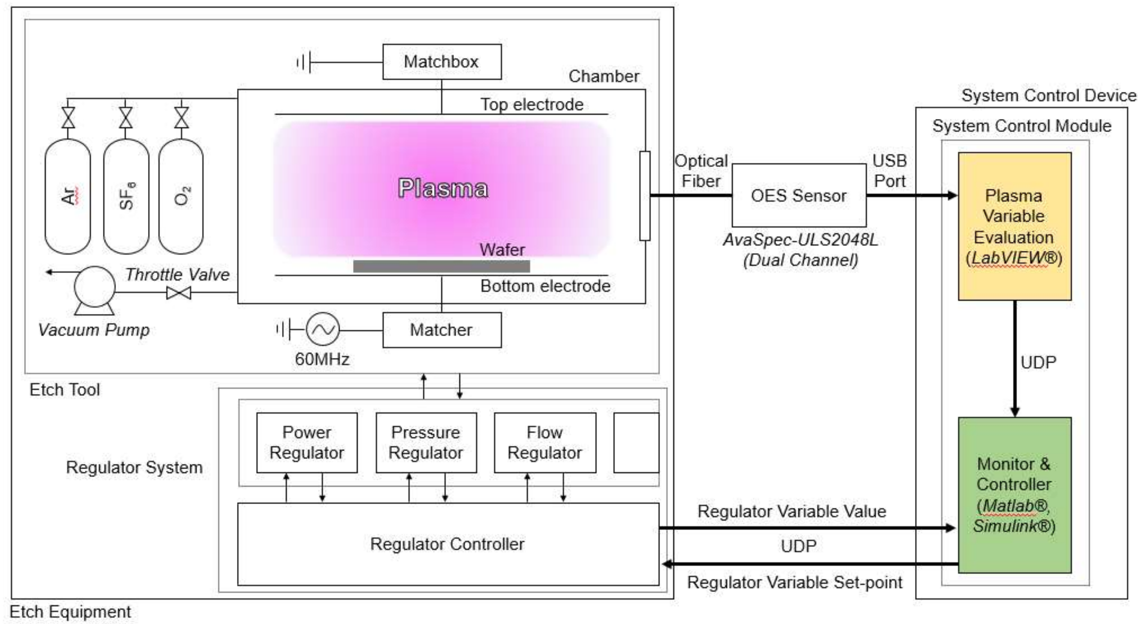

Figure 1-2 Schematic of CCP etching reactor employed in this thesis.

1.4. Outline of the thesis

CHAPTER 1 provides the research motivation and the objectives. Also, the equipment used in this thesis is described in this chapter. CHAPTER 2 presents a design of a MIMO controller. The controller design includes a variable pairing technique and system identification. Then, the tuned controllers with decoupler controllers conduct MIMO control simulations and an Ar plasma variable control experiment. CHAPTER 3 includes disturbance rejection control results of a model predictive controller. The performance of a thoroughly tuned model predictive controller is introduced, taking into account the disturbance that occurs frequently in the plasma-based system. CHAPTER 4 proposes an adaptive model predictive controller which consists of the model predictive controller designed in Chapter 3 and a recursive model parameter estimator. The adaptive model predictive controller is compared to the model predictive controller in the case of O_2 injection as a disturbance in a pure Ar plasma system. Finally, CHAPTER 5 summarizes the key contributions of this thesis and discusses ideas for the future work.

CHAPTER 2. Design of Multi-Input Multi-Output Controller for Plasma-based System*

2.1. Introduction

Since the early 1990s, research results on plasma variable control have begun to emerge. In one of the earliest research conducted in this field of study, a CF_4/O_2 plasma system was modeled and controlled using a relative gain array (RGA), singular value decomposition (SVD), and control simulation through an internal model controller (McLaughlin et al., 1991). Rauf and Kushner (1998) reported integral control results of electron density of Cl_2 plasma in an inductively coupled plasma (ICP) reactor using a virtual plasma equipment model, and Armaou et al. (2001; 1999) demonstrated the abilities of their proportional integral (PI) controllers to enhance the uniformity of the thickness of a wafer in the plasma-enhanced chemical vapor deposition (PECVD) process. With the highly elaborate fundamental models, they succeeded in controlling the uniformity in a SiH_4 plasma environment and CF_4 plasma environment. Chang et al. (2001) performed a PI control of Ar plasma variables in an ICP reactor using a heterodyne interferometer as the sensor and Lin et al. (2009) proposed a fuzzy logic based a PI controller that controls the electron density and ion energy using Cl_2/Ar gas in an ICP etcher. Lastly, Keville et al. (2013) performed an integral control of the electron density of Ar capacitively coupled

*This chapter cites the author's published journal article: Koo, J., Ha, D., Park, D., Roh, H.-J., Ryu, S., Kim, G.-H., Baek, K. H. & Han, C. (2017). Design of optical emission spectroscopy based plasma parameter controller for real-time advanced equipment control. Computers & Chemical Engineering, 100, 38-47.

plasma (CCP) using a hairpin probe as the sensor through an in-depth analysis of the control. Even though those studies show excellent results, it is difficult to directly apply them to semiconductor manufacturing environment because the employed plasma diagnostic tools are invasive to the systems and are also required to modify current plasma reactors for installation. In addition, controllers shown in these studies have SISO schemes where a counter change of another plasma variable during a SISO control action might occur due to the highly interactive plasma characteristics. Thus, a plasma controller using a non-invasive diagnostic tool and enabling consideration of interactions among plasma variables should be re-developed in the semiconductor industry.

In this chapter, an OES based MIMO PID controller is introduced. Since an OES is a default plasma diagnostic tool for every plasma reactor, there is no concern about invasiveness toward process and about installation. In order to estimate plasma variables such as the electron density and electron temperature, line-ratio techniques based on the corona model are employed for our plasma conditions (Boffard et al., 2004; Zhu & Pu, 2010). With these variables treated as CVs, a MIMO plasma variable controller is designed in the CCP reactor described in section 1.3. The MIMO system is identified by pseudo random binary sequence (PRBS) test, SVD, and RGA. The MIMO controller conducts a set-point tracking control simulation which can verify the exist of an interaction effect between MVs and CVs. Futhermore, by applying decoupler controllers that effectively handles the interaction, it finally becomes the MIMO PID controller with decoupler controllers. The proposed controller performs a set-point tracking control experiment in an Ar plasma system.

This chapter is organized as follows. In Section 2.2, theoretical backgrounds are introduced. Those are the explanation of the choice of the plasma variables, of the estimation of plasma variables from OES, of the influence of oxygen in the plasma etching reactor, of SVD and condition number (CN), of RGA method, and of multi-loop control system. Section 2.3 describes the MIMO control results in the Ar plasma system. It contains the result of the variable selection and pairing, of the disturbance rejection performance in SISO systems for demonstrating of controllability, of the simulation result of multi-loop control scheme and decoupling control scheme, and of the set-point tracking test of MIMO controllers with decoupler controllers. Finally, Section 2.4 concludes this chapter.

2.2. Theoretical backgrounds

2.2.1. Estimation of plasma variables from optical emission spectroscopy

An optical emission spectroscopy (OES) is a non-invasive and default plasma sensor under semiconductor manufacturing environment as mentioned in CHAPTER 1. It measures emission in plasma via an optical fiber which is attached on the viewport of chambers. Emission in plasma is generated by a process where an excited particle is converted from its higher energy quantum state to lower energy quantum state. Excitation of a particle is usually done by electron-particle collisions or particle-particle collisions.

In general, the intensity of emission in plasma is obtained by using corona equilibrium. In corona equilibrium, the excited state is formed solely by electron impact excitation, and the electron excitation rate is equal to the photon decay rate (Boffard et al., 2004; Zhu & Pu, 2010). The emission intensity from a particular p^{th} state to k^{th} state is described as Eq. (2-1),

$$\Phi_{pk} = n_0 n_e \int_{E_{thr}}^{\infty} \sigma_{pk}(E) \left(\frac{2E}{m_e}\right)^{\frac{1}{2}} f(E) dE, \qquad \textbf{(2-1)}$$

where n_0 is the number density of ground state atoms, n_e is the electron density, $\sigma_{pk}(E)$ is the excitation cross section from level p into level k as a function of electron energy E, $f(E)$ is the electron energy distribution function (EEDF), and m_e is the electron mass (Boffard et al., 2004).

In practice EEDF, $f(E)$ is assumed as one of the several standard functional forms, which is an one-parameter Maxwellian distribution described by an electron temperature, T_e, like that shown in Eq. (2-2),

$$f(E, T_e) = \frac{2\sqrt{E}}{\sqrt{\pi}(kT_e)^{3/2}} \exp\left(\frac{-E}{kT_e}\right), \tag{2-2}$$

where k is Boltzmann constant. In order to utilize OES for measuring plasma variables, so-called line-ratio technique has been utilized so far (Boffard et al., 2004; Zhu & Pu, 2010). For instance, the ratio of two measured emission lines from different excited states can be described in Eq. (2-3) derived from Eqs. (2-1) and (2-2),

$$\frac{\Phi_{pk}}{\Phi_{ij}} = \frac{\int_{E_1}^{\infty} \sigma_{pk}(E) \exp\left[-\frac{E}{kT_e}\right] EdE}{\int_{E_2}^{\infty} \sigma_{ij}(E) \exp\left[-\frac{E}{kT_e}\right] EdE}. \tag{2-3}$$

where E_1 and E_2 denote the energy threshold in each selected excited state. This is only dependent on the electron temperature. Of course, the two emission lines must be from different excited states with different energy thresholds, E_1 and E_2.

In addition to a line ratio measurement of the electron temperature, it would be useful to have a separate line-ratio measurement that is only a function of the electron density. Boffard *et al.* found that the 357.2nm ($5p_5$)/425.9nm($3p_1$) line ratio serves this purpose. This line ratio is essentially independent of electron temperature, but highly dependent on electron density. In a similar way, this work utilizes several Ar emission lines to estimate electron density and the electron temperature.

The above plasma variables which are the electron density and electron temperature have great significance in plasma etching processes. Considering a plasma etching process conducted by F species plasma, the etch rate (ER) is

affected by the plasma density n_F (cm^{-3}) linearly, thus, ER $\propto n_{\mathrm{F}}$. n_{F} can be expressed by the particle balance equation as follows.

$$K_{wall} n_{\mathrm{F}} v_{th} A = K_{iz} n_e n_g V \qquad \textbf{(2-4)}$$

where K_{wall} is the loss rate to the reactor wall (dimensionless), v_{th} is the thermal velocity (cm/s), A is the effective area for particle loss (cm^2), K_{iz} is the electron-neutral ionization rate constant (cm^6/s), n_e is the electron density (cm^{-3}), n_g is the neutral gas density (cm^{-3}) and V is the discharge model volume (cm^3). Solving for n_{F}, the following equation is obtained.

$$n_F = \frac{K_{iz} n_e n_g V}{K_{wall} v_{th} A}. \qquad \textbf{(2-5)}$$

Here, K_{iz} can be expressed as a function of T_{e} (Lieberman & Lichtenberg, 2005). Therefore, these relations ensure that the electron density and electron temperature are selected as the target plasma variables in estimating the performance of the plasma etching process. Consequently, the electron density and electron temperature which can be measured with the OES are selected as CVs in this work.

2.2.2. The influence of oxygen in plasma etching reactor

Oxygen is one of the species most closely related to the various processes in which a plasma etching reactor is used. It is either used as an additive in some etching processes or released as a by-product, and is also a very effective and economical major source of plasma in the cleaning process. The following is a reaction formula for the dissociation attachment when O_2 is used as an additive to increase the concentration of the etchant gas, CF_4, during Si etching or inhibiting polymer formation:

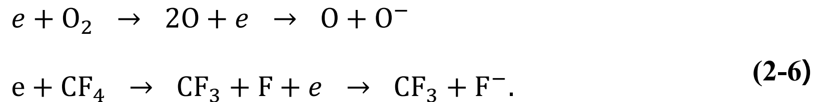

$$e + \mathrm{O_2} \;\rightarrow\; 2\mathrm{O} + e \;\rightarrow\; \mathrm{O} + \mathrm{O^-}$$
$$\mathrm{e} + \mathrm{CF_4} \;\rightarrow\; \mathrm{CF_3} + \mathrm{F} + e \;\rightarrow\; \mathrm{CF_3} + \mathrm{F^-}. \quad \textbf{(2-6)}$$

Oxygen atoms formed by the above reaction easily react with organics used as photoresists to produce reactants such as volatile gases CO, CO_2, and H_2O when fluorine atoms react with Si to cause etching. For ionization reactions that occur frequently in high density plasma, O_2 is ionized as follows.

$$e + \mathrm{O_2} \;\rightarrow\; \mathrm{O_2}^- \;\rightarrow\; \mathrm{O} + \mathrm{O^-} \quad \textbf{(2-7)}$$

where the threshold energy is 4.5 eV. In addition, O_2 is used in conjunction with CF_4 as an etching gas in organic etching processes, though not many. O_2 is also produced as a by-product in Si or Al etching using halogen as (Chung, 2013; Yeom, 2006):

$$\mathrm{Si} + 4\mathrm{Cl} \;\rightarrow\; \mathrm{SiCl_4}$$
$$\mathrm{SiO_2} + 4\mathrm{Cl} \rightarrow \mathrm{SiCl_4} + \mathrm{O_2} \quad \textbf{(2-8)}$$

$$Al_2O_3 + Cl_2 \rightarrow AlCl_3 + O_2. \quad \textbf{(2-9)}$$

O_2 is the most common chemical species used in the plasma cleaning process. The plasma cleaning process is a process for removing impurities and contaminants on the surface by using an energetic plasma. After the short wave ultraviolet (vacuum UV) energy breaks the most organic bonds such as C-H, C-C, C=C and C-O, O_2, plasma's activated species (O_2^+, O_2^-, O_3, O, O^+, O^- etc.) raised from the vacuum UV react with organic contaminants to form H_2O, CO, CO_2 (Pizzi & Mittal, 2003; Shun'ko & Belkin, 2007). As demonstrated above, O_2 is adopted as the disturbance of Ar plasma systems in this thesis because it plays a large role in various processes in which the plasma etching reactor is used.

2.2.3. Singular value decomposition and condition number

Singular value analysis (SVA) and its extensions such as SVD are powerful analytical techniques that can be helpful in solving important control problems such as selection of MVs and CVs and quantification of multivariable directionality (Baek et al., 2013; Seborg et al., 2008; Skogestad & Postlethwaite, 2007). If G is a constant $l \times m$ matrix, any matrix G can be decomposed into its singular value decomposition like Eq. (2-10),

$$G = U_s \Sigma V_s^T, \qquad \textbf{(2-10)}$$

where $\sum$ is a diagonal $l \times m$ matrix with non-negative singular values, $\boldsymbol{\sigma_i}$, arranged in a descending order along its main diagonal. In addition, $\boldsymbol{U_s}$ is an orthonormal $l \times l$ matrix of output singular vectors, $\boldsymbol{u_i}$, and $\boldsymbol{V_s}$ is an orthonormal $m \times m$ matrix of input singular vectors, $\boldsymbol{v_i}$.

That is, the original vector is decomposed into two directional vectors ($\boldsymbol{u_i}$ and $\boldsymbol{v_i}$) and one stretching vector ($\boldsymbol{\sigma_i}$). These characteristics of SVD can be utilized in analyzing a controller which is operated in a linear system model between input and output variables. If we consider a 2×2 linear controller with a steady-state gain *K* in Eq. (2-11), *K* can be decomposed like that shown in Eq. (2-12).

$$Y = KU + D, \qquad \textbf{(2-11)}$$

where *Y* is a CV matrix and *U* is a MV matrix, and *D* is an offset matrix.

$$K = \begin{bmatrix} cos\theta_1 & -sin\theta_1 \\ sin\theta_1 & cos\theta_1 \end{bmatrix} \begin{bmatrix} \sigma_1 & 0 \\ 0 & \sigma_2 \end{bmatrix} \begin{bmatrix} cos\theta_2 & \pm sin\theta_2 \\ -sin\theta_2 & \pm cos\theta_2 \end{bmatrix}^T, \quad \textbf{(2-12)}$$

$$U_s \qquad\qquad \Sigma \qquad\qquad V_s^T$$

where the angles $\boldsymbol{\theta_1}$ and $\boldsymbol{\theta_2}$ depend on the given matrix.

From Eq. (2-12), it is seen that the columns of the matrix $\boldsymbol{V_s}$ represent input directions, and so an input signal is rotated by the transpose of this matrix. In addition, it is illustrated that the rotated vectors are amplified by the matrix $\sum$, and then rotate again at the system output by the matrix $\boldsymbol{U_s}$. Therefore, the gain of the direction for each CV is determined by singular values in the matrix $\sum$, and the analyzing the singular values of gain matrix, *K*, gives insight into control performance.

The insight given by the SVD can be easily quantified by using the ratio of singular values that are defined as the square roots of the eigenvalues of the matrix product $\boldsymbol{K^T K}$. The condition number (CN) of *K* is defined in Eq. (2-13) (Seborg et al., 2008; Skogestad & Postlethwaite, 2007).

$$CN = \frac{\sigma_l}{\sigma_s} \quad \textbf{(2-13)}$$

where $\boldsymbol{\sigma_l}$ is the largest nonzero singular value and $\boldsymbol{\sigma_s}$ is the smallest nonzero singular value.

A large CN indicates at least one direction for CV is either too weak or too strong to be effectively controlled because the gain matrix is ill-conditioned. Therefore, a well-conditioned control strategy can be found by removing MVs or CVs of the control strategy until the CN of the control strategy becomes smaller.

Because a CN has the dependence on scaling of inputs and outputs, there are some scaling methods for minimizing the CN. Skogestad and Postlethwaite (2007) suggested minimized condition number:

$$CN^{*}(K) = \min_{D_1, D_2} CN\,(D_1 K D_2) \tag{2-14}$$

where CN^* is minimized condition number, and $\boldsymbol{D_1}$ and $\boldsymbol{D_2}$ are diagonal scaling matrices. In this chapter, we use the minimized condition number rather than the condition number in Eq. (2-13).

2.2.4. Relative gain array method

RGA is a useful tool to analyze interactions between input and output variables in MIMO control systems (Bristol, 1966; Seborg et al., 2008; Skogestad & Postlethwaite, 2007).

If a control system with *n* CVs and *m* MVs exist, the relative gain between a CV, y_i, a MV, u_j, is defined as ratio of two steady-state gains:

$$\lambda_{ij} = \frac{(\partial y_i/\partial u_j)_u}{(\partial y_i/\partial u_j)_y} = \frac{open - loop\ \ gain}{closed - loop\ \ gain} \tag{2-15}$$

for $i = 1,2, \ldots, n$ and $j = 1, 2, \ldots, m$.

In Eq. (2-15), $(\partial y_i/\partial u_j)_u$ denotes a partial derivative that is evaluated with all of the MVs except u_j held constant. Similarly, $(\partial y_i/\partial u_j)_y$ denotes a partial derivative that is evaluated with all of the CVs except y_i held constant.

The matrix of those relative gains, RGA, denoted by Λ is defined as follows.

$$\Lambda = \begin{bmatrix} \lambda_{11} & \cdots & \lambda_{1m} \\ \vdots & \ddots & \vdots \\ \lambda_{n1} & \cdots & \lambda_{nm} \end{bmatrix}. \tag{2-16}$$

The RGA has several algebraic properties and control properties. For example, the sum of its each row or column is 1 so that it is normalized. Also, it is not affected by scaling and units of input and output variables because of its dimensionless characteristic. In addition, we can get information of control properties of the system: When λ_{ij} is equal to 0, u_j has no effect on y_i. When λ_{ij} is equal to 1, u_j affects y_i without any interaction. In $0 < \lambda_{ij} < 1$ case, the interaction effect has the same direction with the main effect. That is, the interaction assists u_j in controlling y_i. In contrast, in $\lambda_{ij} > 1$ case, the

interaction effect has the opposition direction with the main effect so that u_j needs a larger movement. In $\lambda_{ij} < 0$ case, the system becomes unstable. Thus, the first rule is to avoid negative elements, and the second rule is to select elements close to 1 (Seborg et al., 2008; Skogestad & Postlethwaite, 2007).

2.2.5. Multi-loop control system

Figure 2-1 shows a standard block diagram of a feedback control system. The manipulated variable U is transformed into Y_u through a process transfer function G_p. Similarly, disturbance variable D is transformed into Y_d through a disturbance transfer function G_d. The difference between set-point, Y_{sp}, and summation of Y_u and Y_d becomes error, E, which can be compensated by the controller operation. That is, the controller calculates new U which can minimize E.

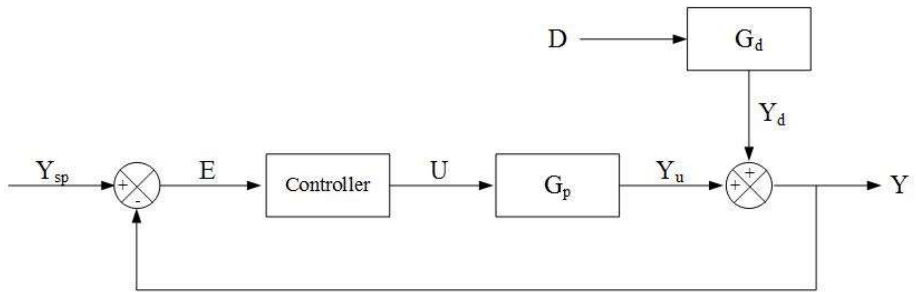

Figure 2-1 Standard block diagram of feedback control system.

Some controllers which enable to minimize error signals have been developed. Among them, the PID controller is one of the most popular controller types, which can be applied in Figure 2-1.

For proportional control mode, the controller output is proportional to the output error,

$$p(t) - \bar{p}(t) = K_c e(t), \tag{2-17}$$

where $p(t)$ and $\bar{p}(t)$ are the controller output and bias value of it, K_c is a controller gain, $e(t)$ is error signal for measured CV in time domain. When a deviation variable $p'(t)$ is defined as $p(t) - \bar{p}(t)$, the transfer function for Eq. (2-17) becomes

$$\frac{P'(s)}{E(s)} = K_c \tag{2-18}$$

in Laplace domain. Likewise, the equations in time domain and Laplace domain for PI control mode is expressed as,

$$p'(t) = K_c \left[e(t) + \frac{1}{\tau_I} \int_0^t e(t^*) dt^*) \right] \tag{2-19}$$

$$\frac{P'(s)}{E(s)} = K_c \left(1 + \frac{1}{\tau_I s} \right) \tag{2-20}$$

where τ_I is integral time. For PID control equation, those equations can be revised as follows.

$$p'(t) = K_c \left[e(t) + \frac{1}{\tau_I} \int_0^t e(t^*) dt^* + \tau_D \frac{de(t)}{dt} \right] \tag{2-21}$$

$$\frac{P'(s)}{E(s)} = K_c\left(1 + \frac{1}{\tau_I s} + \tau_D s\right) \quad \textbf{(2-22)}$$

where τ_D is derivative time.

The integral control mode compensates the offset which can occur at a proportional only control system. In addition, the derivative control mode amends the time response in a proportional only control or a proportional and integral control. In general, the integral control or the derivative control is not used alone. Instead, the combination of those three control modes is widely used (Seborg et al., 2008).

When a target control system is multivariable, the feedback control system shown in Figure 2-1 should consider interactions between input and output variables. Figure 2-2 illustrates a 2 × 2 MIMO control system. In this scheme, the controller 1 adjusts U_1 so as to make Y_1 approach to the set-point. However, U_1 also affects Y_2 via transfer function G_{21}. When Y_2 is changed, the controller 2 adjusts U_2 so as to bring Y_2 back to its set-point, Y_{sp2}. However, in this time, Y_1 is affected through transfer function G_{12}. These control actions proceed simultaneously and continuously until a new steady state is reached. Therefore, unless interaction analysis between input and output is done sufficiently, this control scheme might be able to destabilize or fail to reach both control targets.

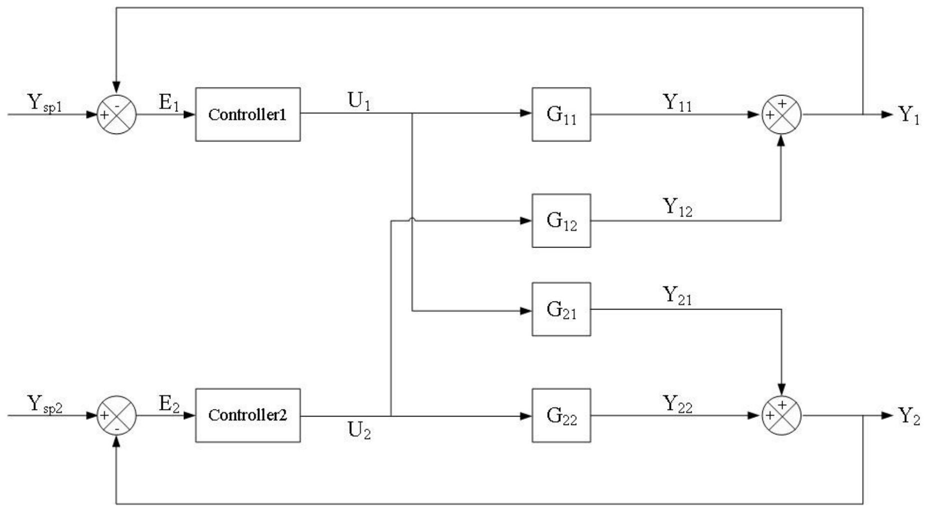

Figure 2-2 Block diagram of multi-loop control system.

One approach to eliminating interactions is to add additional controllers called decoupler controllers. In principle, decoupling control schemes can provide two important benefits (Seborg et al., 2008). Firstly, interactions caused by control actions can be eliminated and so the stability of the closed-loop system is determined independently by the individual feedback control loops. Secondly, a set-point change for one CV has no effect on the other CVs.

Figure 2-3 illustrates one type of decoupling control system for a 2 × 2 process. There are additional decoupler controllers, T_1 and T_2, where the input signal to each decoupler controller is the output signal from each feedback controller. The decoupler controller T_1 is designed to cancel out Y_{21}, which arises from the undesirable process interaction between U_1 and Y_2. Similarly, the decoupler controller T_2 removes the interaction between U_2 and Y_1.

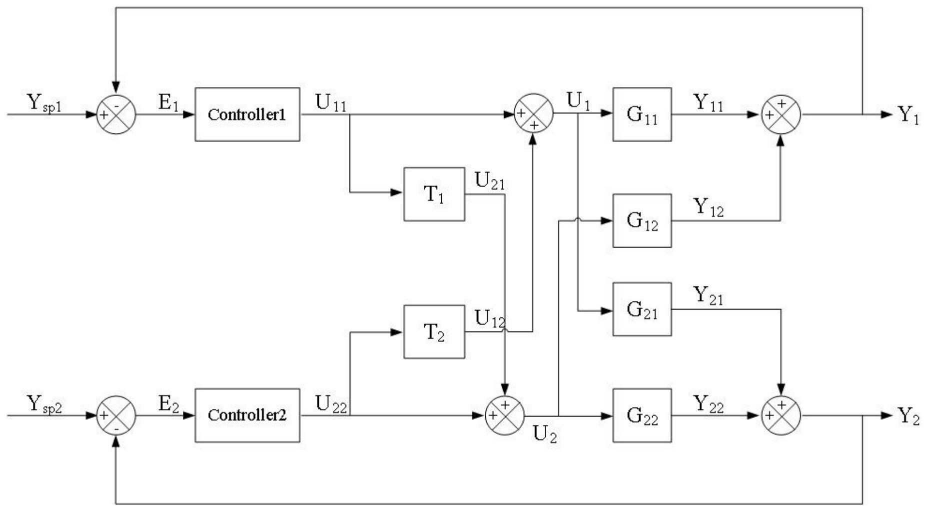

Figure 2-3 Block diagram of decoupling multi-loop control system.

In the next section, the control performances of different schemes shown in Figure 2-1, Figure 2-2, and Figure 2-3 are compared and then the results will be discussed.

2.3. MIMO control results in the Ar plasma system

2.3.1. Variable selection and pairing

In order to design a robust and feasible controller, optimum CVs and MVs should be selected, which cannot be often chosen only by using expert knowledge. Theoretically, a perfect steady-state control is achievable if there are the same numbers of control knobs as outputs. Specifically, the preferred control strategy is a square system with each CV controlled by one MV. To make a reasonable design for the square system, a step-by-step procedure using techniques in Sections 2.2.3 and 2.2.4 is made.

As a first step, the electron density and electron temperature were selected as CVs. They were estimated from OES data by using the technique in Section 2.2.1. As a second step, pseudo random binary sequence (PRBS) tests for individual MVs (60 MHz RF power, pressure, Ar flowrate and 2 MHz RF power) were done with various changes within system linearity in order to determine steady-state relationships. The reference plasma condition is 200 W of 60 MHz RF power, 20 mT of pressure, 100 W of 2 MHz RF power and 400 sccm of Ar flowrate. Regarding to this reference plasma condition, MVs were changed independently by +/- 10 % and waited until plasma reaches steady-state. Through the PRBS test results, the average system gains, average time constants, and average time delays were obtained so that the first order system model approximations were identified. Table 1 summarizes the steady-state gains between MVs and CVs calculated from the PRBS tests.

Table 1 Steady state gain matrix obtained from PRBS tests.

	60 MHz RF power (W)	Pressure (mT)	Ar flowrate (sccm)	2 MHz RF power (W)
Electron density (a.u.)	63.81 (a.u./W)	84.61 (a.u./mT)	0.7195 (a.u./sccm)	1.962 (a.u./W)
Electron temperature (a.u.)	-0.005975 (a.u./W)	-0.07004 (a.u./mT)	-0.0004193 (a.u./sccm)	-0.002871 (a.u./W)

With the gain matrix in Table 1, minimized condition numbers in Eq. (2-14) are calculated for every 2×2 system. For the final step, the relative gains were also calculated for every 2×2 system to compare the feasibilities of each strategy in relation to the interaction effect. Table 2 summarizes the possible control strategies and their minimized CNs and relative gains.

Table 2 Minimized condition numbers and relative gains for every $\mathbf{2 \times 2}$ system.

Strategy	CVs	MVs	CN*	Relative gains			
				λ_{11}	λ_{12}	λ_{21}	λ_{22}
1	**Electron density, Electron temperature**	**60 MHz RF power, Pressure**	**1027**	**1.13**	**-0.13**	**-0.13**	**1.13**
2	Electron density, Electron temperature	60 MHz RF power, Ar flowrate	995220	1.19	-0.19	-0.19	1.19
3	Electron density, Electron temperature	60 MHz RF power, 2 MHz RF power	23748	1.07	-0.07	-0.07	1.07
4	Electron density, Electron temperature	Pressure, Ar flowrate	107024	-2.38	3.38	3.38	-2.38
5	Electron density, Electron temperature	Pressure, Ar flowrate	67887	2.30	-1.30	-1.30	2.30
6	Electron density, Electron temperature	Ar flowrate 2 MHz RF power	421.7	1.66	-0.66	-0.66	1.66

Although there is no threshold of CN* that can decide whether the condition of system is ill or not, a relatively small CN* can be acceptable for the choice of the best case. In this sense, strategy number 1 and 6 are reasonable to select. When it comes to RGA, the strategy number 1 has a pair of relative gains as close as one. Based on the results of SVD and RGA method, the best pairing of MVs and CVs was determined to be 60 MHz RF power - electron density and pressure - electron temperature. The 2×2 first order transfer function system model is described in Table 3.

Table 3 The selected 2×2 first order transfer function system model.

	60 MHz RF power	**Pressure**
Electron density	$\frac{63.81}{0.028s + 1}$	$\frac{84.61}{0.30s + 1}$
Electron temperature	$\frac{-0.005975}{0.20s + 1}$	$\frac{-0.07004}{0.41s + 1}$

2.3.2. Disturbance rejection control results for SISO systems

As described in the previous section, the best strategy of plasma parameter control is the system comprising of 60 MHz RF power (MV_1), pressure (MV_2), electron density (CV_1) and electron temperature (CV_2). Also, based on the RGA method, feasible pairings are 60 MHz RF power - electron density and pressure - electron temperature.

In order to check the controllability of this system, two SISO controls were tested under an intentional disturbance situation. In the SISO control systems, U in Figure 2-1 indicates 60 MHz RF power or pressure and Y indicates electron density or electron temperature. As described in Section 2.2.2, O_2 was injected to pure Ar plasma chamber as a disturbance. Figure 2-4(a) shows a change of electron density by O_2 injection and that after a control operation. On the initial stage, the MV_1 and MV_2 are set to be 200 W and 20 mT, and the CV_1 and CV_2 have steady state value of 21,578 a.u. and 4.451 a.u., respectively. After O_2 injection, the CV_1 is decreased from 21,578 a.u. to 21,198 a.u. and returns to the original value by the control operation. For this control action, the MV_1 is changed to 207 W while the MV_2 remains constant. In a similar way, the electron temperature was controlled in the O_2 injection situation like that shown in Figure 2-4(b). The CV_2 is decreased from 4.423 a.u. to 4.225 a.u. after O_2 injection then returns to the original value by the control action. For this control operation, the MV_2 is changed while MV_1 remains constant. Thereby, the controllability of each is demonstrated to be positive.

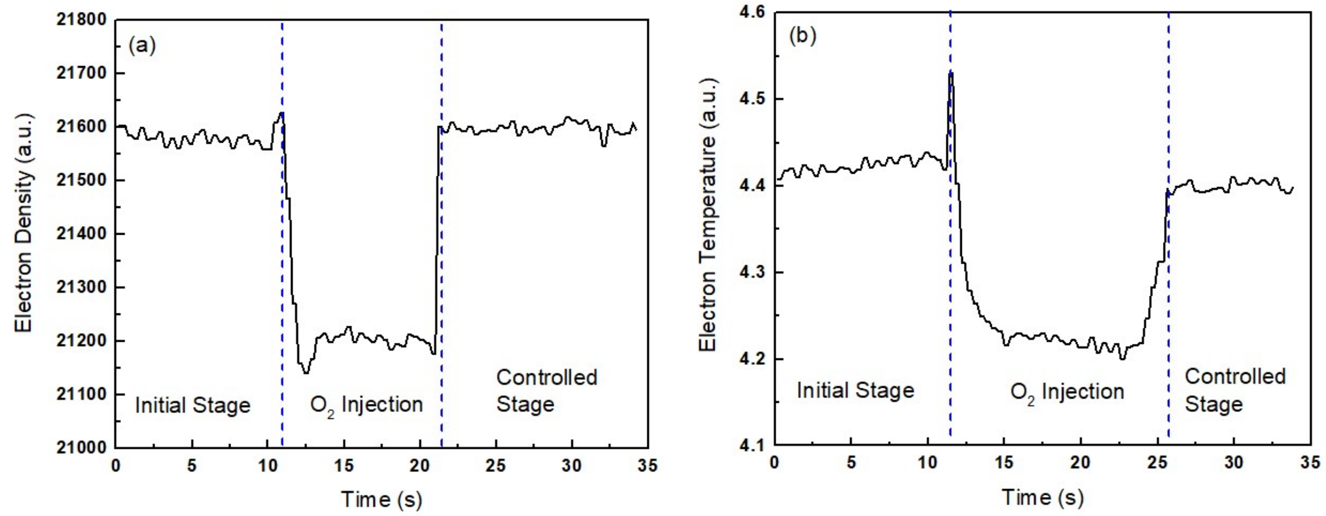

Figure 2-4 Results of SISO disturbance rejection control of (a) the electron density and (b) electron temperature.

Although these SISO controls show an excellent disturbance rejection, it is found that there were interaction effects for each control operation. Figure 2-5 shows that the electron density is affected by the control operation for the electron temperature. When O_2 flows into the plasma etching reactor at 12 s for simulating the disturbance injection situation, the electron density and electron temperature are changed from their original steady-state values to new steady-state values. As soon as the SISO control for electron temperature is activated, the other CV, which is the electron density, moves to the new value that is different from the initial stage value. This concludes that SISO control schemes might not be enough to control plasma variables and a MIMO control scheme which can compensate the interaction effect should be considered for highly complex plasma processes.

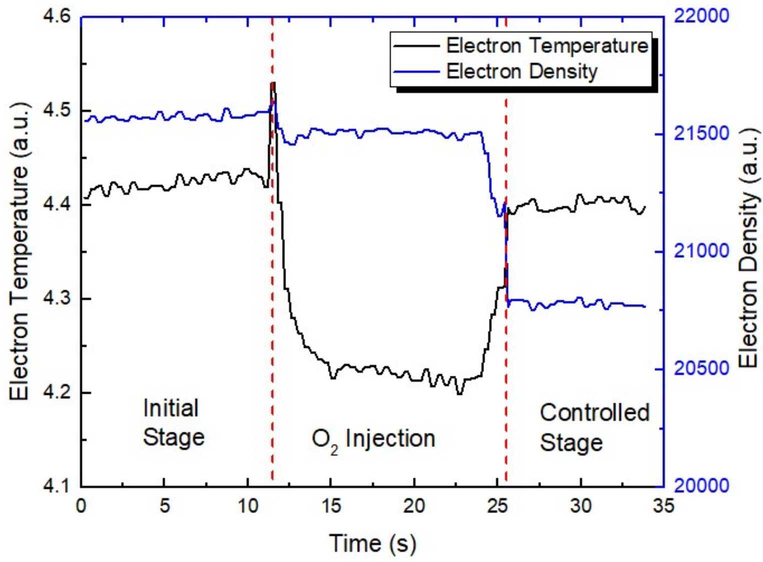

Figure 2-5 Undesirable movement of electron density when electron temperature is controlled.

2.3.3. Simulation of multi-loop control scheme and decoupling control scheme

As described in the previous section, a system with interactions between variables cannot be perfectly controlled by SISO control schemes. Thus, a MIMO control scheme enabling compensation of those interactions is designed by using previously chosen CVs and MVs pairings. A multi-loop controller, a conventional type of a MIMO controller, is designed by the PID tuner application in Simulink® with the obtained transfer functions in Table 3. Like the block diagram shown in Figure 2-2, Y_1 and Y_{sp1} indicate the electron density and the set point of it, respectively. Similarly, Y_2 and Y_{sp2} indicate the electron temperature and the set point of it, respectively. Also, U_1 and U_2 indicate the 60 MHz RF power and pressure, respectively. G_{ab} (a=1, 2, b=1, 2) indicates each transfer function in Table 3. After applying the parameters of the transfer functions to the simulation models, the offline set-point tracking control simulations for controller tuning based on the errors were conducted. With the two tuned PID controllers, a set point tracking test which simultaneously changes the electron density and electron temperature from 21,600 a.u. and 4.480 a.u. to 22,680 a.u. to 4.256 a.u. was conducted. Figure 2-6 and Figure 2-7 show the results of the set point tracking control simulation. Each CV is well controlled as it tracks its target in accordance with the set-point change at 50 s. For the control realization, MVs change at 50 s where the steady state value of MV_1 is changed from 200 W to 214 W and that of MV_2 is changed from 20 mT to 21.8 mT. Therefore, it is demonstrated that the MIMO PID controller are well tuned and has a good ability in conducting simultaneous CV changing control.

These successful control result from the multi-loop controller shows feasibility of MIMO scheme for plasma variable control.

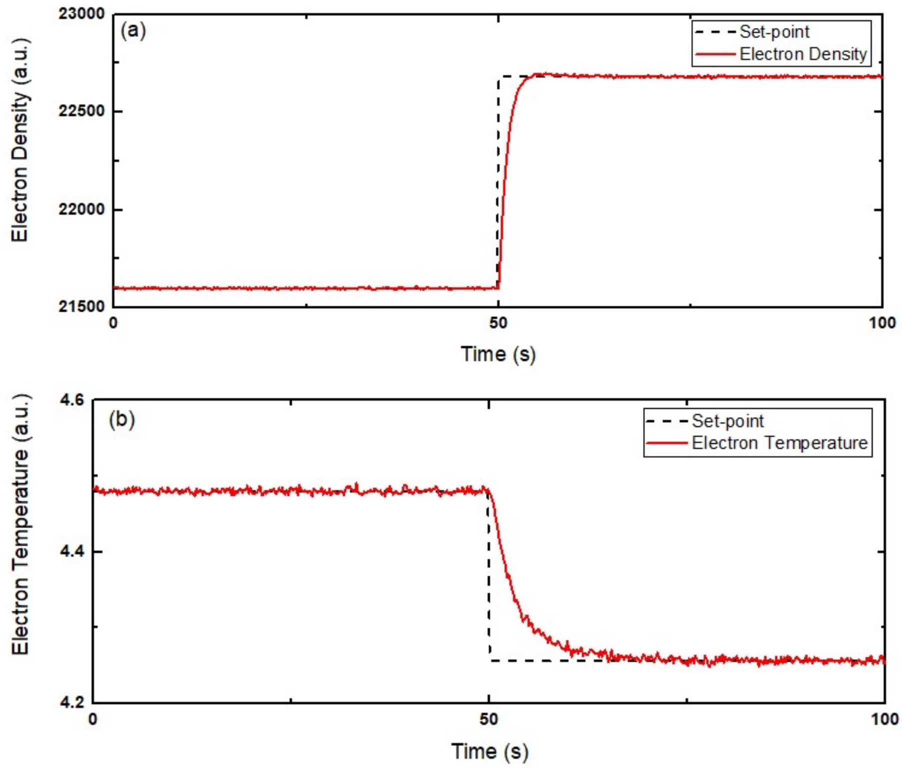

Figure 2-6 Multi-loop control simulation results of (a) electron density (CV_1) movement and (b) electron temperature (CV_2) (without decoupler).

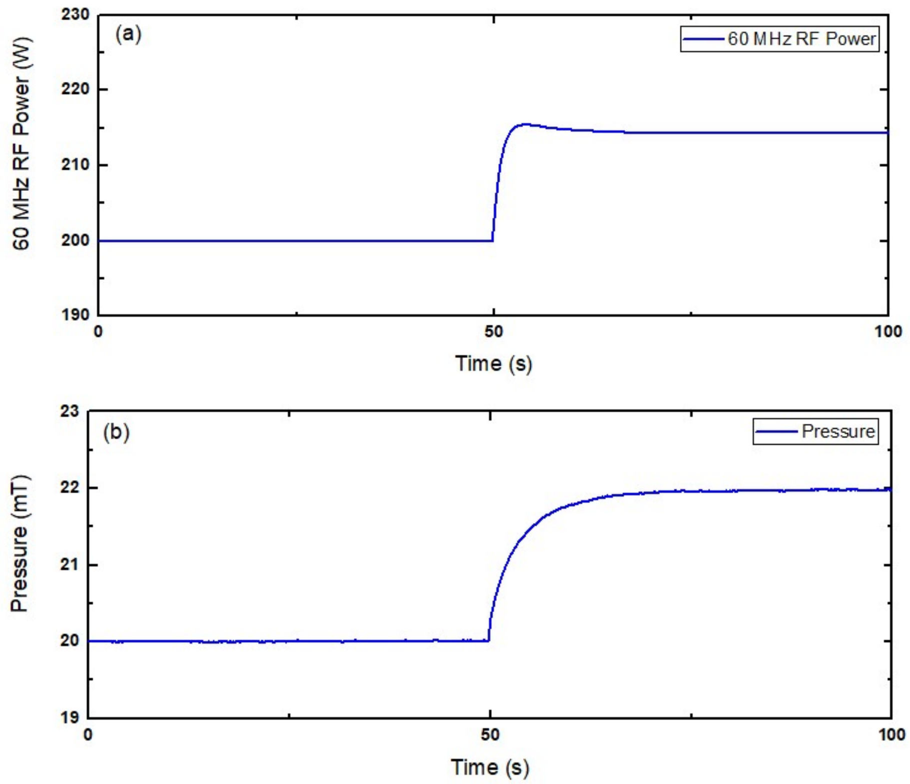

Figure 2-7 (a) 60 MHz RF Power (MV_1) movement and (b) pressure (MV_2) movement during multi-loop control simulation (without decoupler).

Even though the multi-loop control scheme with the two PID controllers shows the successful set-point tracking control result, the simultaneous changes for CV_1 and CV_2 set-points might overlook the system complexity effect. When the set-point change for each CV was done at different time, the effects of interaction with and without decoupler controllers were observed more obviously. For the simulation to show the interaction effect, the set point of the CV_1 was changed to be 22,680 a.u. and after 30 s, the set point of the CV_2 was changed to be 4.256 a.u. in the same control design used in the above. The control simulation result is shown in Figure 2-8 and Figure 2-9. That is, as soon as the set point of CV_1 is changed at 30 s, MVs are changed to control the CV_1. At the same time, the CV_2 is affected by the movement of the MVs in this case. In same way, the undesirable movement of the CV_1 exists at the 60 s. It is clearly demonstrated that the interaction effect disturbs the CVs tracking their set-points.

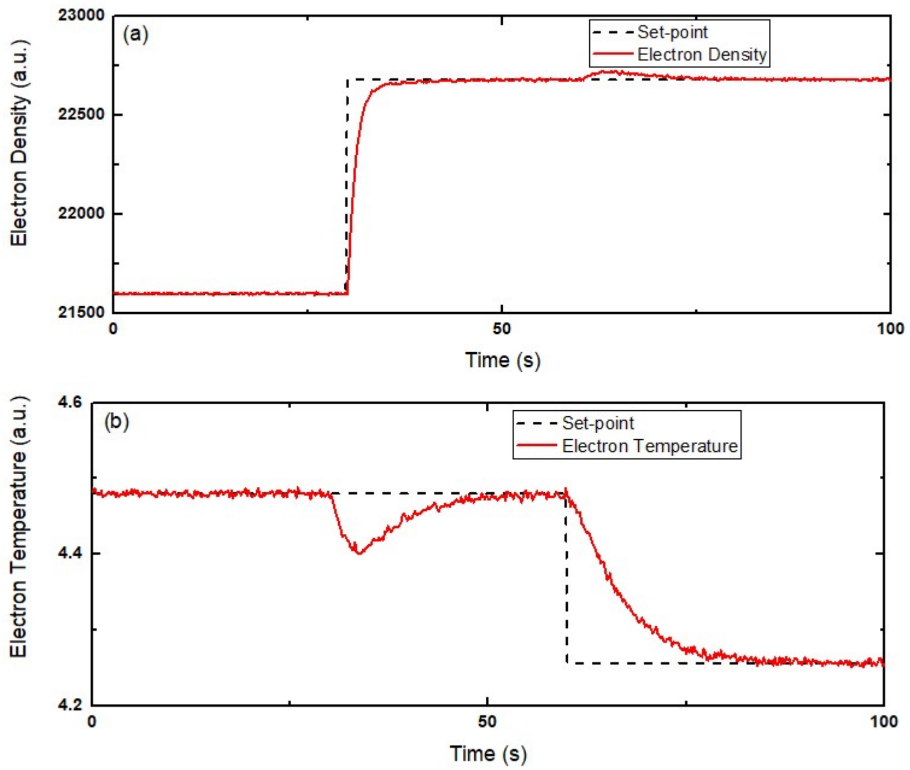

Figure 2-8 Multi-loop control simulation results of (a) electron density (CV_1) and (b) electron temperature (CV_2) (without decoupler).

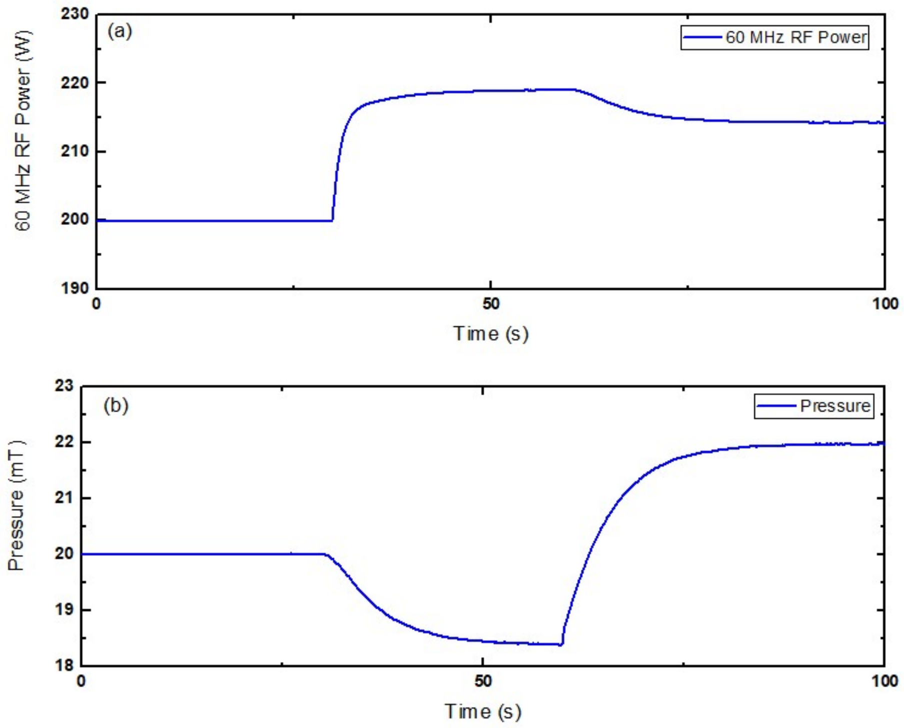

Figure 2-9 (a) 60 MHz RF Power (MV_1) movement and (b) pressure (MV_2) movement during multi-loop control simulation (without decoupler).

For the purpose of removal of the interaction, decoupler controllers discussed in Section 2.2.5 were applied. The following equations are the equations of the decoupler controllers and the design results of it based on Table 3.

$$T_1 = -\frac{G_{21}}{G_{22}}$$
$$T_2 = -\frac{G_{12}}{G_{11}} \qquad \textbf{(2-23)}$$

$$T_1 = \frac{1280(0.41s + 1)}{0.30s + 1}$$
$$T_2 = \frac{9.364(0.028s + 1)}{0.20s + 1} \times 10^{-5}. \qquad \textbf{(2-24)}$$

With these decoupler controllers, the comparison between SISO controllers and the MIMO controller with decoupler controllers were conducted. For the first case, the set-point tracking control for electron density was conducted. Here, the SISO controller has the set-point of electron density but not that of electron temperature. Whereas, the MIMO controller with decoupler controllers has both two set-points of CVs. With the stationary set-point for the electron temperature, the MIMO controller could control the both CVs. In Figure 2-10, the control simulation results of electron density set-point tracking test are shown. As the set-point of electron density was changed at 50 s, both controllers operated well for the electron density control as shown in Figure 2-10(a). However, the electron temperature was deviated from the initial steady state value when there was only the SISO control action as shown in Figure 2-10(b). Whereas, the electron temperature was maintained to its steady state value in the MIMO control mode. The consistency was induced by the pressure adjustment in the MIMO control mode as shown in Figure 2-11(b). The

adjustment affected the electron density, causing the larger movement in the other MV, 60 MHz RF power, than the SISO control mode case, which is illustrated in Figure 2-11(a).

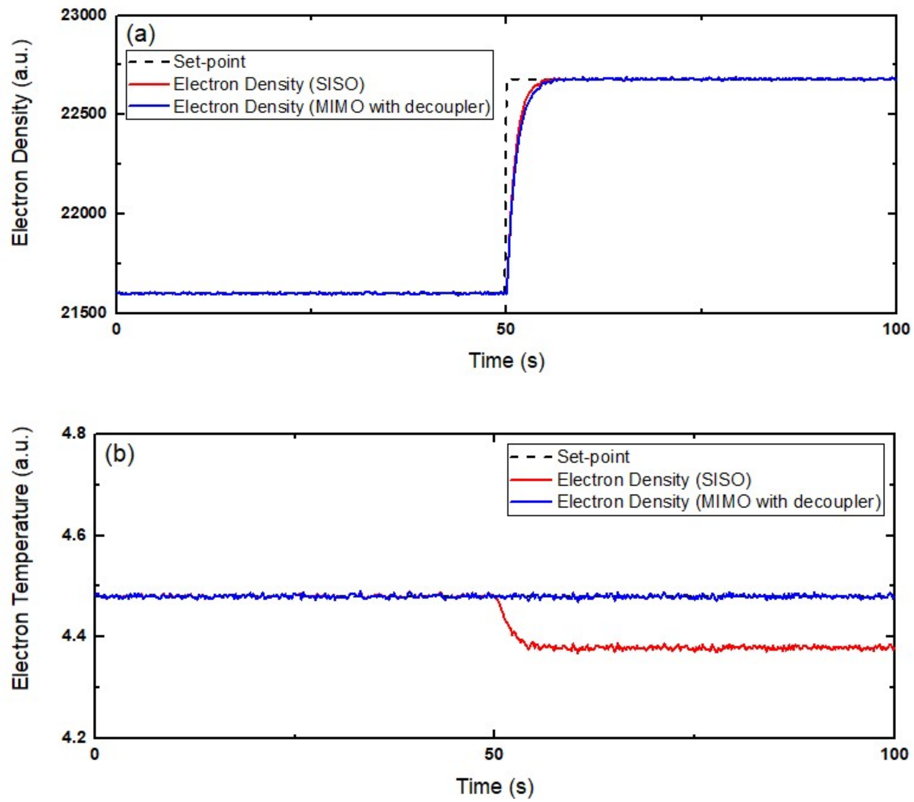

Figure 2-10 The control simulation results of electron density (CV_1) set-point tracking test conducted by the SISO controller (red line) and the MIMO controller with decoupler controllers (blue line).

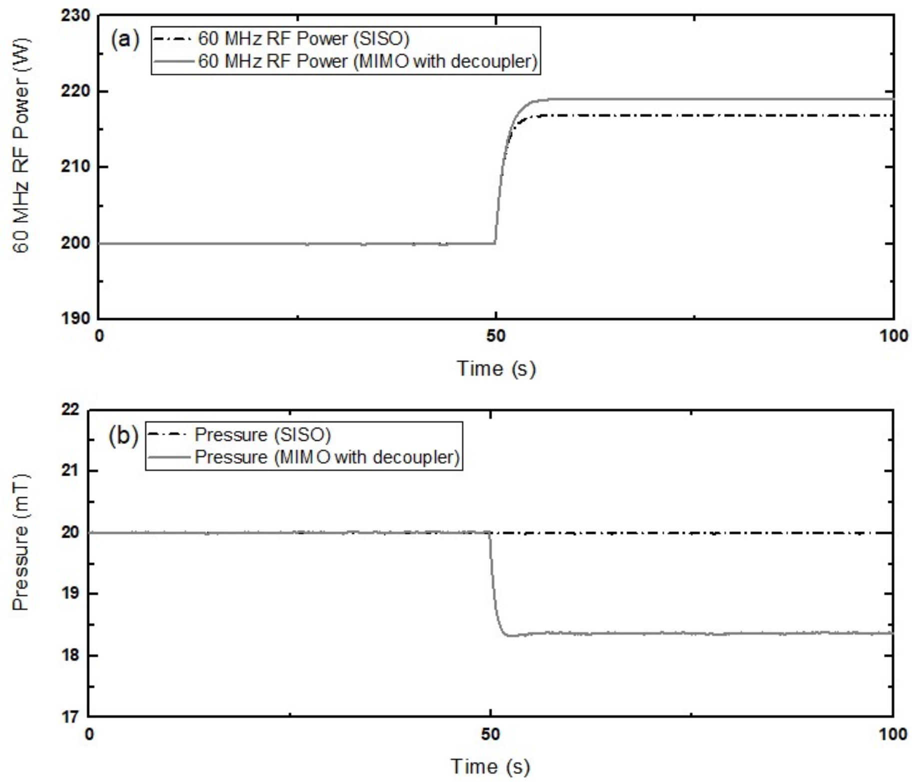

Figure 2-11 (a) 60 MHz RF Power (MV_1) movements and (b) pressure (MV_2) movements during electron density set-point tracking control simulation conducted by the SISO controller (dash dot) and the MIMO controller with decoupler controllers (gray line).

Similar to the above case, an additional comparison through the electron temperature control simulation was conducted. In this case, the second CV, electron temperature was controlled. In Figure 2-12(b), both controllers operated well to make the electron temperature track its set-point. However, the electron density was deviated from the initial steady state value when there was only the SISO control action as shown in Figure 2-12(a). Whereas, the electron density was maintained in the MIMO control mode by the 60MHz RF power adjustment as shown in Figure 2-13(a). The larger movement of pressure in the MIMO control mode than the SISO control mode in Figure 2-13(b) is because of the compensation of the effect from the other MV adjustment.

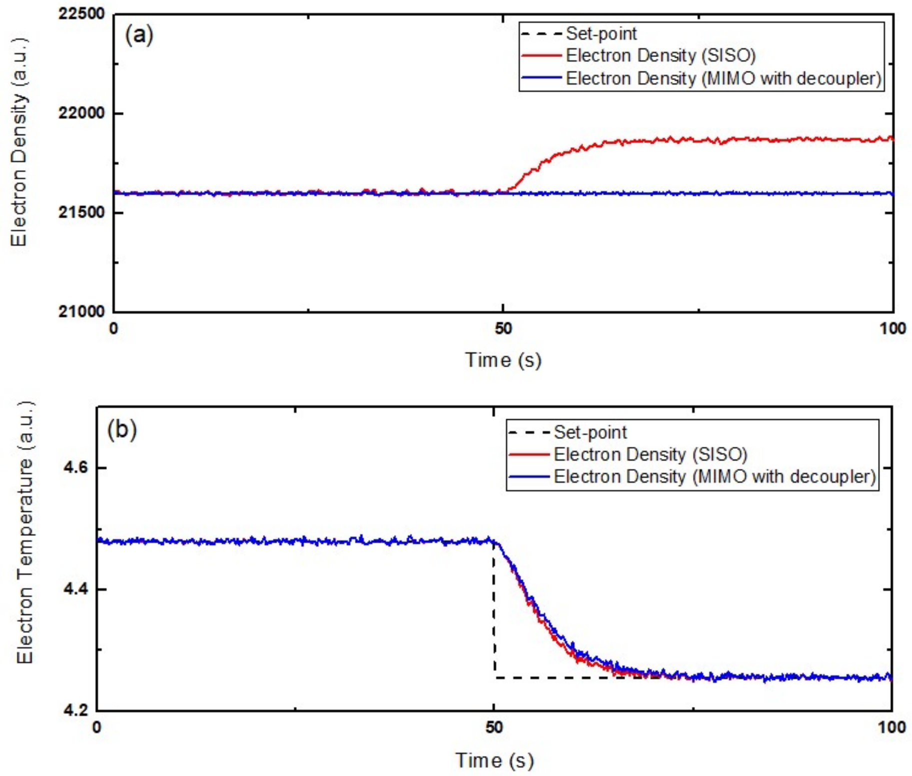

Figure 2-12 The control simulation results of electron temperature (CV_2) set-point tracking test conducted by the SISO controller (red line) and the MIMO controller with decoupler controllers (blue line).

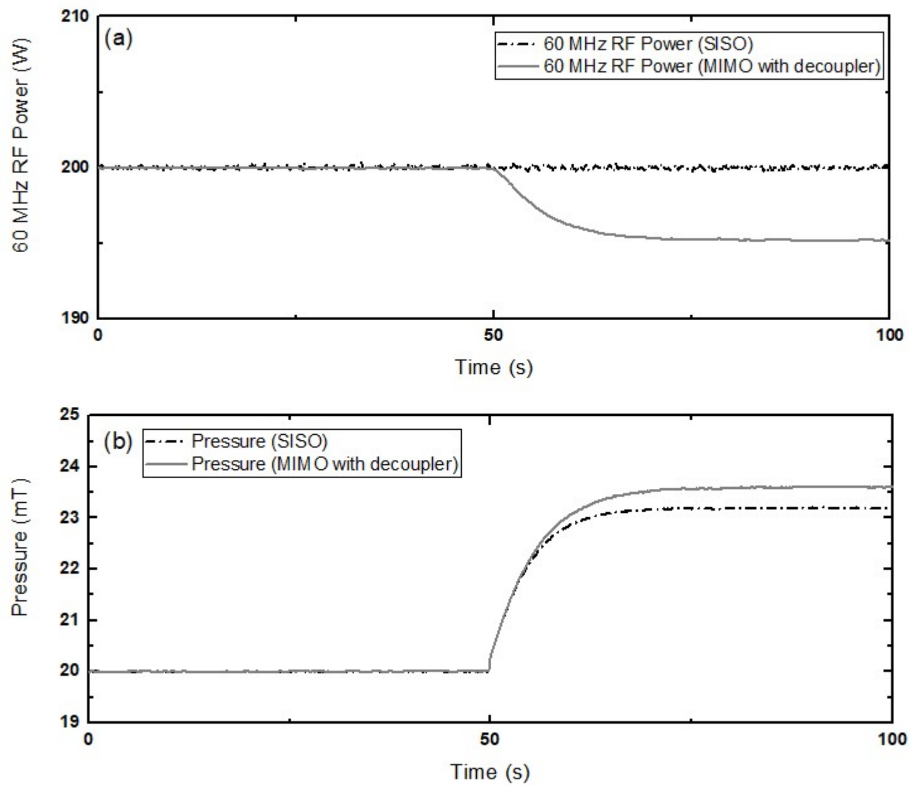

Figure 2-13 (a) 60 MHz RF Power (MV_1) movements and (b) pressure (MV_2) movements during electron density set-point tracking control simulation conducted by the SISO controller (dash dot) and the MIMO controller with decoupler controllers (gray line).

In addition, the same set-point tracking control simulation described in Figure 2-8 was conducted by the MIMO controller with decoupler controllers. In Figure 2-14, the interaction effect shown in Figure 2-8 (red line) does not appear in the decoupler controllers added case (blue line). It is because when the CV_1 tracks its set-point at 30 s, the decoupler controllers T_1 and T_2 compensate the errors by larger movements of the MVs. At 30 s, the movements of the MVs from the decoupler controllers added case (gray line) are larger than that from the only MIMO controller exist case (dash dot) as shown in Figure 2-15. In the same way, the effect of interaction at 60 s is removed beforehand by the decoupler controllers. These simulation results obviously demonstrate that the decoupler controllers are indispensable for MIMO control of plasma variables. Based on the simulation results, a set-point tracking control experiment will be conducted and discussed in the next section.

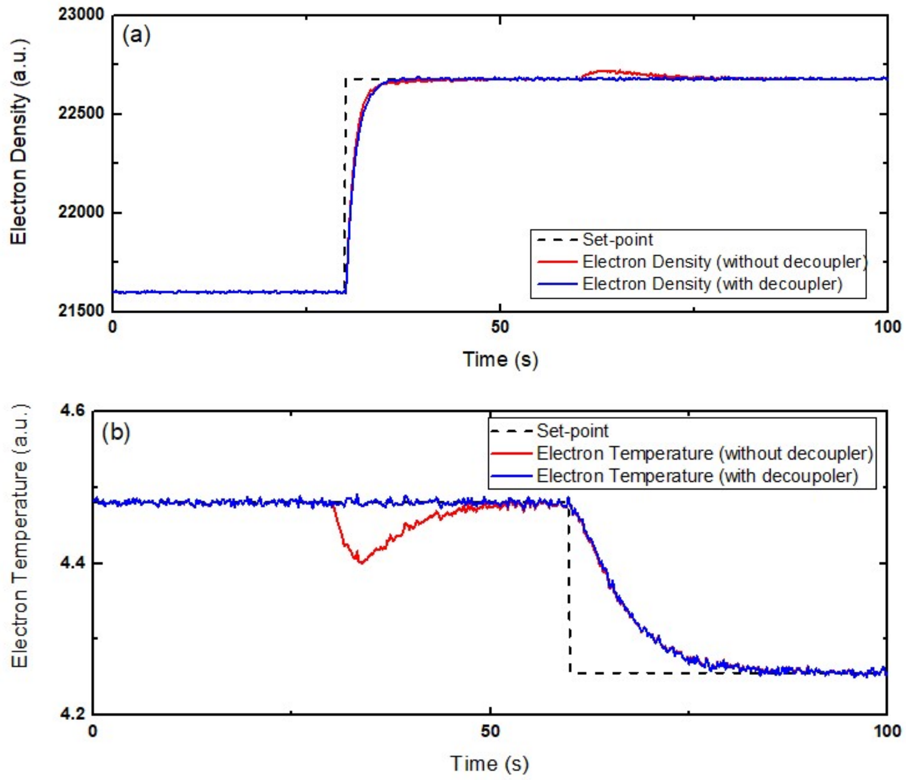

Figure 2-14 Multi-loop control simulation results of (a) electron density (CV_1) movement and (b) electron temperature (CV_2) conducted by the MIMO controller with decoupler controllers (blue line) are compared to the results come from the MIMO controller without decoupler controllers (red line).

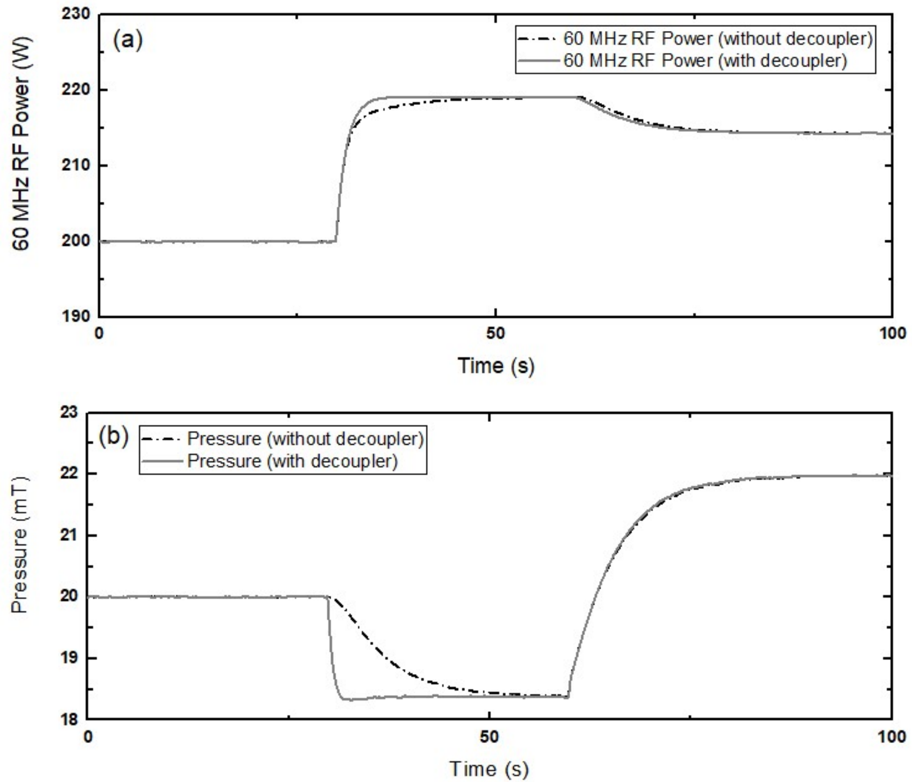

Figure 2-15 (a) 60 MHz RF Power (MV_1) movement and (b) pressure (MV_2) movement during multi-loop control simulation conducted by the MIMO controller with decoupler controllers (gray line) are compared to the MV movements released from the MIMO controller without decoupler controllers (dash dot).

2.3.4. Set-point tracking control experiment of multi-loop controller with decoupler controllers

With the controller introduced in the previous section, a set point tracking experiment was conducted. Some adjustments were done to apply the controller to our plasma etching reactor beforehand. For example, for the real-time control, a pace matching between simulation and experiment was done. The experimental sample time is 0.2 s and the starting reference condition is 200 W of 60 MHz RF power, 20 mT of pressure and 400 sccm of Ar flowrate. As shown in Figure 2-16, the steady state values of the CVs are 21,597 a.u. and 4.479 a.u., respectively, until 20 s at the reference condition. The set point trajectory of the electron density is configured to increase from the reference value to 22,680 a.u. at 20 s and that of the electron temperature is configured to decrease from the reference value to 4.256 a.u. at 50 s. While the electron density increases at 20 s and follows its trajectory well, the MIMO PID controller with the decoupler controllers also works to maintain the electron temperature. Likewise, while the electron temperature tracks its trajectory with decreasing at 50 s, the electron density remains almost constant. Although the decoupler controllers work to reduce the interaction, the oscillation of the electron temperature is observed. The reason of the oscillation was because of the equipment limitation in the settings of the MVs. The values of the MVs had been only able to be positive integers like that shown in Figure 2-17 while the designed controller had released control actions in positive real numbers. However, the equipment has been modified now and can cover entire positive real numbers. This control results verify the feasibility of the MIMO plasma variable control measured by OES through the proposed MIMO PID controller

with decoupler controllers. Therefore, it is expected that the diversity and the development of plasma variable control processes are improved by the proposed control schemes.

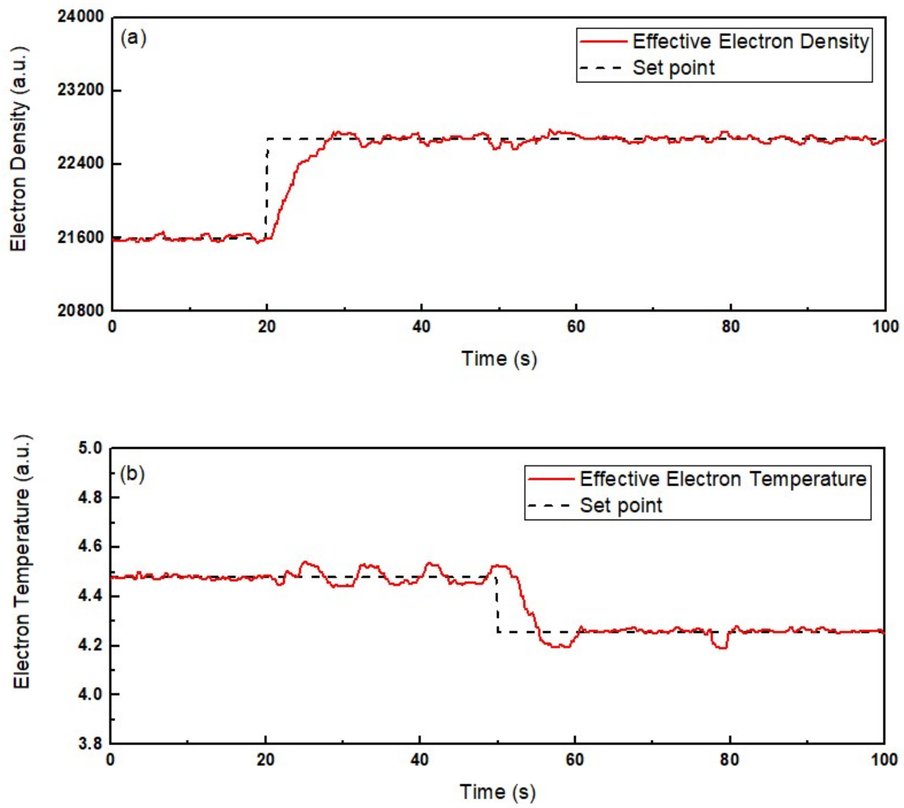

Figure 2-16 Set-point tracking control results of (a) electron density (CV_1) and (b) electron temperature(CV_2)).

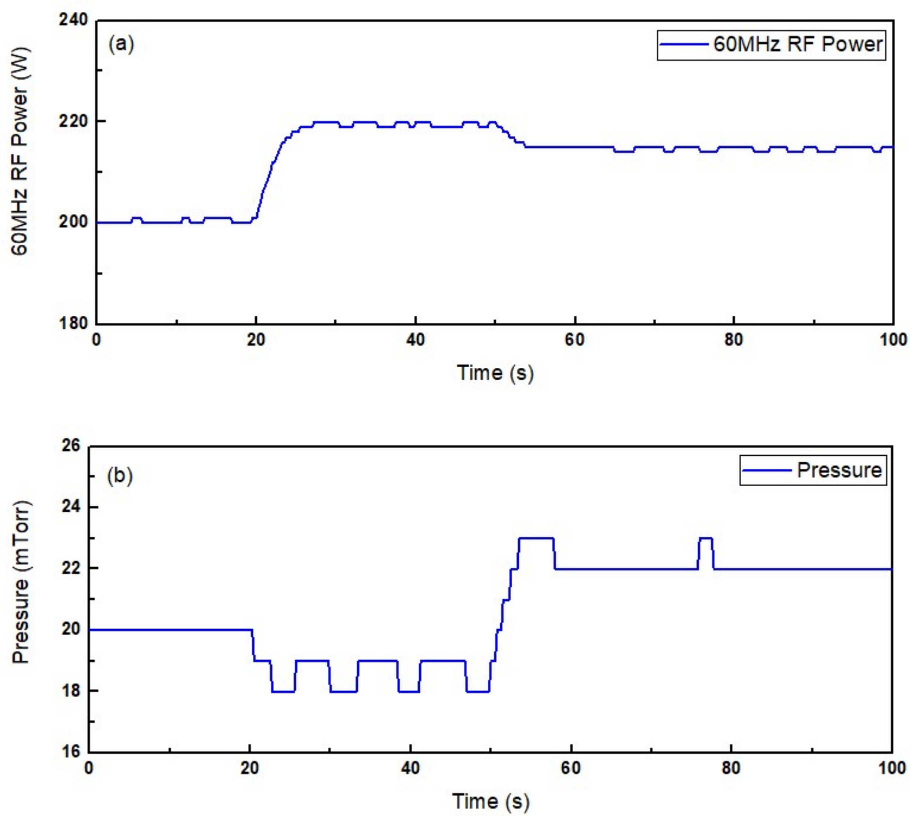

Figure 2-17 The movement of 60 MHz RF power (MV_1) and (b) pressure (MV_2) during the set-point tracking control experiment.

2.4. Concluding remarks

Through this research, a multi-loop controller which controls the electron density and electron temperature in Ar plasma condition. The plasma variables obtained as the CVs by the non-intrusive OES were firstly paired with the instrumental variables as the MVs through SVA and RGA techniques. As a prerequisite of the variable selection and pairing techniques, PRBS tests of all MVs were conducted. Consequently, the best pairing was the electron density – 60 MHz RF power and the electron temperature – pressure. The two SISO systems were then successfully controlled under disturbance rejection tests so that the controllability of each system was demonstrated. However, it was observed that interaction effects between the CVs and MVs which may cause unwanted outcomes still existed. Then, MIMO control simulations were conducted through Simulink®. The two parallel PID controllers were designed based on the 2×2 first order transfer function models and the offline tuning with set-point tracking control simulations. With these controllers, set-point tracking tests that demonstrate the exist of interactions were conducted. The effectiveness of decoupler controllers on plasma variable control was proven by sequential set-point tracking control simulations. As it conducts the reduction of the interaction as well as the set-point tracking control of the both set-points of CVs simultaneously, it demonstrated that the proposed controller shows the better performance than the SISO controller and the MIMO controller without decouplers. Finally, the designed controller was adjusted to be applied to our plasma etching reactor and then was verified its effectiveness by using a set-point tracking control experiment. From these results, it is

concluded that in highly interactive plasma variable control processes, additional modules to compensate interaction should be required even under optimum pairing techniques. Therefore, from this chapter, the possibility of MIMO control of plasma-based system is demonstrated. From the next chapter, more advanced control research will be continued under more realistic plasma conditions in semiconductor manufacturing.

CHAPTER 3. Disturbance Rejection Control of Plasma Electron Density by Model Predictive Controller†

3.1. Introduction

Model predictive control (MPC), one of the most popular control algorithm in recent years, was employed in the defence and petroleum industries for the first time in the 1970s. The typical advantages of MPC is that the interaction between input, output, disturbance variables is able to be captured by the process model and the calculation of optimum set-points can be coordinated with the control calculation (Seborg et al., 2008). Unlike PID control, which only deals with the difference between the current output value and reference value, MPC estimates output states based on given models and calculates estimated output values according to the given conditions to release the optimal MVs. Although the meaningful control results using the PID controller in the previous chapter, there are obvious limitations in relation to the exquisiteness and MPC can overcome this. Therefore, MPC is chosen as the control method for plasma variable control in this chapter for a number of reasons: Since small errors can cause a large loss in the plasma etching process due to the nature of the process, the importance of the sophistication is more emphasized. However, in PID control scheme, some extent of error cannot be overcome due to the

---

†This chapter cites the author's journal article: Koo, J., Park, D., Ryu, S., Kim, G.-H. & Han, C. (under review). Design of a Self-tuning Adaptive Model Predictive Controller using Recursive Model Parameter Estimation for Real-time Plasma Variable Control.

nature of the algorithm. Whereas optimized results are expected in MPC as it calculates the MVs by predicting future trends to a certain horizon range. In addition, MPC can be easily implemented to the system using a first order approximation and is already popularized in the industry level. Most importantly, decoupler controllers as well as PID controllers are highly dependent to the accuracy of the model so that even a very small model-plant mismatch (MPM) can cause a large error. However, in the case of the MPC, it can show its ability in a sensitive plasma-based system because it overcomes some MPM by estimating the output states of the future. Because these advantages are exactly consistent with the characteristics of the plasma-based system, it is essential to use MPC for plasma variable control.

The publication of Lynn et al. (2012) is the only case of attempting to control a plasma variable using MPC. They demonstrated the feasibility of real time virtual metrology (VM) and MPC scheme, especially predictive functional control (PFC), for the electron density and etch rate control. Although the results of these promising experiments demonstrates the merits of the VM and PFC, they overlooked the variety of the plasma-based system. In addition to the using of the hairpin probe, which is an invasive sensor that directly affects the system, there were limits of completing the control algorithm according to the system changes. During plasma etching processes, the chamber wall condition is changed. For example, the chemical composition of a Al_2O_3 chamber wall contains high concentrations of O, Si, and Cl+Br after $HBr/Cl_2/O2$ etching (Cunge et al., 2005). The changed chemical composition of a chamber wall easily affects to the performances of etch processes. Fukasawa et al. (2009)

described the variation of the etch rate depending on the polymer thickness on the chamber walls. They demonstrated that the etch rate performance varies by 30% in relation to the wall conditions. Kim and Aydil (2003) also presented the effects of a chamber wall condition on the etch rate. As such, the wall condition and etch profile are closely related and affect each other cyclically. Thus, as a plasma etching process proceeds, a plasma system continues to change. Therefore, the consideration of time-varying characteristics is indispensable.

In this chapter, an MPC design which considers the variety of plasma systems is conducted. As a disturbance model term is appropriately applied to the MPC algorithm considering drift of the system, the more flexible MPC allows the electron density control to be successfully performed. Moreover, an optimization method of MPC tuning parameters is also essential to maximize MPC abilities. In this work, the Bayesian optimization technique is used to determine the optimal tuning parameters of MPC. Then, disturbance rejection controls are performed through the well-tuned model predictive controller designed by considering all of the above. To simulate a disturbance situation, O_2 is injected to the pure Ar plasma system. The influence of oxygen in plasma etching reactor is described in Section 2.2.2.

The rest of this chapter is organized as follows. In Section 3.2 the concept of MPC and the state estimation algorithm along with the optimization algorithm which are generally used in MPC algorithm are described. Section 3.3 presents a design of model predictive controller for Ar plasma system. It contains system identification of the system and the tuning method of MPC weight parameters used ISE-based Bayesian optimization. Subsequently, the Ar plasma electron

density control simulation results and a control experiment result are shown that conducted the model predictive controller. Section 3.4 provides the results of disturbance rejection control with the disturbance model applied model predictive controller. Finally, Section 3.5 concludes this chapter.

3.2. Model predictive control

3.2.1. Concept of model predictive control

This section briefly describes the concept of MPC. Figure 3-1 shows a block diagram for MPC. The state estimator calculates $y(k+i|k)$, which is the $k+i^{th}$ output prediction calculated at k ($i=1,2,\dots,p$; p is the prediction horizon), using $y(k)$, which is the current measured output released from the process, and the optimal $\Delta u(k+i|k)$, which is the optimal $k+i^{th}$ input calculated at k. The predicted error, which is denoted as $e(k+i|k)$, can be obtained from the $y(k+i|k)$ and $y_{sp}(k+i)$, which is the set-point of the output. Subsequently, the optimizer calculates the optimal control action set for the next step, $\Delta u(k+1+i|k+1)$, utilizing the cost function, and the constraints, $e(k+i|k)$, and $e(k)$ where $e(k)$ denotes the current error. Actually, $\Delta u(k+i|k)$ from the optimizer has a property of $\Delta u(k+m-1|k)=\ \Delta u(k+m|k)=\cdots=\ \Delta u(k+p|k)$ for $j=1,2,\dots,m$ where m is the control horizon ($m<p$). From the set of MV adjustments, $\Delta u(k)$ is applied to the process and $\Delta u(k+i|k)$ is delivered to the state estimator for the calculation of the new output prediction. Thus, the objective of the MPC algorithm is to calculate a sequence of control actions which makes the predicted response going to the set-point in an optimal manner. (Seborg et al., 2008). A basic concept for MPC is illustrated in Figure 3-2.

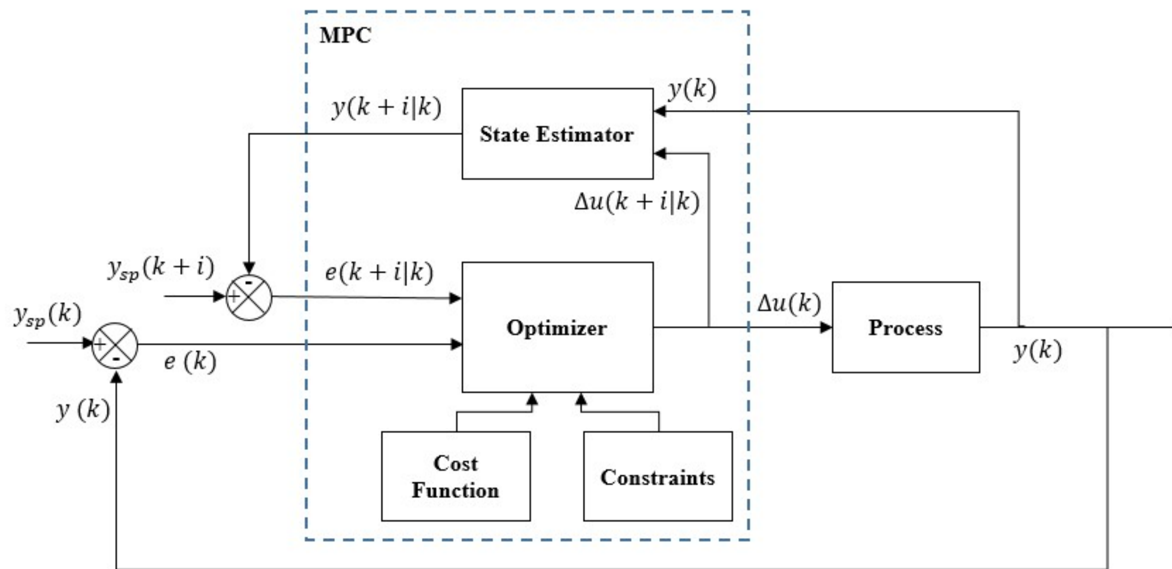

Figure 3-1 Block diagram of MPC.

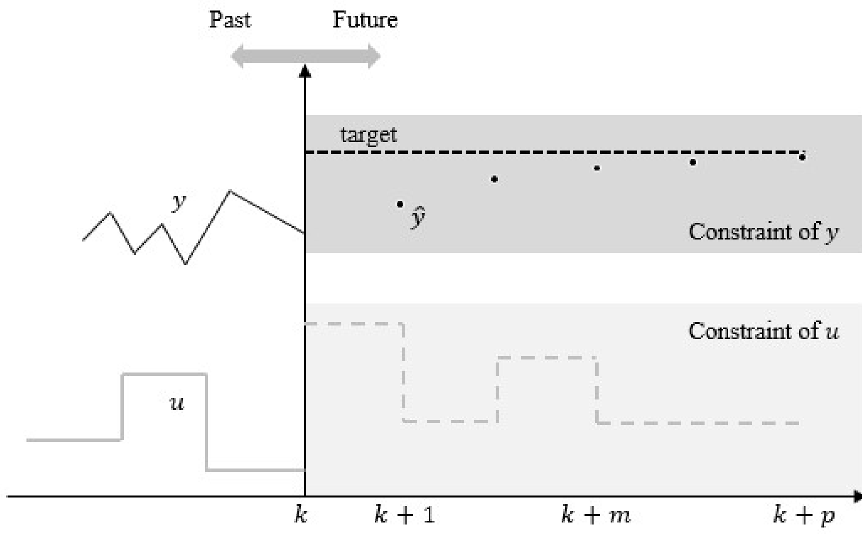

Figure 3-2 Basic concept of MPC.

3.2.2. Description of model predictive control algorithm

3.2.2.1. State estimation algorithm

MPC is fundamentally based on the state space model and uses a steady-state Kalman filter in general. The diagram of the MPC system is shown in Figure 3-3. The MPC system deals with 4 subsystem models which are plant model, input disturbance model, output disturbance model, and measurement noise model.

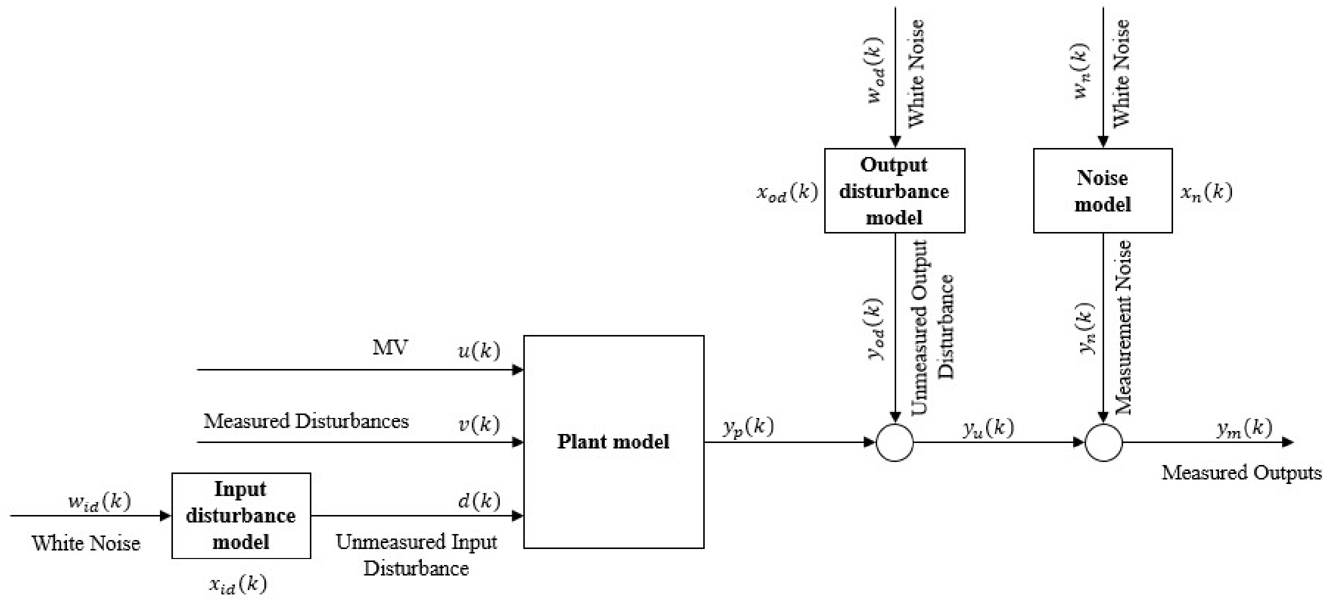

Figure 3-3 Diagram of MPC system based on state space models.

The controller uses its state $x(k)$, $x(k) = [x_p{}^T \ x_{id}{}^T \ x_{od}{}^T \ x_n{}^T]^T$, where each state represents each model. The length of each model state vector x_i is n_{xi} ($i = p$ or id or od or n). In addition, if a input variable, $u_0(k)$, is set as $[u^T(k) \ v^T(k) \ w_{id}{}^T(k) \ w_{od}{}^T(k) \ w_n{}^T(k)]^T$, the state space models are expressed as follows.

For the plant model,

$$\begin{aligned} x_p(k+1) &= A_p x_p(k) + [B_{pu} \ B_{pv} \ B_{pd}][u(k) \ v(k) \ d(k)]^T \\ y_p(k) &= C_p x_p(k) + [D_{pu} \ D_{pv} \ D_{pd}][u(k) \ v(k) \ d(k)]^T, \end{aligned} \quad \textbf{(3-1)}$$

for the input disturbance model,

$$\begin{aligned} x_{id}(k+1) &= A_{id} x_{id}(k) + B_{id} w_{id}(k) \\ y_{id}(k) &= C_{id} x_{id}(k) + D_{id} w_{id}(k), \end{aligned} \quad \textbf{(3-2)}$$

for the output disturbance model,

$$\begin{aligned} x_{od}(k+1) &= A_{od} x_{od}(k) + B_{od} w_{od}(k) \\ y_{od}(k) &= C_{od} x_{od}(k) + D_{od} w_{od}(k), \end{aligned} \quad \textbf{(3-3)}$$

and for the measurement noise model,

$$\begin{aligned} x_n(k+1) &= A_n x_n(k) + B_n w_n(k) \\ y_n(k) &= C_n x_n(k) + D_n w_n(k) \end{aligned} . \quad \textbf{(3-4)}$$

Therefore, the entire system state space model can be expressed as follows.

$$x(k+1) = \begin{bmatrix} A_p & B_{pd}C_{id} & 0 & 0 \\ 0 & A_{id} & 0 & 0 \\ 0 & 0 & A_{od} & 0 \\ 0 & 0 & 0 & A_n \end{bmatrix} x(k) + \begin{bmatrix} B_{pu} & B_{pv} & B_{pd}D_{id} & 0 & 0 \\ 0 & 0 & B_{id} & 0 & 0 \\ 0 & 0 & 0 & B_{od} & 0 \\ 0 & 0 & 0 & 0 & B_n \end{bmatrix} u_0(k) \quad \textbf{(3-5)}$$

$$y_m(k) = \begin{bmatrix} C_p & D_{pd}C_{id} & C_{od} & C_n \end{bmatrix} x(k) + \begin{bmatrix} 0 & D_{pv} & D_{pd}D_{id} & D_{od} & D_n \end{bmatrix} u_0(k).$$

where y_m is the measured output obtained by a measurement sensor, especially the OES in this thesis.

With this model structure, the parameters from the previous step calculation, and the current data, the state estimator determines the predicted states, $x(k+i|k)$, and the predicted outputs, $y(k+i|k)$ (for $i = 1, 2, \dots, p$). The detailed estimation algorithm is described below.

First of all, the estimator calculates the revised state estimate, x^{rev}, from the actual input value and the optimal input value, which are denoted as u^{act} and u^{opt}, from the previous step. Then it computes the innovation, $e(k)$:

$$x^{rev}(k|k-1) = x(k|k-1) + B_u[u^{act}(k-1) - u^{opt}(k-1)] \quad \textbf{(3-6)}$$

$$e(k) = y_m(k) - [C_m x^{rev}(k|k-1) + D_{mv}v(k)] \quad \textbf{(3-7)}$$

where B_u denotes $[B_{pu} \;\; 0 \;\; 0 \;\; 0]^T$, C_m denotes $\begin{bmatrix} C_p & D_{pd}C_{id} & C_{od} & C_n \end{bmatrix}$, and D_{mv} is equivalent to D_{pv}. Afterwards, the current state $x(k|k)$ and the one step predicted state $x(k+1|k)$ are updated as follows.

$$x(k|k) = x^{rev}(k|k-1) + Me(k) \quad \textbf{(3-8)}$$

$$x(k+1|k) = Ax^{rev}(k|k-1) + B_u u^{opt}(k) + B_v v(k) + Le(k) \quad \textbf{(3-9)}$$

where M and L are Kalman gains and B_v denotes $[B_{pv} \ 0 \ 0 \ 0]^T$. Here, $u^{opt}(k)$ is delivered from the optimizer that solve the quadratic program (QP) after $x(k|k)$ is obtained by Eq. (3-8). The detailed algorithm determining $u^{opt}(k)$ will be introduced in Section 3.2.2.2.

In the case of the output variable prediction, the estimator assumes that the white noise inputs, which are w_{id}, w_{od}, and w_n, are zero and the predicted plant outputs are noise-free. Thus, each $y(k+i|k)$ is obtained by as follows (for $i = 1, 2, \ldots, p$).

$$x(k+i|k) = \ Ax(k|k) + B_u u(k|k) + B_v v(k) \quad \textbf{(3-10)}$$

$$y(k+i|k) = Cx(k+i|k) + D_v v(k+i|k) \quad \textbf{(3-11)}$$

where D_v is equivalent to D_{pv}. As descripted in Section 3.2.1, the predicted output values obtained from Eq.(3-11) are used as critical parameters to solve the optimization problem of MPC (Ogunnaike & Ray, 1994; Seborg et al., 2008).

3.2.2.2. Optimization algorithm

In general, a solution of the control signal of MPC which is based on the quadratic criterion determines the adjustment of MVs until the next control interval. In this study, the following alternative cost function is used as the objective function $J(z_k)$ for the control signal which is expressed as follows.

$$J(z_k) = \sum_{i=1}^{p-1} [e_y{}^T(k+i)Qe_y(k+i) + \Delta u^T(k+i)R\Delta u(k+i)] \quad \textbf{(3-12)}$$

where k is the current control interval, p is the prediction horizon, e_y is the difference between reference value of plant output and the predicted value of plant output, Δu is the input movement, Q and R are positive-semi-definite weight matrices which should be tuned by engineers, and z_k is the QP decision which minimizes the objective function given as follows.

$$z_k{}^T = [\Delta u(k|k)^T \;\; \Delta u(k+1|k)^T \ldots \;\; \Delta u(k+m-1|k)^T \ldots \;\; \Delta u(k+p-1|k)^T] \quad \textbf{(3-13)}$$

where m is the control horizon and $\Delta u(k+i|k)$ is the $k+i^{\text{th}}$ adjustment of input calculated at k. After the control horizon, all $\Delta u(k+i|k)^T$ are constant. Therefore, $\Delta u(k+m-1|k)^T = \Delta u(k+m|k)^T = \cdots = \Delta u(k+p-1|k)^T$ as mentioned in Section 3.2.1.

During the optimization there should be set the inequality constraints of input and output variables in most cases. Typically, these constraints are configured through upper bounds and lower bounds as follows.

$$\Delta u^-(k) \le \Delta u(k+i|k) \le \Delta u^+(k) \quad \textbf{(3-14)}$$

$$y^-(k) \le y(k+i|k) \le y^+(k) \qquad i = 1,2,\dots,p \quad \textbf{(3-15)}$$

where $\Delta u^-(k)$ and $\Delta u^+(k)$ denotes the lower and upper bounds for the adjustments of the input variable and $y^-(k)$ and $y^+(k)$ denotes that of the output variable. However, the hard constraints of variables can cause the infeasible solutions. Qin and Badgwell (2003) proposed the constraint softening method by involving slack variables, ${s_i}^u$ and ${s_i}^y$. That is, the revised inequality constraints are (Qin & Badgwell, 2003; Seborg et al., 2008):

$$\Delta u^-(k) - {s_i}^u \le \Delta u(k+i|k) \le \Delta u^+(k) + {s_i}^u \quad \textbf{(3-16)}$$

$$y^-(k) - {s_i}^y \le y(k+i|k) \le y^+(k) + {s_i}^y. \quad \textbf{(3-17)}$$

Considering this soften inequality constraints, the output variable is predicted using the obtained z_k and the controller state estimates, enabling the calculation of the difference between the reference output and the predicted output, e_y, for the next time step. Subsequently, the QP decision for the next time step can be solved. Then the released $\Delta u(k+i|k+1)$ is delivered to the state estimator and the $\Delta u(k+1)$ signal is used for manipulating the relate instrument variables of the device (for $i = 2{:}\,p+1$).

3.3. Design of model predictive controller for Ar plasma system

3.3.1. System identification of Ar plasma system

As a prerequisite, PRBS test for 60 MHz power – electron density transfer function model was conducted. The reference values for the 60 MHz power, $\bar{u}$, is 300 W, and the electron density, $\bar{y}$, is $4.19 \times 10^{10}\ a.u.$ respectively. The obtained first order transfer function model is:

$$Y(s) = \frac{1.559 \times 10^7}{1 + 0.01810s} U(s) \times e^{-0.1392s} \quad \textbf{(3-18)}$$

where $Y(s)$ and $U(s)$ are output and input variables in Laplace domain, respectively. That is, the plant model gain, K_p, is $1.559 \times 10^7\ a.u./\mathrm{W}$, the time constant, τ, is 0.018 s, the time delay, t_d, is 0.1392 s. Then, for the controller tuning in the discrete time domain, the continuous model was discretized and was expressed as follows.

$$y(z) = \frac{7.005 \times 10^6 z + 7.601 \times 10^6}{z - 0.06317} u(z) \times z^{-3}. \quad \textbf{(3-19)}$$

Also, when a system model is used for model predictive controller, the controller needs a model in the form of a state space structure so that the identification for a state space model was conducted. All input and output variables from now on are preprocessed data obtained by scaling the deviation variables, $x_m - \bar{x}$ $(x \in \{u, y\})$. The scale factor of y, which is denoted as y^*, is $2.3 \times 10^9\ a.u.$ and the scale factor of u, which is denoted as u^*, is set to be 10 W. The scale factor of u has only a scaling effect and does not have any numerical meanings. Thus, u and y denote:

$$u = \frac{u_m - \bar{u}}{u^*}$$

$$y = \frac{y_m - \bar{y}}{y^*} \quad \textbf{(3-20)}$$

from now on. The details of scaling method will be described in Sections 4.2.2 and 4.4.1. From the system identification, the plant model in the state space structure is expressed as follows.

$$x_p(k+1) = \begin{bmatrix} 0.06317 & 0 & 0 & 0 \\ 1 & 0 & 0 & 0 \\ 0 & 1 & 0 & 0 \\ 0 & 0 & 1 & 0 \end{bmatrix} x_p(k) + \begin{bmatrix} 10 \\ 0 \\ 0 \\ 0 \end{bmatrix} u(k) \quad \textbf{(3-21)}$$

$$y_p(k) = [0 \;\; 0 \;\; 0.003046 \;\; 0.003305] x_p(k) + [0] u(k).$$

3.3.2. Optimal MPC weight parameters from integral squared error based Bayesian optimization

Based on the plant model previously identified, an offline tuning of a model predictive controller was performed. As described in Section 3.2.2.2, the ability of a model predictive controller is ultimately determined by the weight parameters tuning, Q and R. There are many proposed ways of tuning methods, however, in this thesis, Bayesian optimization which is one of the most popular optimization methods in recent is used for the thorough tuning. In this section, a brief introduction to the concept of Bayesian optimization is described below with Figure 3-4 and is followed by the application of the optimization method to the model predictive controller.

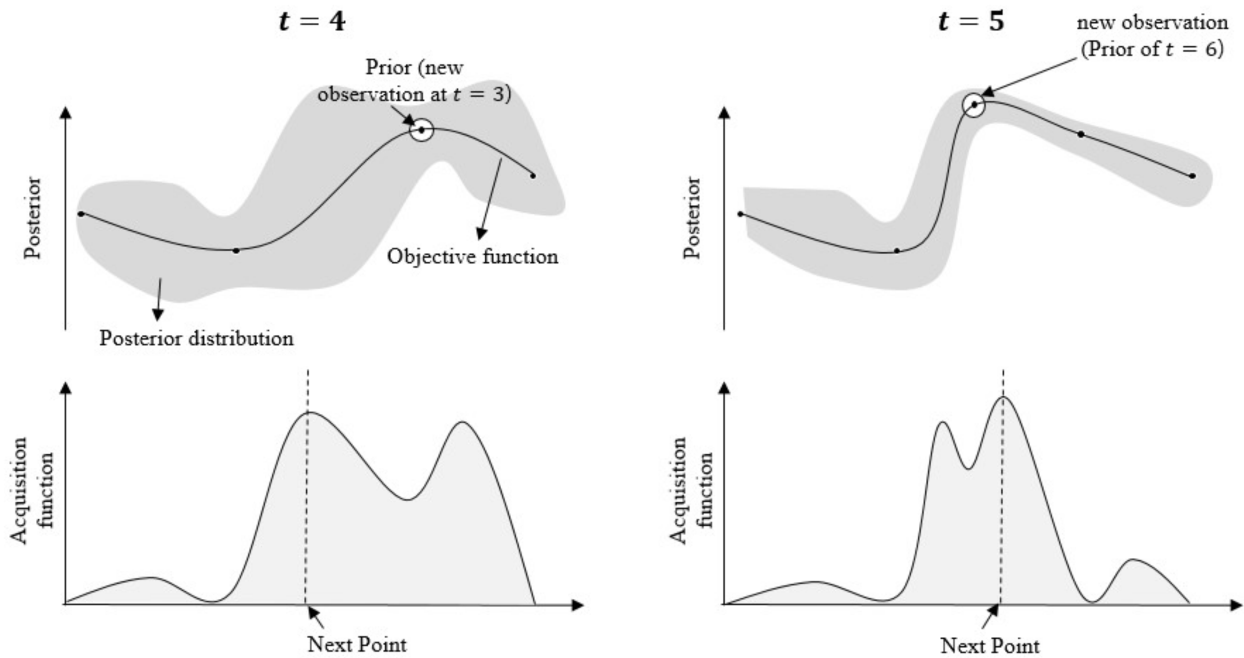

Figure 3-4 Concept of Bayesian optimization algorithm.

Bayesian optimization is a sequential analysis for global optimization of black-box functions. It treats the objective function as a random function and places a prior over it. In the top of the left side of Figure 3-4, the function evaluation at $t = 4$ is obtained from the prior which is the new observation at $t = 3$, and then a posterior distribution over the objective function is constructed. Subsequently, the posterior distribution constructs an acquisition function shown in the bottom of the left side of Figure 3-4. The acquisition function determines where the next query point should be. The new observation at $t = 4$ is ready for constructing the next posterior distribution by being the prior at $t = 5$ (Mockus, 2012; Močkus, 1975; Shahriari et al., 2016).

Utilizing the Bayesian optimization method, the optimal Q and R can be calculated with the constraints of $0 \leq Q \leq 0.1$ and $0.9 \leq R \leq 1$ for the feasible optimization. The upper and lower limits are dependent to the scale of errors of CVs and that of adjustments of MVs as shown in the objective function in Eq. (3-2). With the constraints a model predictive controller was applied to the developed system model in order to conduct an offline tuning. A random number set-point of the electron density is inserted on the controller, then, the Bayesian optimization of 100 trial for the optimal Q and R was performed where the objective function is integral squared error (ISE) of the CV. Therefore, the objective function can be expressed as:

$$[Q \;\; R]^* = \underset{\substack{0 \leq Q \leq 0.1 \\ 0.9 \leq R \leq 1}}{\operatorname{argmin}} f(Q, R) \tag{3-22}$$

where the $f(Q, R)$ is the ISE function given as:

$$f(Q,R) = \int (y_{sp}(t) - y(Q,R,t))^2 dt. \tag{3-23}$$

For the discrete time domain, $f(Q,R)$ is expressed as:

$$f(Q,R) = \sum (y_{sp}(k) - y(Q,R,k))^2. \tag{3-24}$$

With the constraint of MV being between -30 and 30 and the constraint of MV rate being between -1 and 1, the obtained $[Q \;\; R]^*$ is [0.0322 0.9882]. The model predictive controller designed with these weight parameters will conduct electron density control simulations and an experiment from the next section.

3.3.3. Experimental results of Ar plasma electron density control

Based on the system modelling in Section 3.3.1 and the tuning of the model predictive controller in Section 3.3.2, a set-point tracking test of Ar plasma electron density was conducted. The experimental sample time is 50 ms and the starting reference condition is 300 W of 60 MHz RF power, 20 mT of pressure, and 500 sccm of Ar flowrate. Figure 3-5 shows the performance of the tuned controller. As demonstrated by this control result, the model predictive controller effectively performs the set-point tracking control in a situation where the drift is not significant. That is, the initial system and model of it are not significantly different during the control operation. However, such a negligible mismatch between the system and model is possible only in an ideal situation and is difficult to realize in an actual industrial unit. In the following section, the performance of this ideally tuned model predictive controller will be shown in the simulations wherein time-varying systems are assumed.

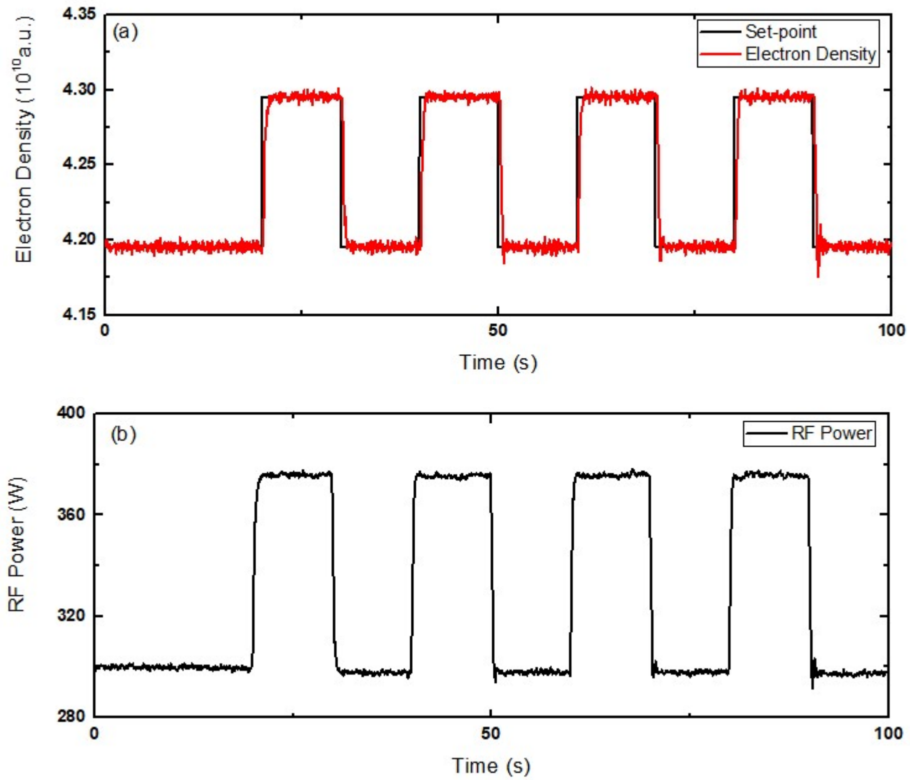

Figure 3-5 Result of set-point tracking control of a drift-free Ar plasma system conducted by the Model predictive controller. (a) The CV, which is the electron density, tracks the set-point of it when (b) the MV, which is the RF power, changes to achieve the control.

3.4. Disturbance rejection control using model predictive controller

3.4.1. Development of time-varying system model for control simulation

Even though the Ar plasma electron density was well controlled through the thoroughly tuned model predictive controller as shown in the previous section, this is only the control case in the situation that is very ideal and has gaps with reality. In actual plasma processing systems, the wall condition and etch profile affect each other cyclically as mentioned in Section 3.1. Therefore, the plasma-based systems are very variant and it should not be ignored. In this section, considering system drift which is the most frequent disturbance in plasma-based systems, a time-varying system model is developed by Simulink®.

The main concept of the development is that a system gain drift and offset drift which are the most frequent drifts are applied to the existing transfer function system model. A block diagram of the time-varying system model is shown in Figure 3-6. The system gain is multiplied by the system gain drift parameter, GD, for every sample time. It can represent the effect of O_2 plasma components that affect a pure Ar plasma system. In addition, the offset drift is simulated by adding the offset drift parameter, OD, to the output variable for every sample time. The OD is a parameter reflecting that the measurement of the output variable is shifted in one direction with time. This is largely caused by the OES measurement error with the long exposure time.

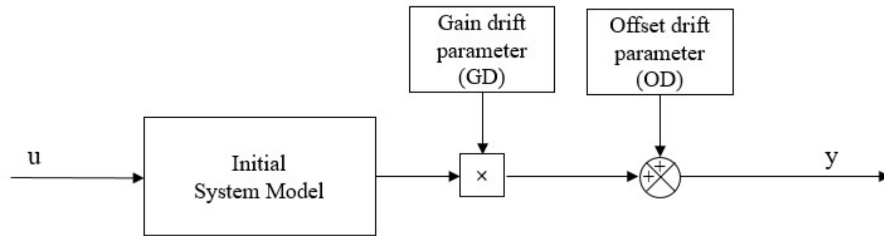

Figure 3-6 Block diagram of time-varying system model affected by the system gain drift and the offset drift.

In Figure 3-7, the offset drift effect as a result of long time exposure (about 40 min) of the OES is proven. At about 1250 s, a disturbance was injected. Although any disturbance affects to the system within 1250 s, the two plasma variables are drifted gradually. Similarly, in the latter part, the variables also do not maintain the steadiness.

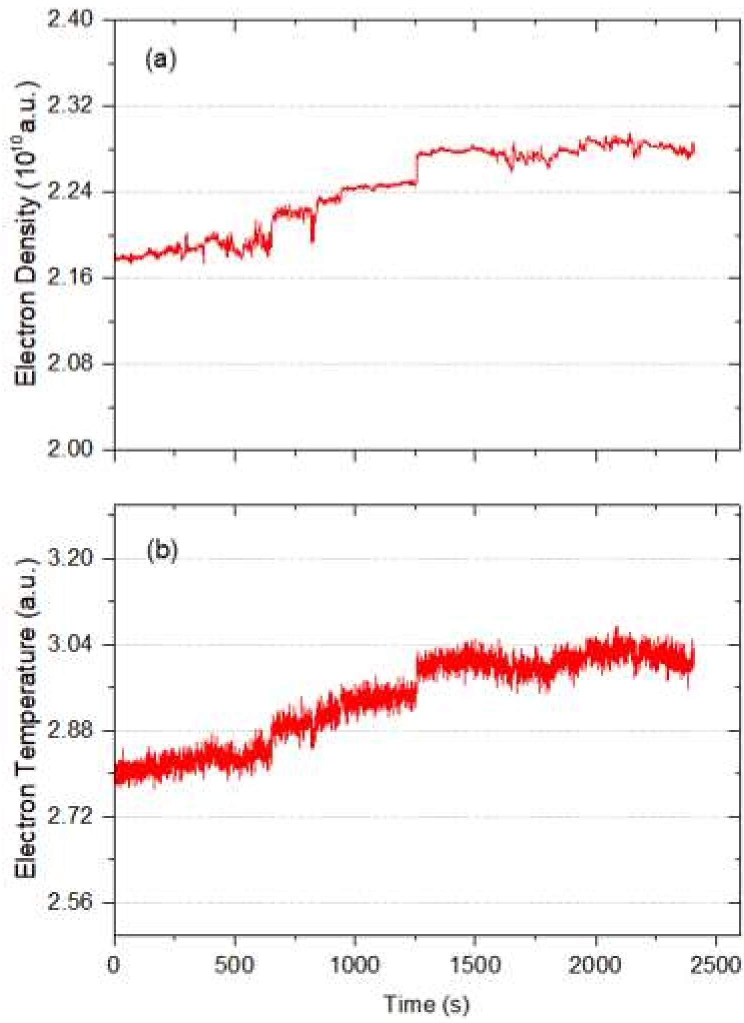

Figure 3-7 Offset drift effect as a result of long time exposure of OES (about 40 min.).

The setting of the GD and OD can vary in accordance with processes and situations by engineers. Thus, the appropriate values of them can be helpful for tuning of a model predictive controller.

3.4.2. Design of model predictive controller for disturbance rejection control

For disturbance rejection control, the previously designed model predictive controller is revised by setting the output disturbance model and noise disturbance model which are suitable for the plasma-based system as described in Section 3.2.2.1. The output disturbance model $\mathcal{M}_{od}$ and noise disturbance model $\mathcal{M}_n$ were set by regarding them as a ramp function and a white Gaussian, respectively. The output disturbance model is considered a ramp function because the most representative form of disturbances in plasma-based systems is the steady system drift, which appears even in the stable plasma state as mentioned in the previous section. The noise disturbance can be set as white Gaussian, the value of which can be obtained from the OES measurement noise. The disturbance models in discrete form can be expressed as follows.

$$\mathcal{M}_{od} = \frac{2.174}{z-1}$$
$$\mathcal{M}_n = 4.348. \tag{3-25}$$

Disturbance rejection control in time-varying system models was then simulated by applying two types of drift, the GD and OD.

In Figure 3-8, the control result is described in the situation where the system gain increases with no offset drift. The sample time of simulations is 50 ms. In this case, the GD is set to be 1.015/s and the OD is 0. As shown in Figure 3-8, as the system gain increases, a lower value of the MV is required for a certain CV. From the control simulation result, shown in Figure 3-8(a), the model predictive controller no longer shows the excellent performance as

described in Section 3.3.3. This is because the incorrect output estimation due to the MPM in the latter part of the simulation hinders the model predictive controller from releasing the appropriate optimal signals. In the early stage, the tuning parameters of the model predictive controller are the appropriate values for the system, however, in the latter stage, the electron density is controlled as if the MPC weight parameters are tuned aggressively.

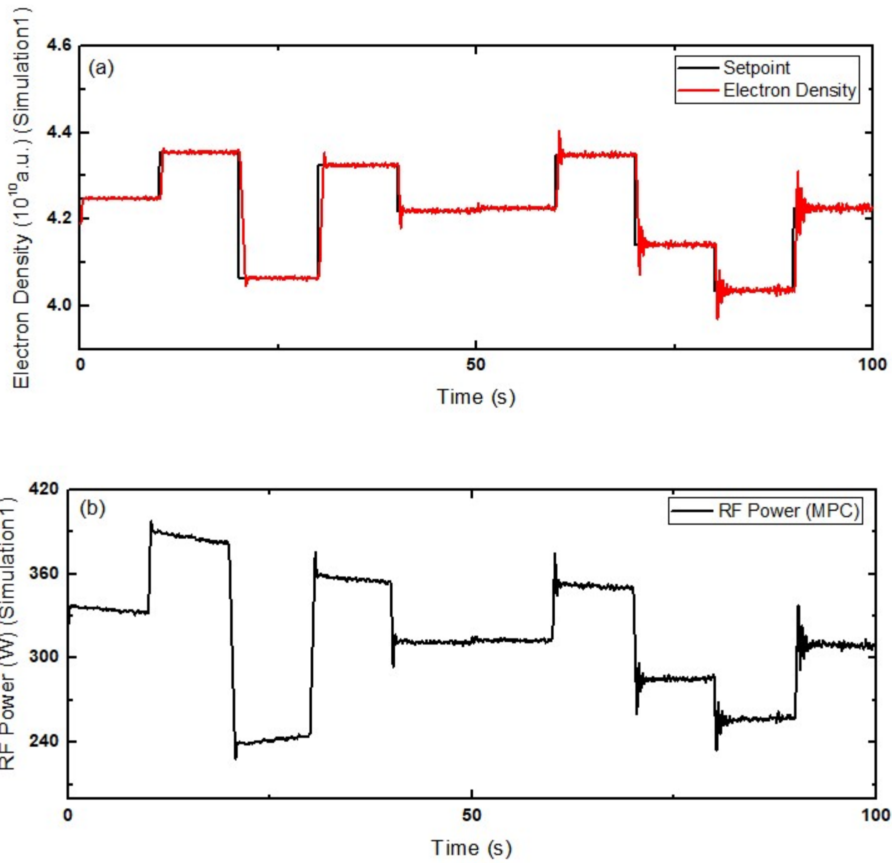

Figure 3-8 Simulation results of set-point tracking control of a gain increasing system conducted by the model predictive controller. (a) The CV, which is the electron density, tracks the set-point of it when (b) the MV, which is the RF power, changes to achieve the control.

Similarly, Figure 3-9 shows the control simulation result when the system gain decreases with no offset drift. The GD is 0.992/s and the OD is 0. It shows the opposite result with respect to the previous case. The model predictive controller operates robustly with the change in the system.

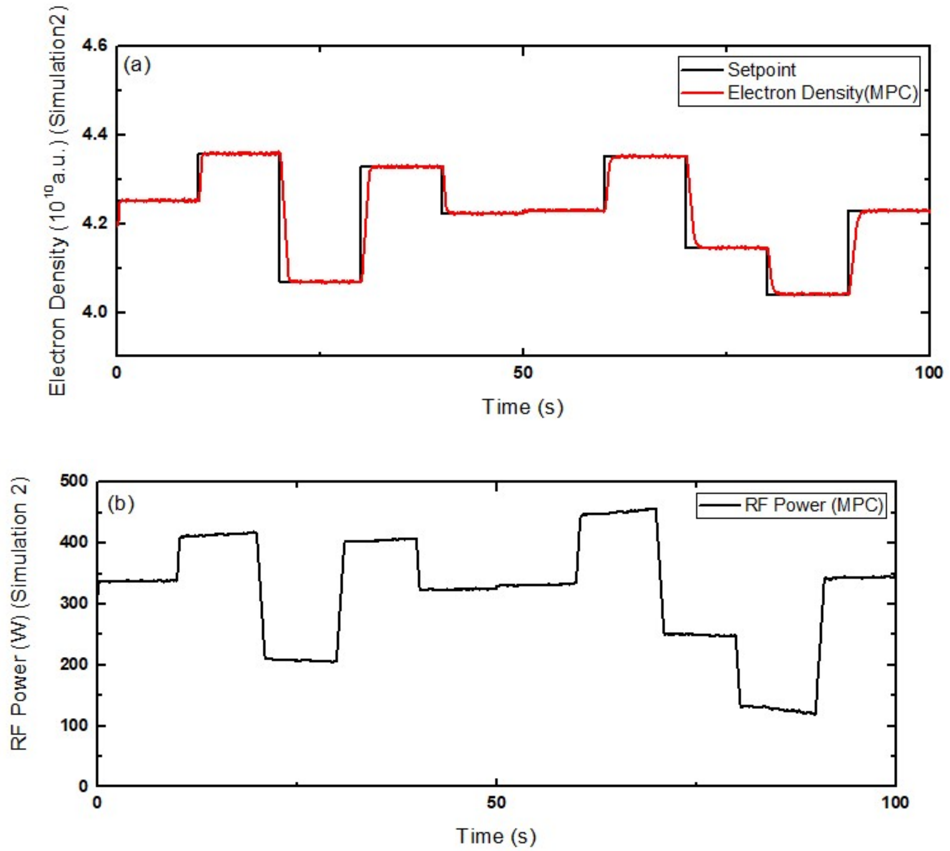

Figure 3-9 Simulation results of set-point tracking control of a gain decreasing system conducted by the model predictive controller. (a) The CV, which is the electron density, tracks the set-point of it when (b) the MV, which is the RF power, changes to achieve the control.

To observe the effect of the offset drift, a simulation was conducted in the absence of the system gain drift, the result of which is shown in Figure 3-10. The GD is 0 and the OD is -2×10^7 $a.u.$/s. In this case, although the CV is measured to be lower with the passage of time, the performance of the model predictive controller does not deteriorate until the end. The offset drift is observed with the increase in the MV, as shown in Figure 3-10(b). It demonstrates that when the system is unchanged with no system gain drift, the well-tuned model predictive controller can overcome the continuous offset drift. It seems that the good performance is maintained because the accuracy of the state estimation is improved by setting the appropriate output disturbance model.

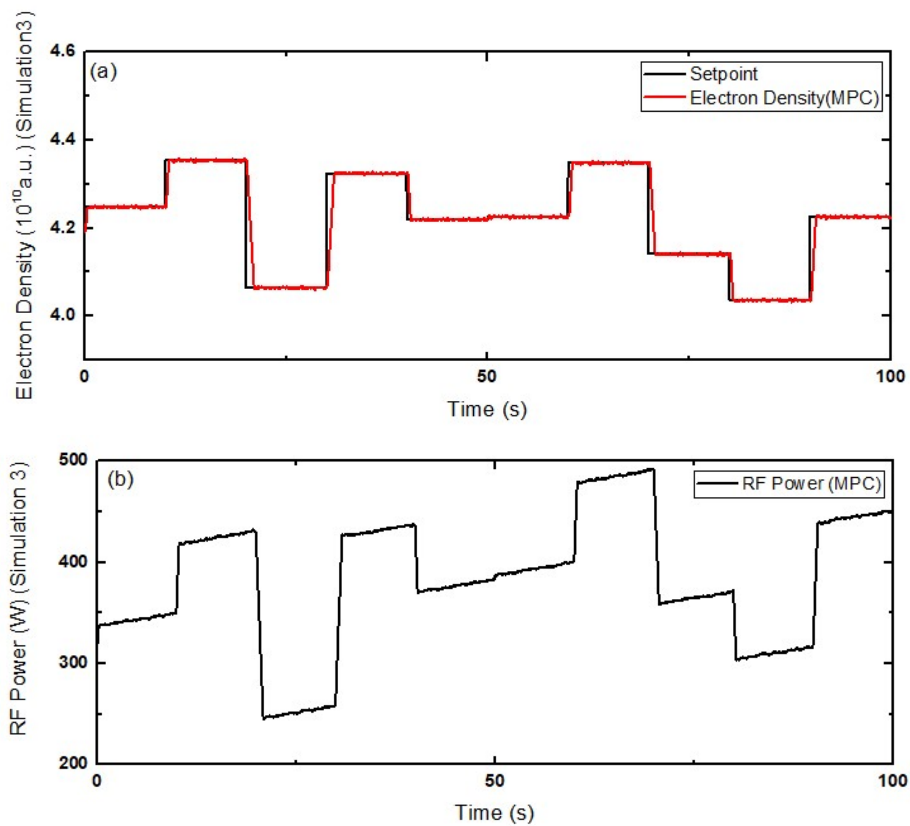

Figure 3-10 Simulation results of set-point tracking control of an offset drift system conducted by the model predictive controller. (a) The CV, which is the electron density, tracks the set-point of it when (b) the MV, which is the RF power, changes to achieve the control.

Figure 3-11 shows the simulation result for the case wherein the two types of drifts exist. The GD is 1.012/s and the OD is -8×10^6 $a.u.$/s. For the case wherein the increase in the system gain and the decrease in the offset drift occur simultaneously, though the model predictive controller can overcome the disturbance caused by offset drift, it shows poor performance due to the system gain drift at the end.

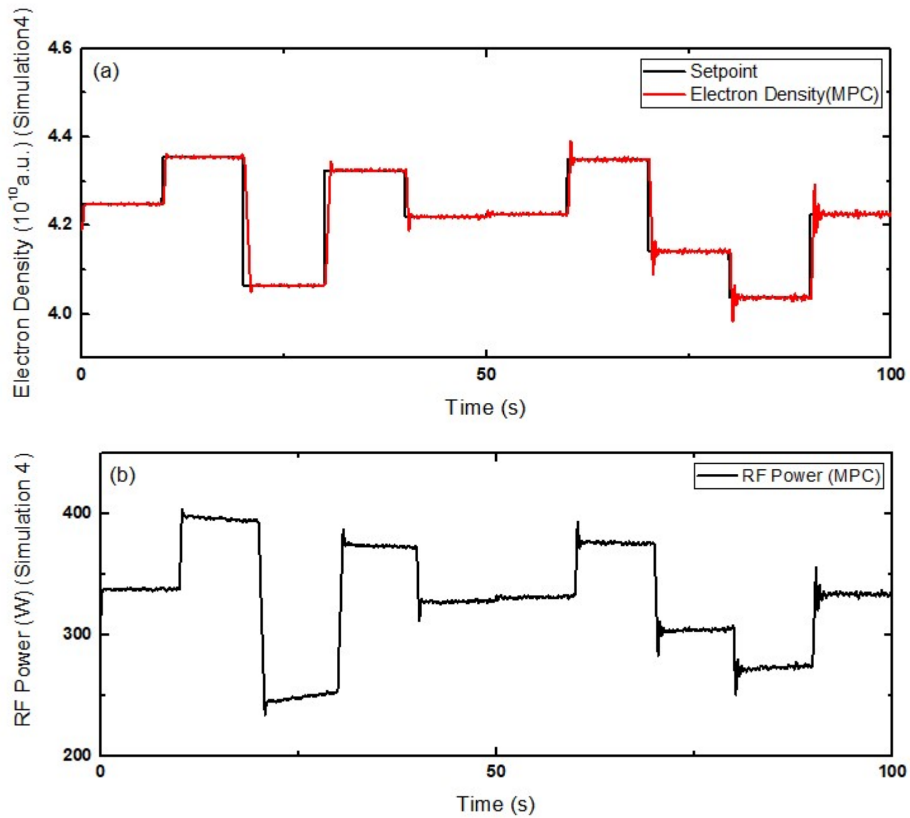

Figure 3-11 Simulation results of set-point tracking control of a gain increasing system with an offset drift conducted by the model predictive controller. (a) The CV, which is the electron density, tracks the set-point of it when (b) the MV, which is the RF power, changes to achieve the control.

These simulation results demonstrate that the model predictive controller shows its limits on the control in time-varying systems especially in system gain changing cases, even though the MPC tuning has been thoroughly performed to estimate the controller state accurately. In the next section, the performance of the model predictive controller will be shown where O_2 is injected into a pure Ar plasma system continuously as a disturbance. The result will be compared to the simulation results described in this section.

3.4.3. Experimental result of disturbance rejection control in Ar/O_2 plasma system

With the model predictive controller described in the previous section, a random set-point tracking control experiment was conducted where a disturbance was artificially applied. The experimental starting condition is equivalent to that of Section 3.3.3. The experimental sample time is 50 ms and the starting reference condition is 300 W of 60 MHz RF power, 20 mT of pressure, and 500 sccm of Ar flowrate. In addition, the disturbance was made by injecting O_2 continuously at 1 sccm/s. When O_2 is injected, the amount of the electron density is gradually increased. In addition, the system itself is changed from a pure Ar plasma system to an Ar/O_2 plasma system. Therefore, both types of drift described in the previous section occur.

As illustrated in Figure 3-12(a), the model predictive controller shows the great performance in the early stage when drift is not yet severe (before 50s). However, it shows the poor performance in the latter stage due to the MPM induced by the enough drift effect. The model predictive controller operates aggressively toward the latter half. Therefore, it is demonstrated that when O_2 plasma is continuously injected to the Ar plasma, an increase in the system gain is observed, which corresponds to the first simulation shown in the previous section. The gradual increase of RF power, as shown in Figure 3-12(b), indicates the presence of the significant offset drift at the same time, which is similar to the simulation 3. This offset drift does not seem to have a significant effect on the model predictive controller performance, as demonstrated in the previous section. Overall, the continuous injection of O_2 plasma to the pure Ar

plasma system results in a time-varying system wherein the system gain drift and offset drift occur simultaneously similar to simulation 4, though the amounts of drift are not exactly equal to that in the simulation.

According to the experimental results, there are limits even with the well-tuned model predictive controller to control the plasma variable in time-varying Ar/O_2 plasma system. Therefore, a more advanced control technique is required.

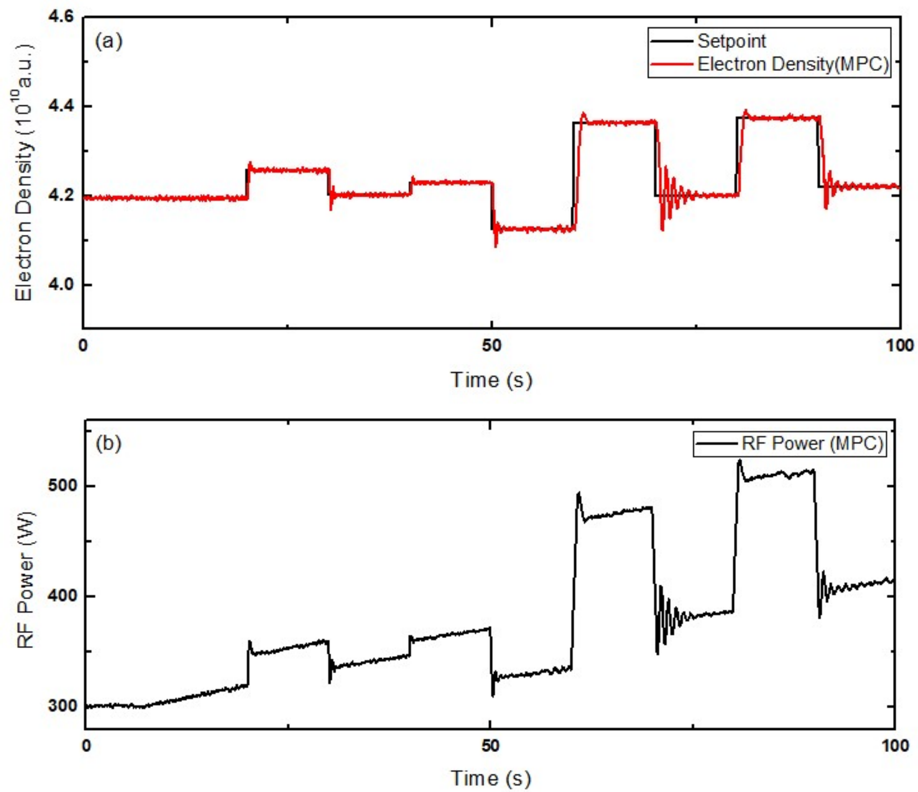

Figure 3-12 Experiment result of set-point tracking control of an Ar/O_2 plasma system with an artificial drift induced by O_2 plasma, conducted by the model predictive controller. (a) The CV, which is the electron density, tracks the set-point of it when (b) the MV, which is the RF power, changes to achieve the control.

3.5. Concluding remarks

In this chapter, a design of a model predictive controller which conducts electron density control and its performance were described. At first, the basic concept of MPC and the optimization algorithm of it were explained. Then, the controller design for a pure Ar plasma system was conducted. The plant model for the MPC was obtained by the approximation through a PRBS test. Subsequently, ISE-based Bayesian optimization technique was used for MPC weight parameters tuning. The performance of it was verified by conducting a set-point tracking test on the electron density of pure Ar plasma without drift. However, such a small MPM case is possible only in an ideal situation and is difficult to realize in an actual industrial unit. Therefore, in the model predictive controller, the output disturbance model was set in relation to the system gain drift and offset drift, which are the most typical drift in plasma-based systems. The noise disturbance model was also set as white Gaussian which can be driven from OES measurement noise. However, although the thorough tuning was conducted, control simulations in the presence of disturbance revealed limitations of the controller. Four simulations were performed wherein the two types of drift were applied to the system model. The simulation results showed that the controller can work well for a disturbed case, but obviously showed its limits in the other cases. Actually, it was confirmed by an electron density control experiment in a time-varying Ar/O_2 plasma system. When O_2 is injected continuously into the pure Ar plasma system as a disturbance, the control performance obviously deteriorated in the latter part of the experiment.

Therefore, applying more advanced control techniques is indispensable and will be covered in the next chapter.

CHAPTER 4. Design of Adaptive Model Predictive Controller for Plasma Etching Reactor[‡]

4.1. Introduction

As demonstrated in CHAPTER 3, The MPC with an output disturbance model overcomes the offset drift but cannot solve the problem that the system itself changes like the system gain drift. However, time-varying system problems frequently occur in actual processes dealing with plasma, and severe MPMs occur within a batch and/or between batches. Therefore, a control strategy based on a stationary model has its limitations, a problem which can be effectively solved by an adaptive control scheme.

A standard diagram of adaptive control methods is illustrated in Figure 4-1. Once the input and output data, u and y, are entered into the adjustment mechanism part, the adjustment mechanism decides the new controller parameters and delivers it to the controller. The type of the updated controller parameters is determined according to the adaptive control algorithm which an engineer uses. As an example, when the model parameter estimation is used as an adaptive control algorithm, the type of the updated controller parameters is

[‡]This chapter cites the author's journal article: Koo, J., Park, D., Ryu, S., Kim, G.-H. & Han, C. (under review). Design of a Self-tuning Adaptive Model Predictive Controller using Recursive Model Parameter Estimation for Real-time Plasma Variable Control.

the model parameter vector. Based on the updated controller parameters, the controller is adjusted then the new values of manipulated variables are released from the revised controller. Adaptive control is classified into three major methods: scheduled adaptive control, model reference adaptive control, and self-tuning adaptive control. In the scheduled adaptive control, which is the most basic form of the adaptive control scheme, the remedies are preprogrammed in anticipation of all possible situations. Thus, it takes advantage of prior knowledge and performs process control adaptively, depending on the situation encountered by the system. This method is effective when an engineer has complete prior knowledge and anticipation of the entire process. However, when this is not the case, self-adaptive schemes that employ a learning mechanism should be used. The model reference adaptive control, which is one of the self-adaptive schemes, uses a constant reference model. Here, the reference model output and the actual process output are compared, and the controller parameters are adjusted accordingly. However, as this technique uses a fixed model, if the difference between the model and the actual system becomes significant, it would be difficult to realize the control. The other self-adaptive method, which is the self-tuning adaptive control, is a technique that estimates the model parameters based on the process inputs and outputs and then applies them to the controller in real time. Although this method is more challenging than the others (as it allows the most freedom to the controller causing potential instability), it is best suited for processes

wherein unexpected situations occur frequently or when a system is time-varying (Ogunnaike & Ray, 1994).

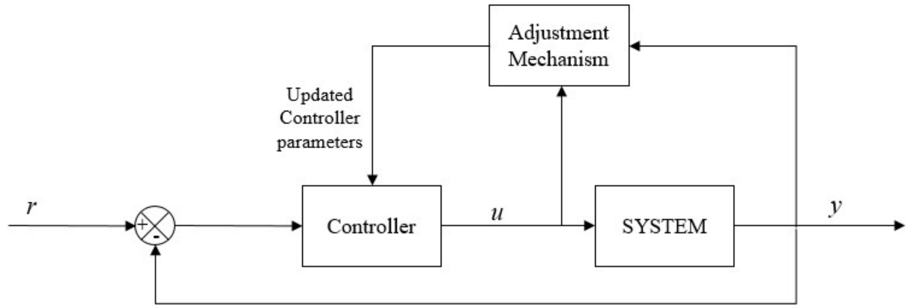

Figure 4-1 Standard block diagram of adaptive control methods.

In some conventional chemical processes, the adaptive control schemes have been employed based on MPC. Most studies have focused on tuning MPC weights or adjusting state observers adaptively. Kothare et al. (1997) and Lakshmanan and Arkun (2010) proposed scheduled adaptive MPC (AMPC) strategies by combining a linear parameter varying method with an model predictive controller as early AMPC schemes. Al-Ghazzawi et al. (2001) presented a self-tuning strategy based on the linear approximation between predicted outputs and MPC tuning parameters. In their study, sensitivity of closed-loop responses to the MPC tuning parameters was used for online tuning. Waschl et al. (2011) proposed an automatic tuning of the state observer through combining an adaptive estimation method with multi-model, and also proposed a tuning of MPC weights by applying an additional optimization loop to the MPC algorithm. A few studies have realized self-tuning AMPC by adaptively applying the updated model parameters to the model predictive controller. Tsai et al. (2003) and Chalupa (2009) reported excellent process control results on an oil-cooling machine system and a pendulum system, respectively, using model predictive controllers combined with online system identification. Fukushima et al. (2007) proposed a new parameter estimation algorithm that can be used to predict the error over the prediction horizon for a robust MPC method based on a comparison model. As demonstrated in the above research, AMPC studies have contributed to the development of self-adaptive control. However, previous studies presented their results at the simulation stage or defined the meaning of real-time conservatively as batch-to-batch or run-to-run.

Moreover, there is no successful application of AMPC to a plasma-based system. In fact, no attempts have been made to apply any adaptive control methods to such systems.

In summary, as a plasma-based system is very sensitive and time-varying, it requires flexible handling in the event of any disturbances. This requires an adaptive control structure for a real-time control. This chapter proposes an AMPC method for the electron density of Ar plasma in the CCP chamber, measured using the OES. The thoroughly tuned model predictive controller from the previous chapter will be combined with a recursive model parameter estimator, wherein the estimated model parameters are updated in real time at the sample time level through a recursive least squares (RLS) algorithm.

The outline of this chapter is as follows. Section 4.2 introduces the two typical recursive model parameter estimations. One is the recursive least squares algorithm using forgetting factor and the other is that using Kalman filter interpretation. In Section 4.3, the adaptive model predictive control algorithm which is formed by an MPC algorithm combined with the recursive least squares algorithm. Finally, Section 4.4 describes a scaling method and an adaptive model predictive controller design process. Subsequently, the results of Ar plasma electron density control simulations and experiment that compare the conventional model predictive controller designed in CHAPTER 3 and the adaptive model predictive controller designed in this chapter. Finally, Section 4.5 concludes this chapter.

4.2. Recursive model parameter estimation

One of the most popular online model parameter estimation algorithms is the recursive algorithm, which can be used to estimate the model parameters through the input and output measurements and the immediately preceding model parameter estimates. As such, the main advantage of the recursive algorithm is that it is computationally less burdensome, making it suitable for online and embedded applications. In this section, the most widely used recursive algorithm, i.e., the RLS algorithm, is described.

4.2.1. Recursive least squares algorithm with forgetting factor

The RLS algorithm is based on the concept of minimizing the difference between the plant output and the model output and can be expressed as follows.

$$\hat{\theta}(t) = \underset{\theta}{argmin} \sum_{k=1}^{t} \beta(t,k)[y(k) - \varphi^T(k)\theta]^2 \quad \textbf{(4-1)}$$

where θ is the model parameter vector, $\hat{\theta}(t)$ is the estimate of the model parameter at time *t*, $\varphi(k)$ is the regression vector at time k (i.e., $\varphi(k) = [-y(k-1) \ldots - y(k-n_a) \;\; u(k-1) \ldots u(k-n_b)]^T$ for the autoregressive exogenous (ARX) structure where n_a and n_b are the number of previous output and input terms respectively), and $\beta(t,k)$ is the weighting function. For more accuracy, the above equation is a weighted least-square criterion where the weighting function $\beta(t,k)$ has the following property:

$$\beta(t,k) = \lambda(t)\beta(t-1,k), \qquad 0 \le k \le t-1$$
$$\beta(t,t) = 1. \quad \textbf{(4-2)}$$

$\lambda(t)$ is the forgetting factor, and λ is determined as follows

$$\lambda = 1 - 1/T_0 \quad \textbf{(4-3)}$$

when the system remains approximately constant over T_0 samples. The value of λ is recommended to be in the range from 0.98 to 0.995 (Ljung, 1999). The following equations can be obtained by solving Eq. (4-1) analytically:

$$
\begin{aligned}
\hat{\theta}(t) &= \bar{R}^{-1}(t)f(t) \\
\bar{R}(t) &= \sum_{k=1}^{t} \beta(t,k)\varphi(t)\varphi^{T}(t) \\
f(t) &= \sum_{k=1}^{t} \beta(t,k)\varphi(t)y(t)
\end{aligned} \tag{4-4}
$$

From Eq. (4-4), the final recursive form of the parameter estimation with $P(t) = \bar{R}^{-1}(t)$, which is the parameter covariance matrix, can be seen as follows.

$$
\begin{aligned}
\hat{\theta}(t) &= \hat{\theta}(t-1) + K(t)\left[y(t) - \varphi^{T}(t)\hat{\theta}(t-1)\right] \\
K(t) &= P(t)\varphi(t) = \frac{P(t-1)\varphi(t)}{\lambda(t) + \varphi^{T}(t)P(t-1)\varphi(t)} \\
P(t) &= \frac{1}{\lambda(t)}\left[P(t-1) - \frac{P(t-1)\varphi(t)\varphi^{T}(t)P(t-1)}{\lambda(t) + \varphi^{T}(t)P(t-1)\varphi(t)}\right].
\end{aligned} \tag{4-5}
$$

To use the recursive algorithm, the value of $P(0)$ is required, which implies the confidence in the initial model parameter estimate, i.e., $\hat{\theta}(0)$. In this algorithm, λ is a design variable to be chosen by an engineer. Thus, the performance of the estimator can be determined accordingly. As the recommended value of λ is less than 1, as shown in Eq. (4-3), the weight of the old measurements is set lower than those of the newer ones. In other words, the lower the value of λ, the more susceptible the estimator becomes to parameter changes. On the other hand, the greater the value of λ, the less sensitive is the estimator (Söderström & Stoica, 1989). As shown in Eq. (4-5),

λ prevents $P(t)$ from taking a value of zero, which naturally prevents the value of $K(t)$ from tending to zero.

4.2.2. Recursive least squares algorithm with Kalman filter interpretation

Another common approach to estimating the model parameters underlying the Kalman filter interpretation is to take the model parameter as the state of the output. In other words,

$$\begin{aligned} \theta(t+1) &= \theta(t) + w(t) \\ y(t) &= \varphi^T(t)\theta(t) + v(t) \end{aligned} \quad \textbf{(4-6)}$$

where $w(t)$ and $v(t)$ are white Gaussians with $Ew(t)w^T(t) = R_1(t)$ and $Ev(t)v^T(t) = R_2(t)$. When calculated analogously as shown in the previous section, the recursive form of $\hat{\theta}(t)$ can be written as follows.

$$\begin{aligned} \hat{\theta}(t) &= \hat{\theta}(t-1) + K(t)\left[y(t) - \varphi^T(t)\hat{\theta}(t-1)\right] \\ K(t) &= P(t)\varphi(t) = \frac{P(t-1)\varphi(t)}{R_2(t) + \varphi^T(t)P(t-1)\varphi(t)} \\ P(t) &= P(t-1) - \frac{P(t-1)\varphi(t)\varphi^T(t)P(t-1)}{R_2(t) + \varphi^T(t)P(t-1)\varphi(t)} \\ &\quad + R_1(t). \end{aligned} \quad \textbf{(4-7)}$$

Unlike in the algorithm wherein the forgetting factor is used, the engineer must consider three parameters in this case: $P(0), R_1(t)$, and $R_2(t)$. As their relative values are important than their absolute values, the number of parameters to be considered can be reduced through a scaling method. The scaling method used in this thesis involves considering $R_2(t)$ as the reference parameter, which can be obtained from the estimated output and the real output. Thus, setting the scale factor of y such that $R_2(t)$ is equal to 1 allows the

engineer to consider only two parameters, namely the scaled values of $P(0)$ and $R_1(t)$.

Like the case of the RLS algorithm with the forgetting factor, this algorithm requires $P(0)$ value to be set. In this algorithm, $R_1(t)$, which is the process noise covariance matrix, is a design variable. As shown in Eq. (4-7), higher values of $R_1(t)$ result in more susceptible estimators with respect to parameter changes, whereas lower values of $R_1(t)$ result in less sensitive estimators. In other words, if $R_1(t)$ is too high, the fluctuation in the model parameter estimates increase because of the increase in the uncertainty of the estimation. On the other hand, if $R_1(t)$ is too low, the estimation of the model parameters is inconsistent with respect to any changes in the system. Similar to the effect of λ, $R_1(t)$ prevents $P(t)$ and $K(t)$ from having a value of zero.

The advantage of Kalman filter interpretation over the forgetting factor case is that an engineer can set the time variations for each model parameter (Ljung, 1999). Therefore, if the number of model parameters is greater than 1, the RLS algorithm with the Kalman filter interpretation shows better accuracy compared to the case wherein the forgetting factor is used. This advantage has a significant effect on discrete systems wherein the time delay is considered. In a time-delayed discrete system, there are model parameters that must be fixed to 0 because of the time delay. In this case, if the model parameters are not separately estimated, the parameters due to the time delay cannot be maintained at zero. However, a plasma etching reactor causes time-delay due to several factors such as a delay from a matcher. These factors must be considered in a

plasma system in order to improve the sophistication of control. Therefore, the model parameter estimator equipped with the RLS algorithm with Kalman filter interpretation is very suitable for the plasma etching reactor. Consequently, the controller with the model parameter estimator can show higher performance in plasma etching processes. In this work, the RLS algorithm with Kalman filter interpretation is chosen for the model parameter estimation.

4.3. Adaptive model predictive control algorithm

An adaptive model predictive controller can be obtained by combining the model predictive controller with the recursive model parameter estimator introduced in the previous sections, as shown in Figure 4-2.

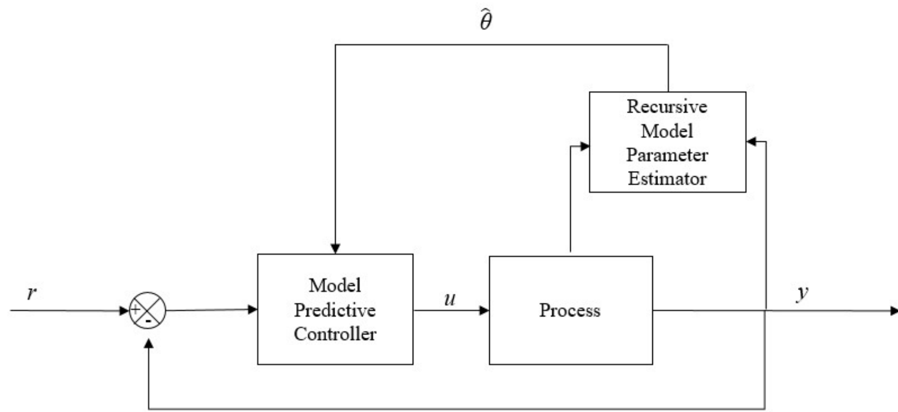

Figure 4-2 Block diagram of adaptive model predictive control.

To realize the combined structure, the following algorithm is proposed.

Step 1: Identify the initial system model parameters and define $P(0)$ and $R_1(0)$.

Step 2: Measure the input and output variables, $u^{act}(k-1)$ and $y_m(k)$.

Step 3: Convert the $k-1$th model parameter estimate, i.e., $\hat{\theta}(k-1)$, to the form of state space model to apply it to the model predictive controller.

Step 4: Calculate the controller state predictions and the output predictions of the model predictive controller with respect to prediction horizon, $x(k+i|k)$ and $y(k+i|k)$ for $i=1{:}p$. Subsequently, compute the next control action $u^{opt}(k)$ from the QP decision z_k based on Eq. (4-1).

Step 5: Update $P(k)$ using Eq. (4-7).

Step 6: Calculate the kth model parameter estimate $\hat{\theta}(k)$.

Step 7: Apply $u^{opt}(k)$ to the plant.

Step 8: Repeat Step 2 to 7.

Figure 4-3 shows the flowchart of the algorithm for better understanding. The less burdensome computation, which is the main advantage of the recursive algorithm, can be attributed to the use of only the immediately preceding data, as shown in the flowchart. Therefore, it can be used in real time up to the sample time level, making the algorithm suitable for plasma-based systems considering their time-varying and sensitive characteristics.

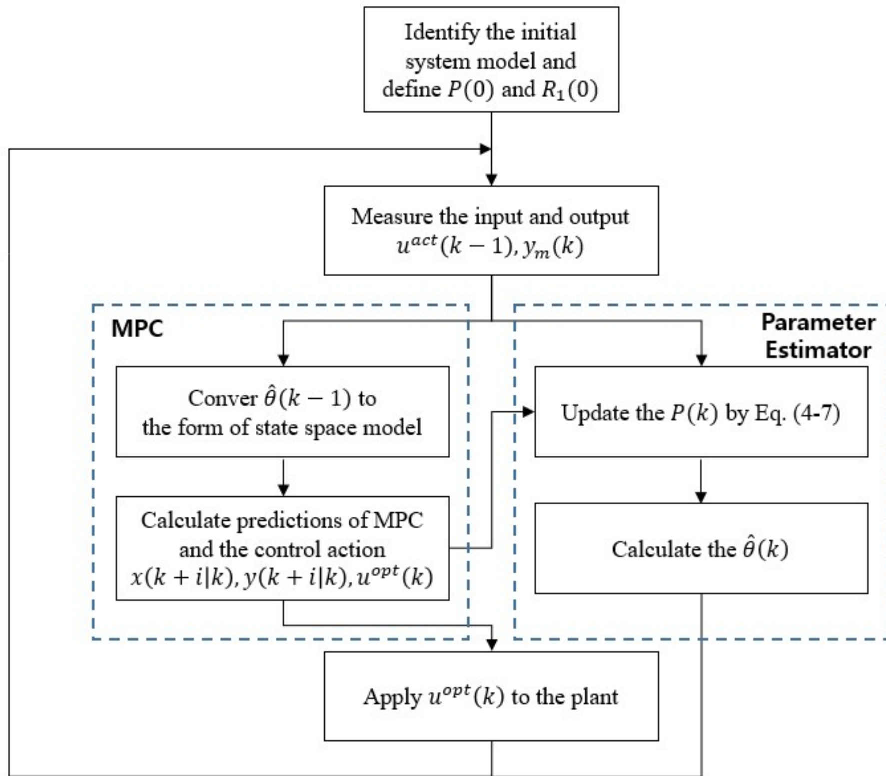

Figure 4-3 Flowchart of the proposed AMPC.

4.4. Time-varying system control using adaptive model predictive controller

4.4.1. Initial system identification (Scaling method)

The initial system model used in this chapter is equivalent to the model obtained in Section 3.3.1. However, additional modeling is also done in ARX form for the parameter estimator. The structure of the model which is released from the estimator is ARX type, therefore a state space model converter should be inserted between the estimator and model predictive controller. The ARX is given as follows.

$$A(z)y(k) = B(z)u(k) + e(k)$$
$$A(z) = 1 + a_1 z^{-1} + a_2 z^{-2} + \cdots \qquad \textbf{(4-8)}$$
$$B(z) = b_1 z^{-1} + b_2 z^{-2} + \cdots \ ,$$

therefore, the model parameter vector is $\theta = [\boldsymbol{a}^T, \boldsymbol{b}^T]^T = [a_1, \ldots a_{n_a}, b_1, \ldots, b_{n_b}]^T$. For the scaled model parameter vector, the scale factors of input and output variables, u^* and y^*, are 10 and 2.3×10^9 respectively as same as the values in Section 3.3.1. It results from treating $R_2(t)$ as the reference parameter as described in Section 4.2.2. In other words, based on the OES measurement data of the electron density, $R_2(t)$ is set as a unit white Gaussian in Eq. (4-6) and $Ev(t)v^T(t) = R_2(t)$. The obtained initial model parameter estimate via this scaling method is $\hat{\theta}(0) = [\boldsymbol{a_0}^T, \boldsymbol{b_0}^T]^T$ where $\boldsymbol{a_0}^T = [-0.0632, 0, 0, 0]$ and $\boldsymbol{b_0}^T = [0, 0, 0.0305, 0.0330]$. As a_3, a_4, b_1, and b_2 are the terms induced from the

system time delay, they must be fixed to zero and should not be changed adaptively during recursive model parameter estimation.

4.4.2. Design of adaptive model predictive controller for time-varying system

As mentioned in Section 4.2.2, the design parameters of the recursive model parameter estimator are $P(0)$ and $R_1(t)$ after using the scaling method. Here, $R_1(t) = R_1(0) = R_1$, thus, a constant value. The effective system model parameters are only a_1, a_2, b_3, and b_4 as mentioned in the previous section. Therefore, the tuning parameters of the recursive model parameter estimation algorithm, i.e., $P(0)$ and R_1, are 4×4 diagonal matrices, which can be obtained using the Bayesian optimization method similar to the method described in Section 3.3.2. When the optimization was conducted, the variances for a_2 and b_3, which are the second and third diagonal terms of R_1, were deliberately set to very small values. This is because a_2 and b_3 are the terms formed by converting the continuous system model to the discrete system model so that these are hardly affected by the drift of the actual system. The expression of ISE-based Bayesian optimization of the recursive model parameter estimator is as follows.

$$[P(0)\ \ R_1]^* = \underset{\substack{P(0)_{min} \leq P(0) \leq P(0)_{max} \\ R_{1min} \leq R_1 \leq R_{1max}}}{\operatorname{argmin}} g(P(0)\ \ R_1) \tag{4-9}$$

where $P(0)_{min}$, $P(0)_{max}$, R_{1min} and R_{1max} is the constraints for the feasible optimization and the $g(P(0)\ \ R_1)$ is the ISE function given as follows.

$$g(P(0)\ \ R_1) = \int (y_{sp}(t) - y(P(0), R_1, t))^2 dt. \tag{4-10}$$

For the discrete time domain, $g(P(0)\ \ R_1)$ is expressed as follows.

$$g(P(0)\ \ R_1) = \sum (y_{sp}(k) - y(P(0), R_1, k))^2. \quad \textbf{(4-11)}$$

The upper and lower limits of $P(0)$ and R_1 are dependent to the system variety. Of course, it is advantageous to set the limit values that exactly reflects how much the system change is, however, it is not the essential requirement to select the perfect values. Proper values can also lead to a good control result.

With the recursive model parameter estimator and the model predictive controller, random set-point tracking tests were conducted, wherein the system gain drift and offset drift were applied to the system model. At each simulation, the offline tuning of the recursive model parameter estimator was done, then the control simulation was performed. Here, the MPC weight parameters, Q and R, 0.0322 and 0.9882 which is equivalent to the values used in Sections 3.4.2 and 3.4.3.

In Figure 4-4 and Figure 4-5, the control result is shown in the situation where the system gain increases with no offset drift as same situation as Figure 3-8. The sample time of simulations is 50 ms. The GD is set to be 1.015/s, and the OD is 0. In this case, the optimal design parameters were obtained as $diag(P(0)^*)^T = [4.51\ \ 0.00\ \ 0.00\ \ 0.353] \times 10^{-6}$ and $diag({R_1}^*)^T = [4.70\ \ 0.00\ \ 0.00\ \ 9.08] \times 10^{-7}$ where the $P(0)^*$ and ${R_1}^*$ denote $P(0)$ and R_1 of $[P(0)\ \ R_1]^*$ in Eq. (4-9), respectively. The adaptive model predictive controller considers the system changes adaptively through the model parameter estimation, thereby performing a significantly better control than the model predictive controller. The model parameter estimates, shown in

Figure 4-6(a) and (b), mitigate the MPM, thus ensuring that the adaptive model predictive controller does not operate aggressively. This is because the state estimation by the MPC algorithm in the AMPC algorithm is much more accurate than the only MPC algorithm used case owing to the adaptively updated model parameters. For the numerical performance, the mean absolute percentage error is (MAPE) used for comparing the two controllers. The MAPE is defined as in Eq. (4-12).

$$MAPE\ \ (\%) = \frac{1}{N}\sum_{k=1}^{N}\left|\frac{e(k)}{y_{set}(k)}\right| \times 100\% \tag{4-12}$$

where N is the number of samples, $y_{set}(k)$ is the set-point value of kth sample, and $e(k)$ is the error of kth sample which is equivalent to $y_{set}(k) - y(k)$. Based on Eq. (4-12), the MAPE for MPC is 0.195% and that for AMPC is 0.163% which shows 16.5% increased performance in MAPE. In addition, the electron density which shows 99% accuracy for the set-point value is recommended to plasma etching processes. This is because the deviation with 1% accuracy is allowed in plasma etching processes, which means only 1% deviation is allowed to the electron density based on Section 2.2.1. Therefore, the comparison of the number of samples which deviate from 1% accuracy is also conducted. When n_{y_d} denotes the number of deviated sample, n_{y_d} for MPC is 85 and that for AMPC is 71 which shows 16.5% increased performance in y_d.

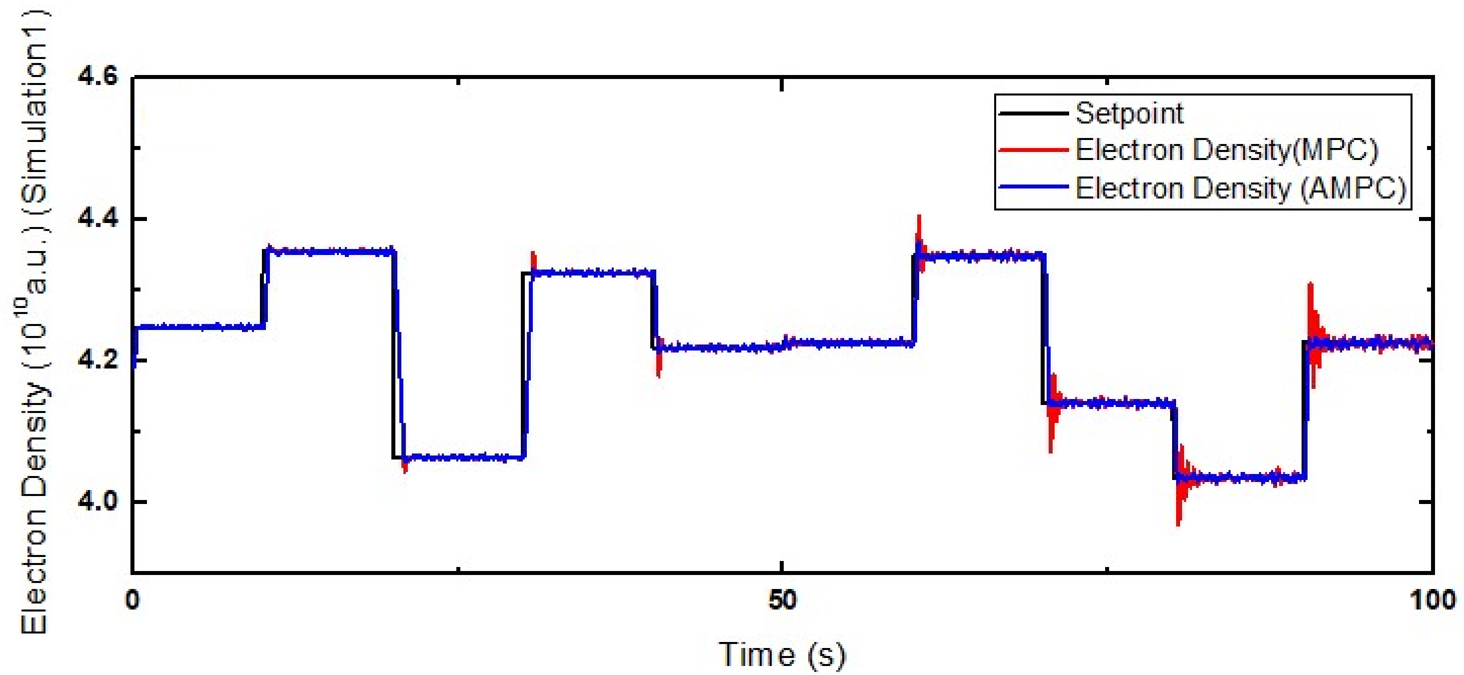

Figure 4-4 Simulation results of set-point tracking control of a gain increasing system conducted by the model predictive controller (red line) and the adaptive model predictive controller (blue line). The CV, which is the electron density, tracks the set-point of it.

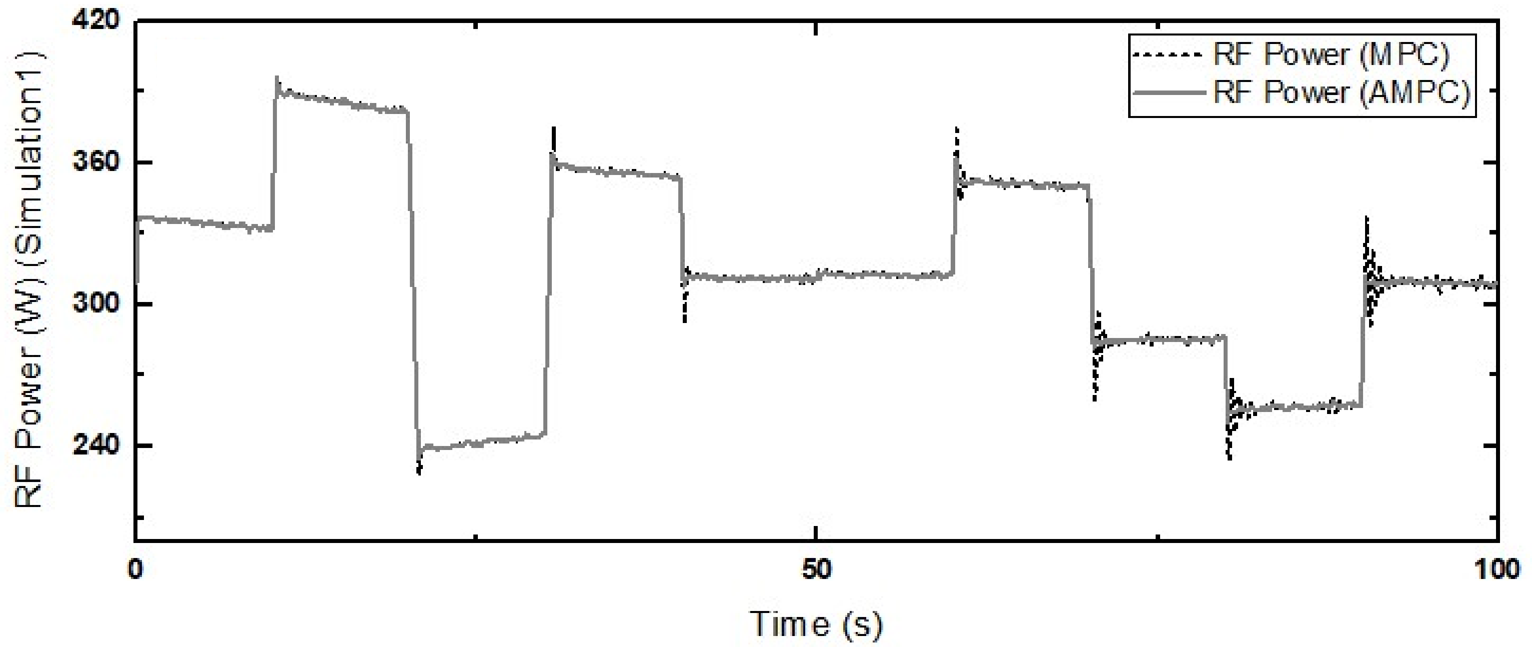

Figure 4-5 The MV (RF power) movements released from the model predictive controller (black dot) and the adaptive model predictive controller (gray line) in simulation 1.

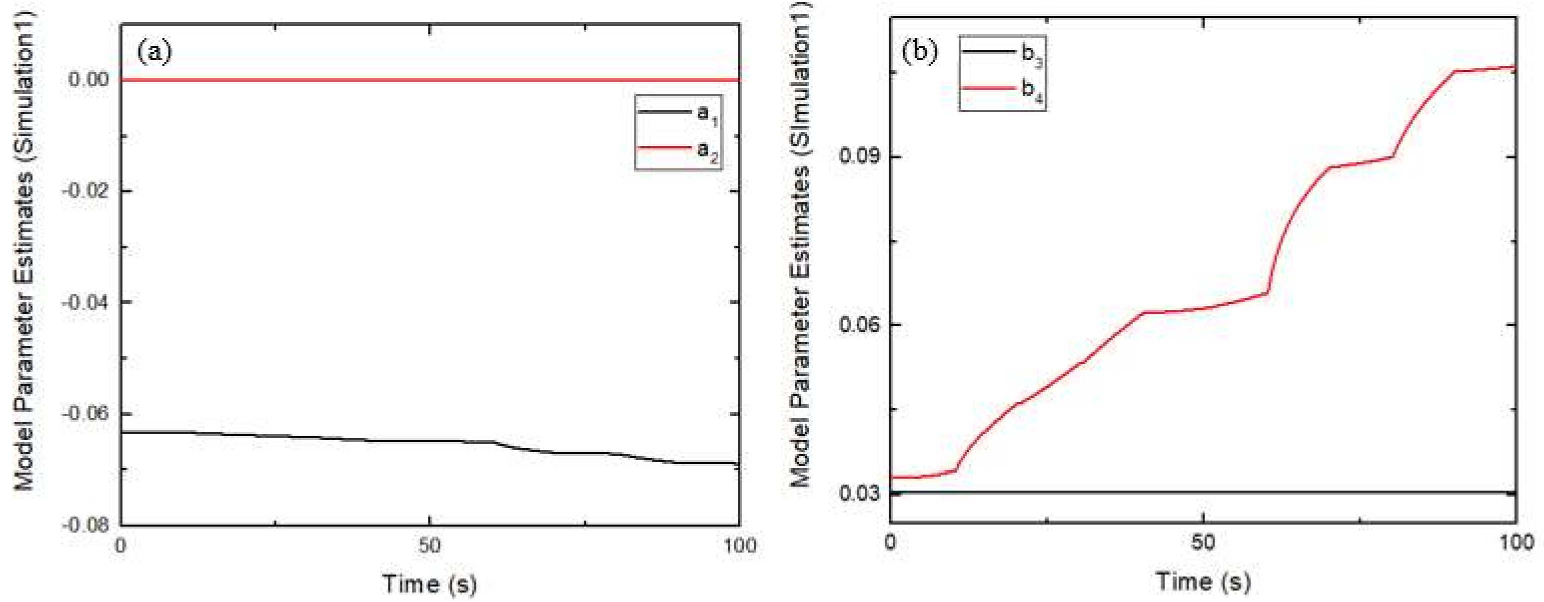

Figure 4-6 The model parameters estimated by the recursive model parameter estimator in simulation 1.

Figure 4-7 and Figure 4-8 shows the control simulation result when the system gain decreases with no offset drift as same situation as Figure 3-9. The GD is 0.992/s and the OD is 0. The optimal design parameters were set to be same as the first simulation case. The model predictive controller operates robustly with the change in the system. Whereas the adaptive model predictive controller shows the excellent performance again through the estimation of the time-varying system model parameters as shown in Figure 4-9(a) and (b). The MAPE for MPC is 0.292% and that for AMPC is 0.268% which shows 8.17% increased performance in MAPE. In addition, n_{y_d} for MPC is 158 and that for AMPC is 156 which shows 1.27% increased performance in y_d.

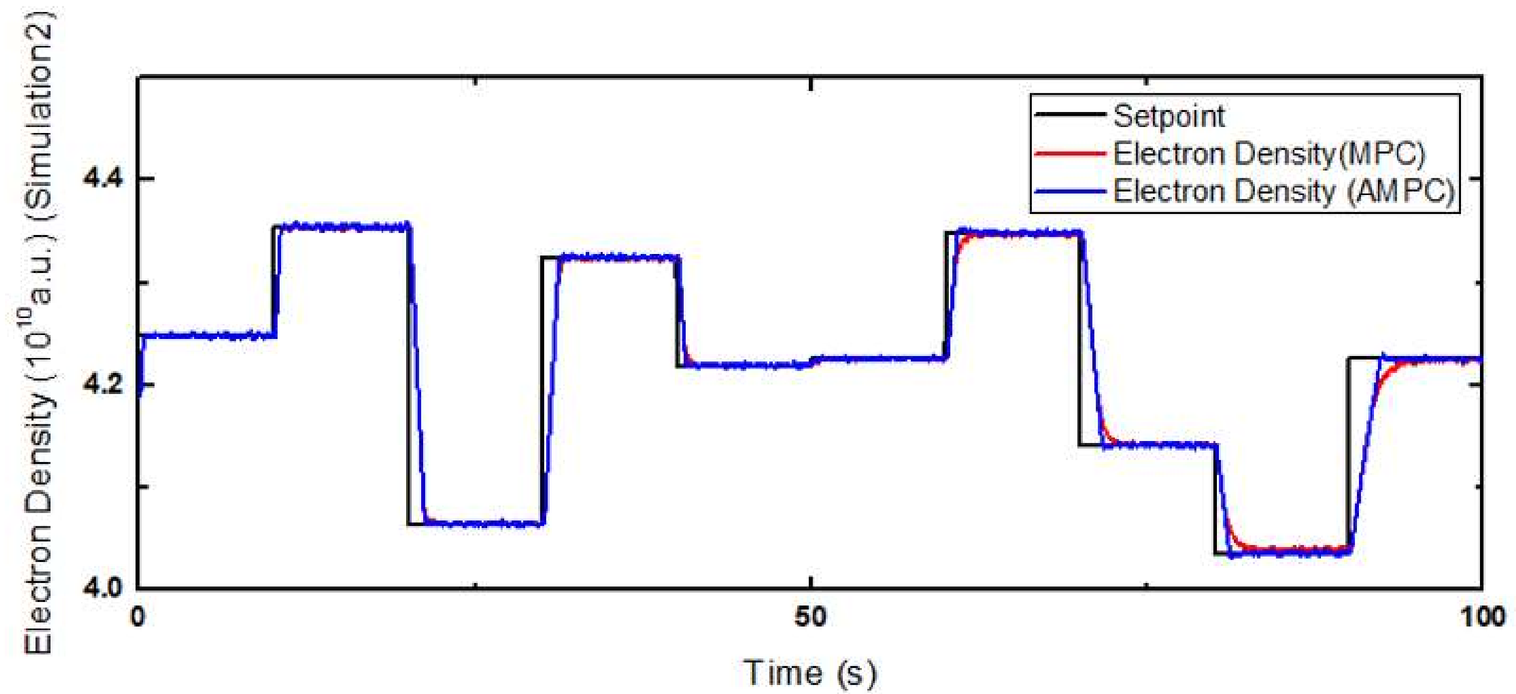

Figure 4-7 Simulation results of set-point tracking control of a gain decreasing system conducted by the model predictive controller (red line) and the adaptive model predictive controller (blue line). The CV, which is the electron density, tracks the set-point of it.

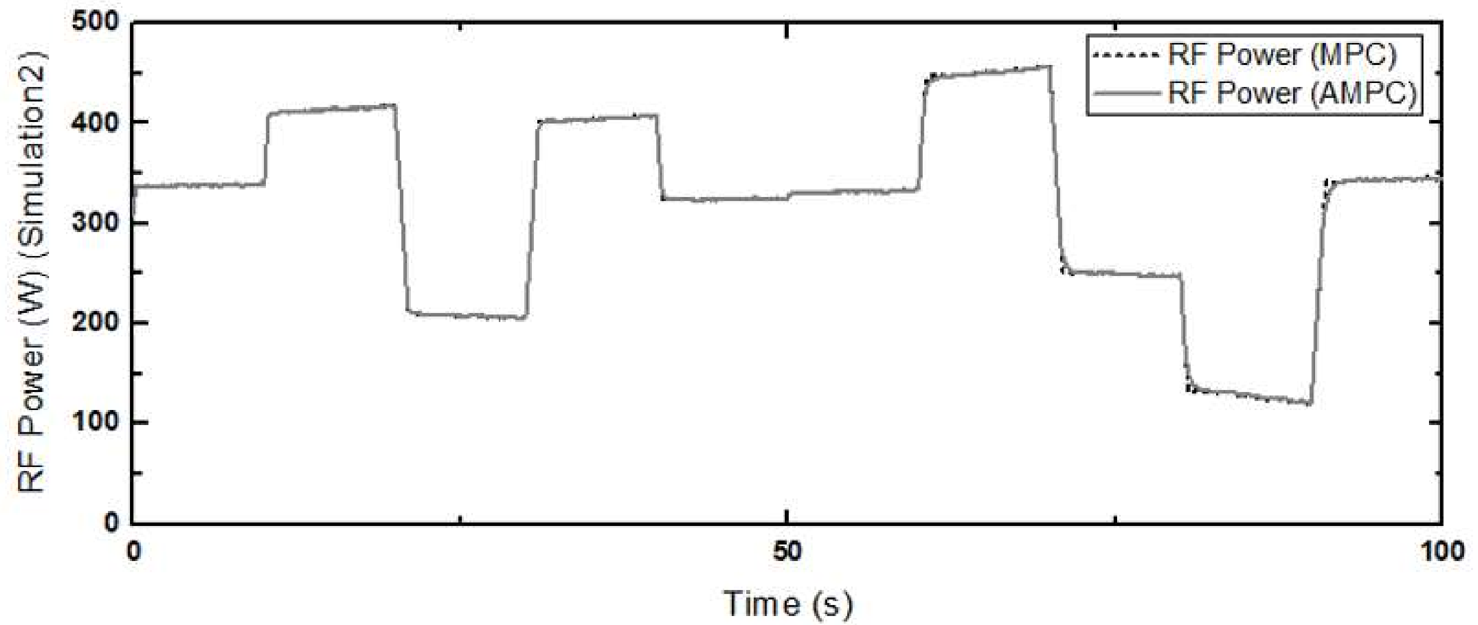

Figure 4-8 The MV (RF power) movements released from the model predictive controller (black dot) and the adaptive model predictive controller (gray line) in simulation 2.

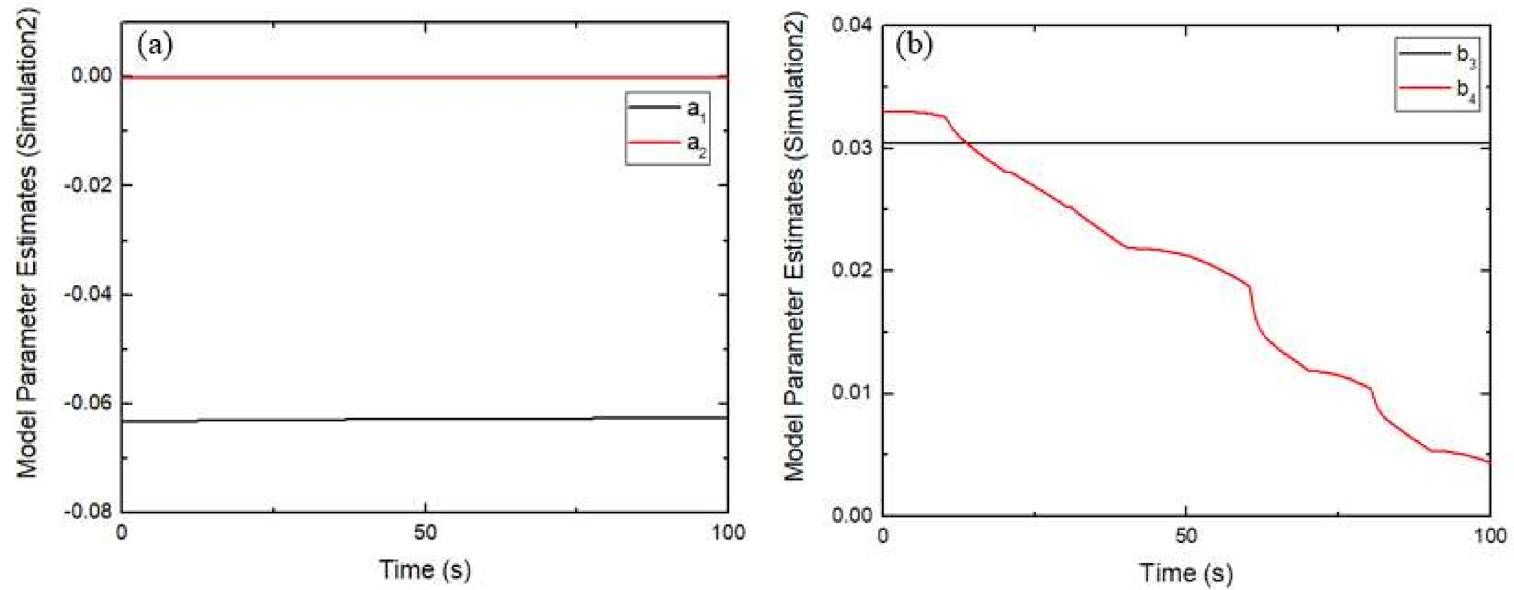

Figure 4-9 The model parameters estimated by the recursive model parameter estimator in simulation 2.

Figure 4-10 and Figure 4-11 shows the simulation results of offset drift only case. The GD is 0 and the OD is -2×10^{7} $a.u.$/s. The optimal design parameters were $diag(P(0)^{*})^{T} = [4.51 \;\; 0.00 \;\; 0.00 \;\; 0.353] \times 10^{-6}$ and $diag({R_{1}}^{*})^{T} = [4.70 \;\; 0.00 \;\; 0.00 \;\; 9.08] \times 10^{-10}$. The model parameter estimates for the adaptive model predictive controller are shown in Figure 4-12(a) and (b). The MAPE for MPC is 0.189% and that for AMPC is 0.189% which shows almost same performance. For n_{y_d} comparison, the two control methods show equal performance where the both n_{y_d} for the methods are same as 96. This result verifies that the well-tuned model predictive controller as well as the adaptive model predictive controller performs the set-point tracking control well wherein the offset drift exists only.

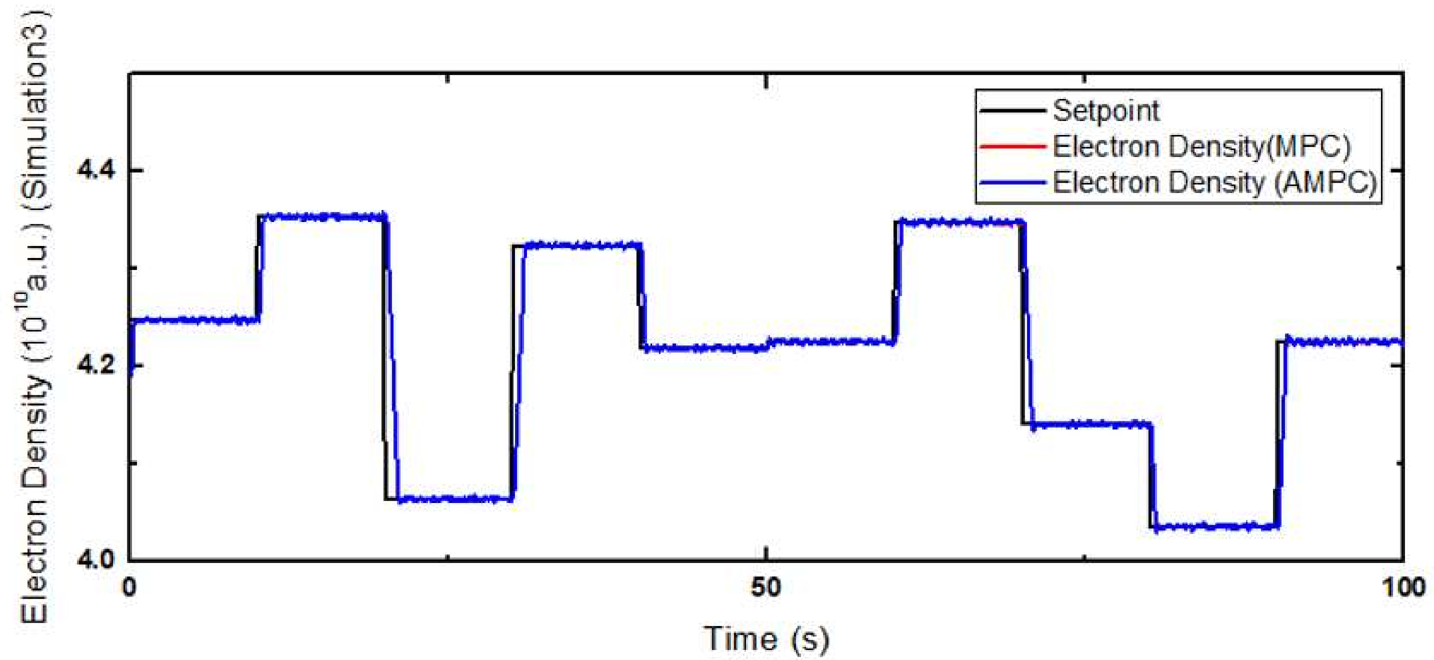

Figure 4-10 Simulation results of set-point tracking control of an offset drift system conducted by the model predictive controller (red line) and the adaptive model predictive controller (blue line). The CV, which is the electron density, tracks the set-point of it.

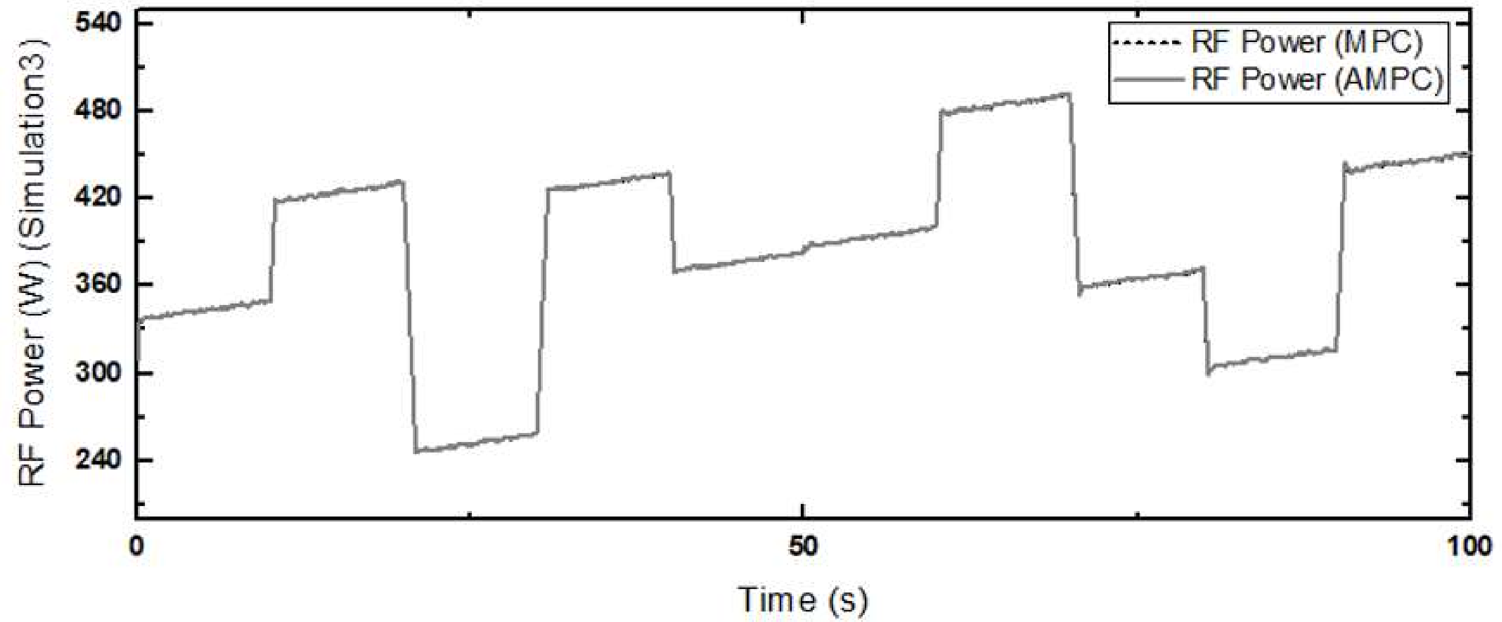

Figure 4-11 The MV (RF power) movements released from the model predictive controller (black dot) and the adaptive model predictive controller (gray line) in simulation 3.

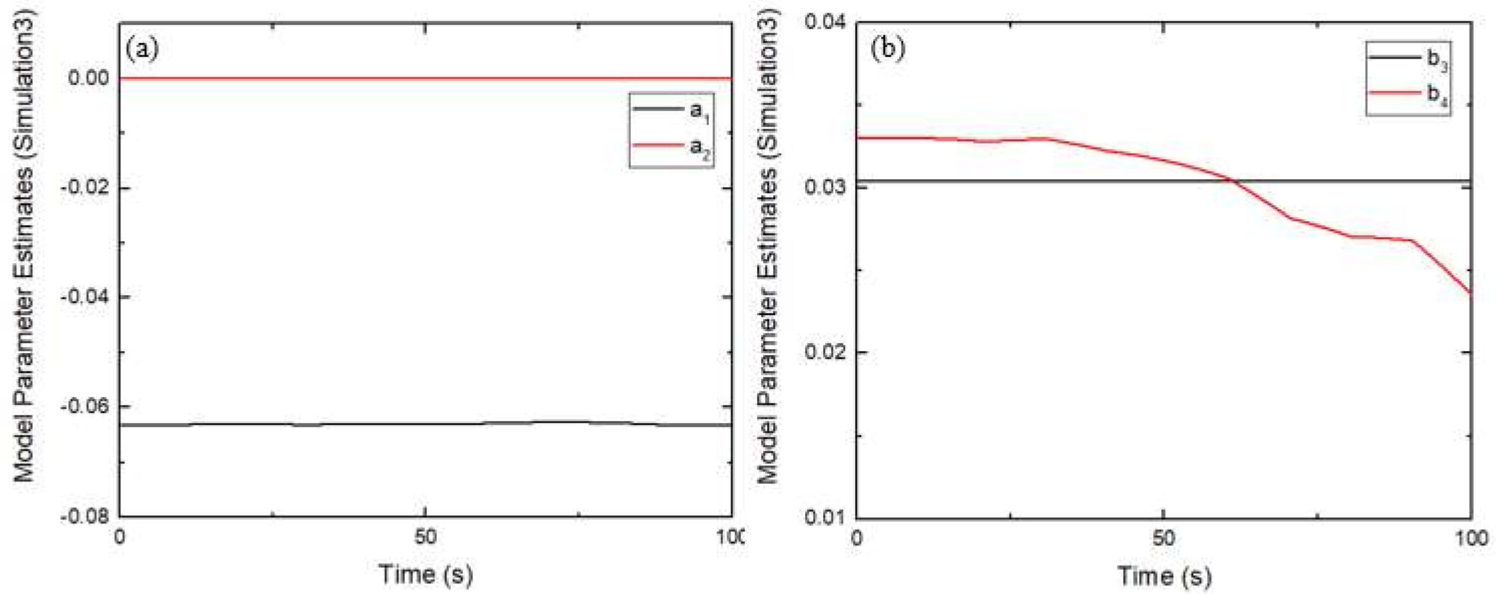

Figure 4-12 The model parameters estimated by the recursive model parameter estimator in simulation 3.

Finally, The control simulation result for the case wherein the two types of drift exist is shown in Figure 4-13 and Figure 4-14. The GD is 1.012/s and the OD is $-8 \times 10^6\ a.u.$ /s. The optimal design parameters were $diag(P(0)^*)^T = [4.51\ \ 0.00\ \ 0.00\ \ 0.353] \times 10^{-6}$ and $diag({R_1}^*)^T = [0.470\ \ 0.00\ \ 0.00\ \ 9.08] \times 10^{-7}$. For the case wherein the increase in the system gain and the decrease in the offset drift occur simultaneously, the model predictive controller cannot overcome the system gain drift effect. Whereas, the adaptive model predictive controller shows excellent performance till the last with the estimation of model parameters as shown in Figure 4-15(a) and (b). The MAPE for MPC is 0.184% and that for AMPC is 0.172% which shows 6.37% increased performance in MAPE. In addition, n_{y_d} for MPC is 81 and that for AMPC is 75 which shows 7.41% increased performance in n_{y_d}. Therefore, it is obviously demonstrated that the control in the time-varying systems is not perfectly done even with the thoroughly tuned model predictive controller and should be conducted with the adaptive model predictive controller. The recursive model parameter estimator allows the model predictive controller to make more accurate controller state estimation by the adaptive modification of the plant model, thus showing remarkable control results. Based on the above simulation results, the performances of the two controllers in an experiment where an artificial drift is introduced will be compared in the next section.

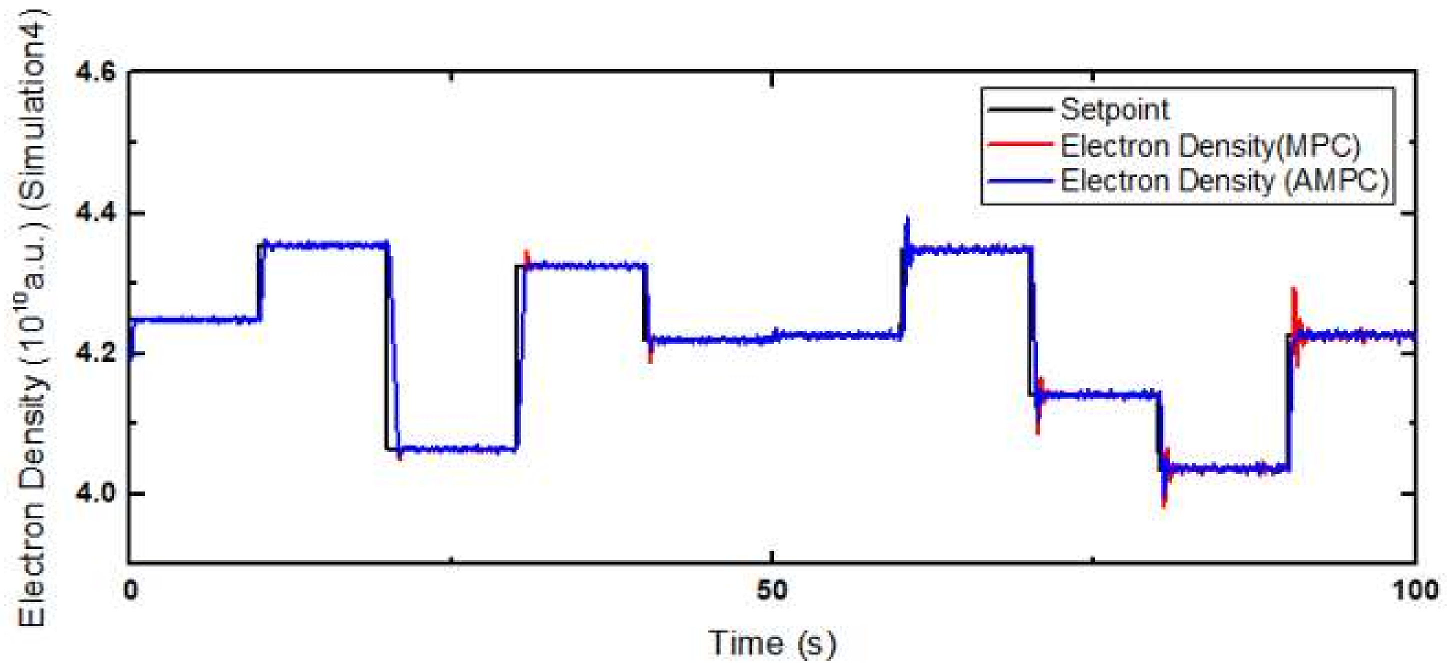

Figure 4-13 Simulation results of set-point tracking control of a gain increasing with an offset drift system conducted by the model predictive controller (red line) and the adaptive model predictive controller (blue line). The CV, which is the electron density, tracks the set-point of it.

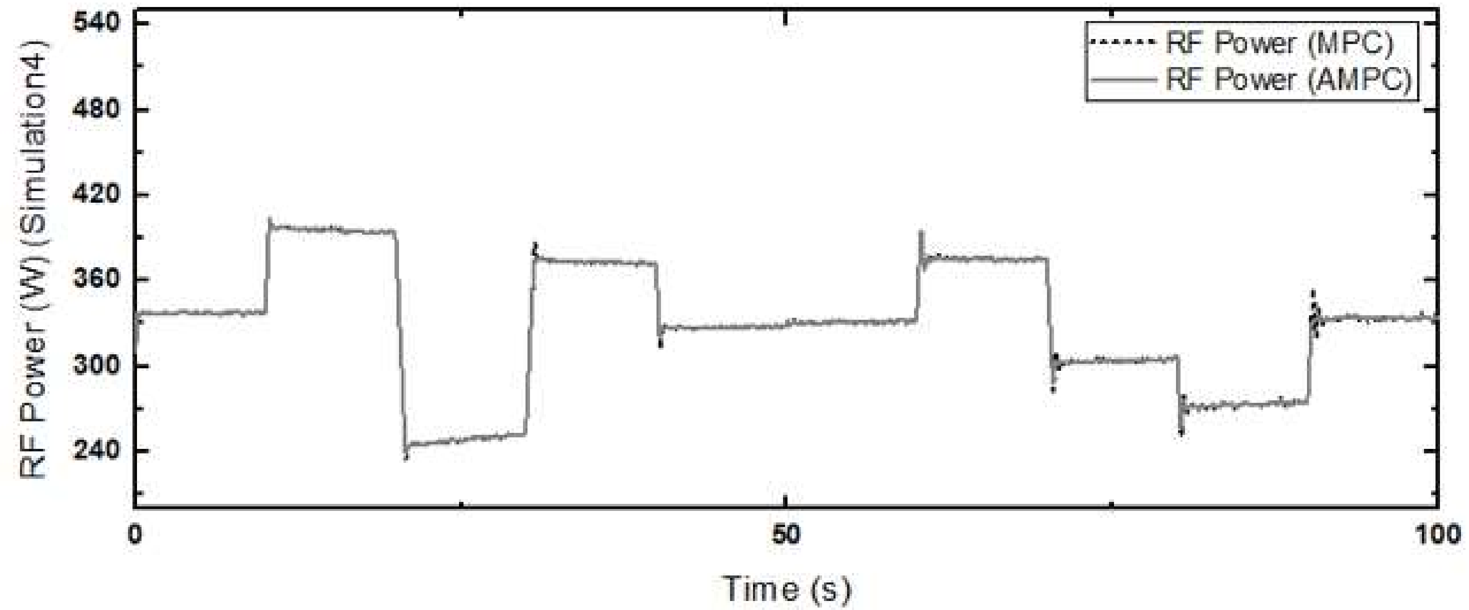

Figure 4-14 The MV (RF power) movements released from the model predictive controller (black dot) and the adaptive model predictive controller (gray line) in simulation 4.

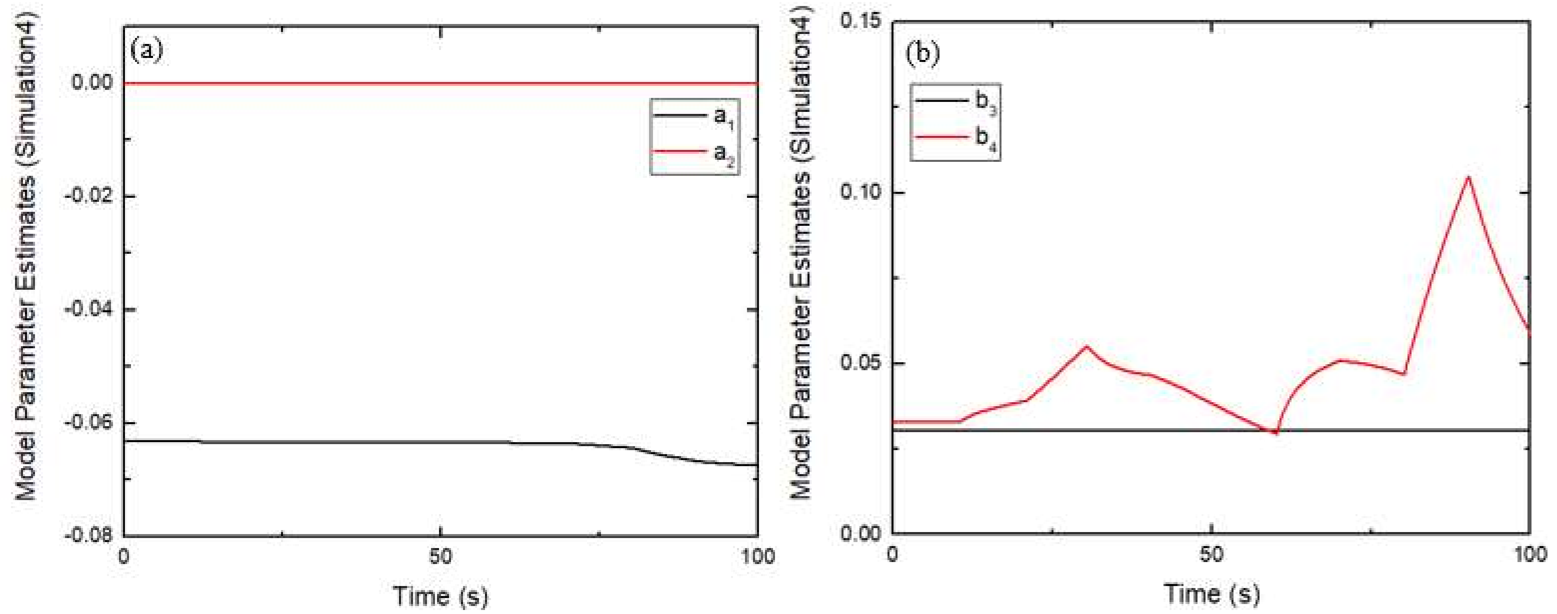

Figure 4-15 The model parameters estimated by the recursive model parameter estimator in simulation 4.

4.4.3. Set-point tracking control results in drifted system

With the adaptive model predictive controller described in the previous section and the model predictive controller from the previous chapter, a random set-point tracking test was conducted wherein the system drift was artificially applied. The detailed experimental condition is that the experimental sample time is 50 ms and the starting reference condition is 300 W of 60 MHz RF power, 20 mT of pressure and 500 sccm of Ar flowrate which is equivalent to that of Section 3.3.3. In addition, the disturbance was made by injecting O_2 at 1 sccm/s as explained in Section 3.4.3. With the offline tuning of the recursive model parameter estimator, the optimal design parameters are $diag(P(0)^*)^T = [6.04\ \ 0.00\ \ 0.00\ \ 0.560] \times 10^{-6}$ and $diag({R_1}^*)^T = [7.18\ \ 0.00\ \ 0.00\ \ 2.34] \times 10^{-11}$. In addition, the MPC weight parameters, Q and R, are equivalent to the values used in Sections 3.4.2 and 3.4.3, which are 0.0322 and 0.9882. As illustrated in Figure 4-16, both controllers show great performance in the early stage when the drift is not yet severe (before 50s). However, the advantage of the adaptive model predictive controller is evident in the latter half. As described in Section 3.4.3, the performance of model predictive controller deteriorates due to the MPM, however, that of the adaptive model predictive controller does not. The MPM comes from the increase of nonlinearity of the system which is induced by the high ratio of O_2 plasma to Ar plasma in the latter half. From the comparison of the control results in simulations and the experiment, the severity of nonlinearity in the experiment

is larger than that of the simulations. To mitigate the deterioration of the controller performance, the recursive model parameter estimator adaptively sends the updated model parameter estimates to the model predictive controller in the AMPC case. Thereby, the adaptive model predictive controller maintains its ability till the end. The model parameters estimated by the recursive parameter estimator during control is illustrated in Figure 4-18(a) and (b). With the real-time updating of the model parameters, the adaptive control result shows much better performance even in the case of enough drift existence in the latter part. The numerical performances calculated using MAPE and n_{y_d} show the improvements of 24.7% and 30.4% for the adaptive model predictive controller, compared to that of the model predictive controller. The MAPE for MPC is 0.190% and that for AMPC is 0.143%. In addition, n_{y_d} for MPC is 92 and that for AMPC is 64.

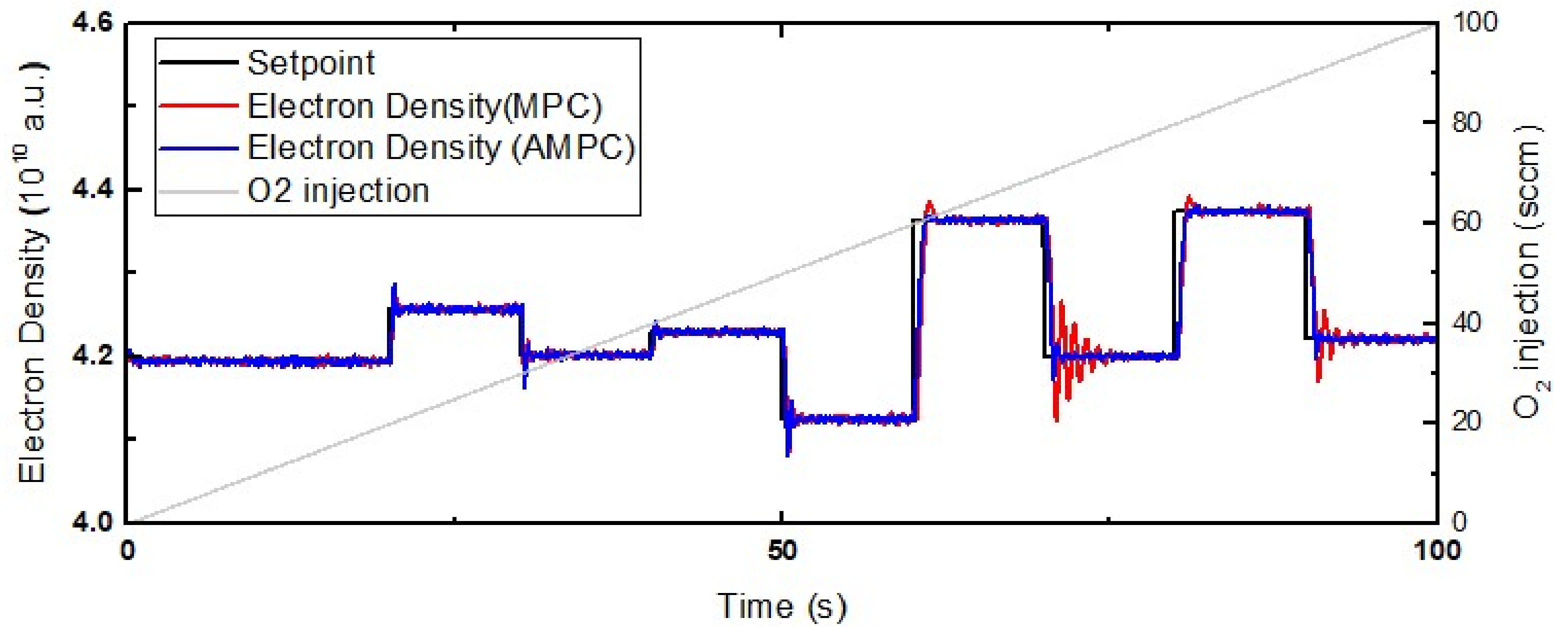

Figure 4-16 Experiment result of set-point tracking control of an Ar plasma system with an artificial drift induced by O_2 plasma (light gray, right axis), conducted by the model predictive controller (red line, left axis) and the adaptive model predictive controller (blue line, left axis). The CV, which is the electron density, tracks the set-point of it.

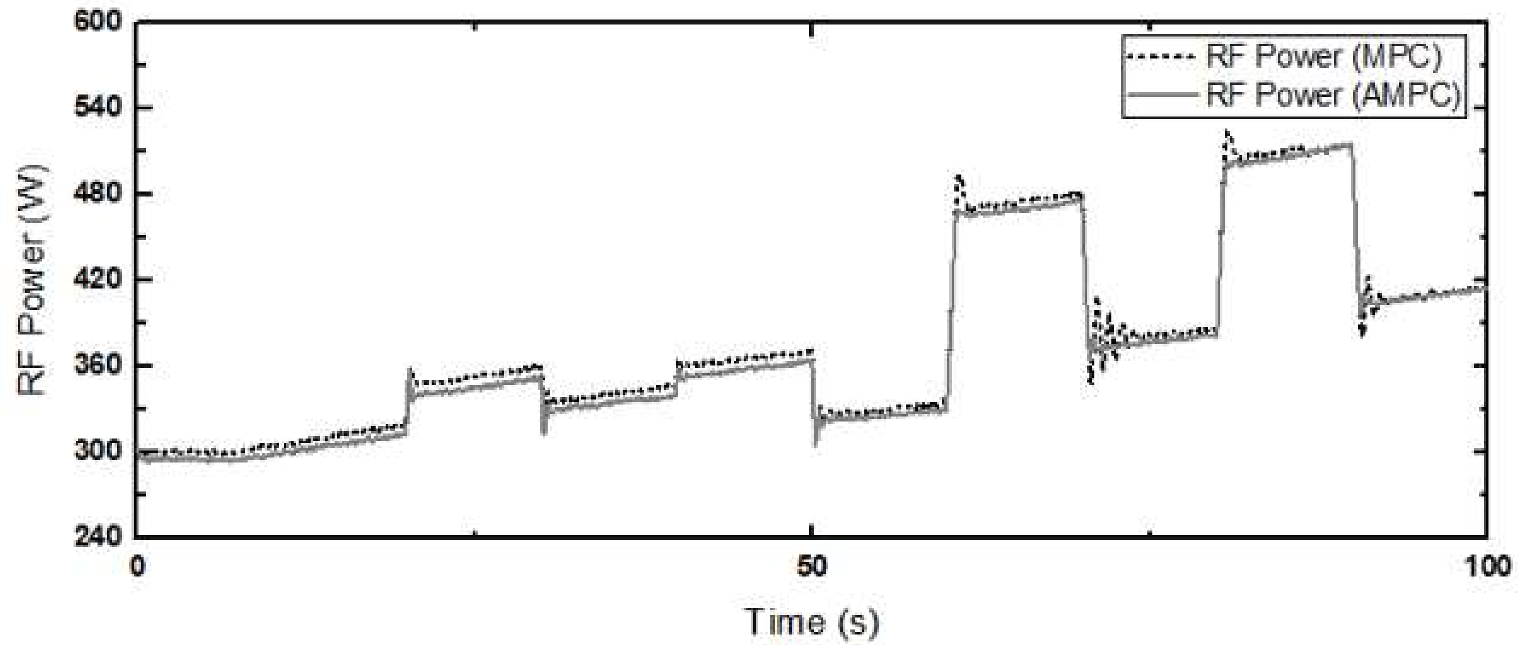

Figure 4-17 The MV (RF power) movements released from the model predictive controller (black dot) and the adaptive model predictive controller (gray line) in the experiment.

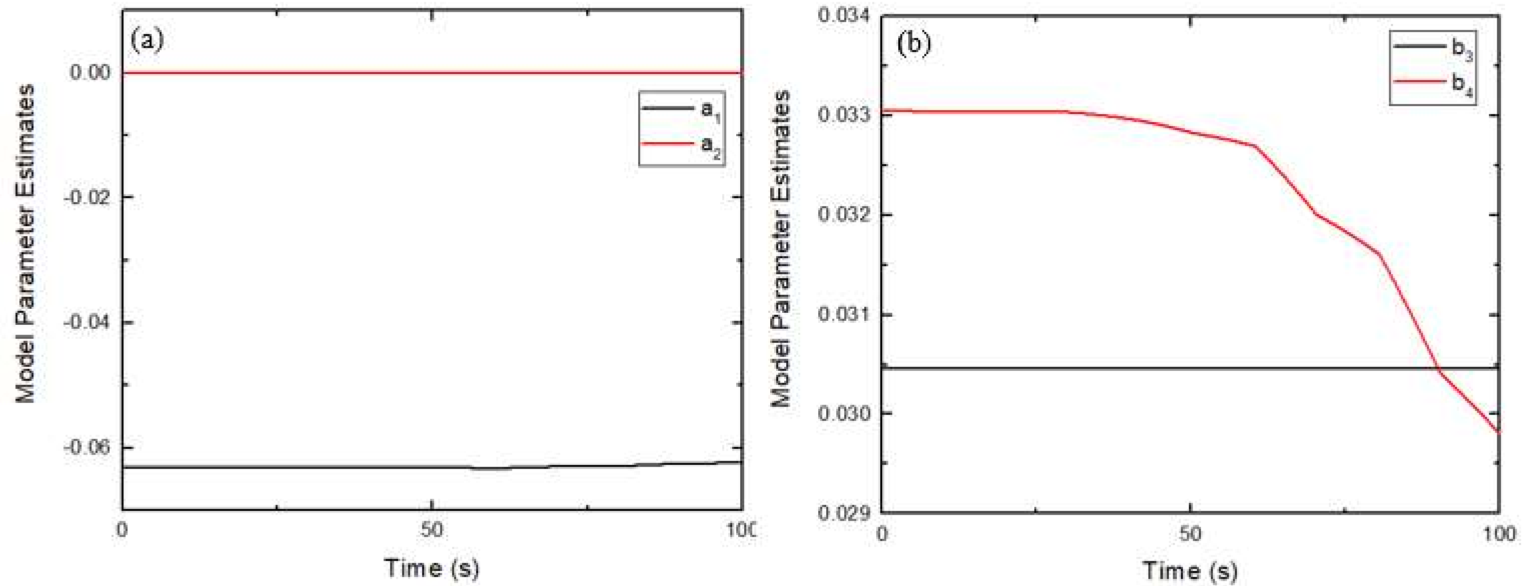

Figure 4-18 The model parameters estimated by the recursive model parameter estimator in the experiment.

The overview of control results discussed in Section 4.4.2 and 4.4.3 are shown in Table 4 and Table 5. In Table 4, the MAPE for both control methods and its performance index γ_{MAPE} are expressed. Here, γ_{MAPE} represents the increased performance of AMPC compared to that of MPC based on MAPE, which is defined as follows.

$$\gamma_{MAPE}(\%) = \frac{\mathrm{MAPE(MPC)} - \mathrm{MAPE(AMPC)}}{\mathrm{MAPE(MPC)}} \times 100\% \qquad \textbf{(4-13)}$$

where MAPE(MPC) and MAPE(AMPC) are the MAPE for MPC and AMPC, respectively. In Table 5, the number of deviated samples n_{y_d} for both control methods and its performance index γ_n are expressed. Here, γ_n represents the increased performance of AMPC compared to that of MPC based on n_{y_d}, which is defined as follows.

$$\gamma_n(\%) = \frac{n_{y_d}(\mathrm{MPC}) - n_{y_d}(\mathrm{AMPC})}{n_{y_d}(\mathrm{MPC})} \times 100\% \qquad \textbf{(4-14)}$$

where $n_{y_d}(\mathrm{MPC})$ and $n_{y_d}(\mathrm{AMPC})$ are n_{y_d} for MPC and AMPC, respectively.

Table 4 The overview of MPC and AMPC results in set-point tracking tests based on MAPE (%) and γ_{MAPE} (%).

	MAPE(MPC)	**MAPE(AMPC)**	$\boldsymbol{\gamma_{MAPE}}$
Simulation 1	0.195	0.163	16.5
Simulation 2	0.292	0.268	8.17
Simulation 3	0.189	0.189	-0.144
Simulation 4	0.184	0.172	6.37
Experiment	**0.190**	**0.143**	**24.7**

Table 5 The overview of MPC and AMPC results in set-point tracking tests based on $\boldsymbol{n_{y_d}}$ and $\boldsymbol{\gamma_n}$ (%).

	$\boldsymbol{n_{y_d}}$**(MPC)**	$\boldsymbol{n_{y_d}}$**(AMPC)**	$\boldsymbol{\gamma_n}$
Simulation 1	85	71	16.5
Simulation 2	158	156	1.27
Simulation 3	96	96	0
Simulation 4	81	75	7.41
Experiment	**92**	**64**	**30.4**

The simulations and experiment result definitely demonstrates that the adaptive model predictive controller is the much more effective controller for the plasma-based systems where drifts are frequent. In addition, better control results can be expected through the adaptive control wherein continuous parameter estimation is incorporated for time-varying systems. Moreover, the experiment results demonstrate that the proposed controller can show excellent control performance even in the system with much larger disturbance than the actual situation due to the high ratio of O_2 plasma to Ar plasma. This successful AMPC result is expected to further enhance the quality of many control processes that require high sophistication and flexibility.

4.5. Concluding remarks

An adaptive model predictive controller that can performs the real-time electron density control in Ar/O_2 plasma system at the sample time level was developed in this chapter. The strategy involved designing the adaptive model predictive controller that is well suited to the time-varying nature of the plasma-based system by applying a recursive model parameter estimator, which has little computational complexity, to the finely tuned model predictive controller. The RLS algorithm with Kalman filter interpretation was used for the online model parameter estimation. The algorithm has much more advantages in comparison to the RLS algorithm with the forgetting factor in consideration of time delay induced by a plasma etching reactor. The initial values of the parameter covariance matrix and the process noise covariance matrix were considered prerequisites for the recursive model parameter estimation. These parameters were optimized by ISE-based Bayesian optimization. The performance of the adaptive model predictive controller was verified by performing control simulations wherein two types of drift were applied to the system model and by conducting a set-point tracking control experiment in an Ar plasma system with an artificial drift induced by O_2 plasma. The adaptive model predictive controller shows 24.7% better performance in terms of the MAPE and 30.4% better performance in terms of n_{y_d} compared to the conventional model predictive controller for the real-time control at the sample time level. In fact, the relatively high ratio of O_2 plasma to Ar plasma in the latter part of this experiment represents the situation with larger disturbance

than actual plasma-based processes. Therefore, these results demonstrate that the adaptive model predictive controller using the recursive model parameter estimator can operate successfully in plasma-based systems and is expected to make a significant contribution to control processes that require high sophistication and flexibility.

CHAPTER 5. Conclusion

5.1. Summary of contributions

This thesis considered a design of adaptive model predictive controller for the CCP etching reactor. First of all, the possibility of MIMO control was demonstrated. Through the PRBS tests, SVA, and RGA, the optimal variable selection, variable pairing, and the system identification of 2×2 first order transfer function models were conducted. As a prerequisite, the selection of CVs was described by the particle balance equation. For the check of controllability, two SISO disturbance controls were performed. In this case, O_2 which is a key chemical in plasma etching processes was used as a disturbance. In order to reduce the interaction effects, decoupler controllers were applied to the MIMO controller. Being compared to the SISO controller and MIMO controller without decoupler controllers by set-point tracking control simulations, the proposed controller showed the better performance. Then, it excellently conducted a 2×2 MIMO control of the Ar plasma electron density and electron temperature. The results demonstrate that the possibility of MIMO plasma variable control. After that, a design of a model predictive controller which can conduct electron density control and its performance were described. Resulting from the cyclical affection between the wall condition of plasma etching reactor and the etch profile, the time-varying characteristics of plasma-based system was considered in the MPC design. The output disturbance model and noise disturbance model were set to the MPC algorithm

considering system gain drift and offset drift, which are the most typical drift types in plasma-based systems. For thorough design, ISE-based Bayesian optimization technique was used for MPC weight parameters tuning. Then, the model predictive controller performed control simulations of the Ar plasma electron density. Four simulation results wherein the system gain drift and offset drift showed that the controller can work well for some disturbed cases, but its limits were clearly observed. Finally, the limitations were confirmed by the electron density control experiment in the time-varying Ar/O_2 plasma system. The control performance deteriorated in the latter part. The control results demonstrate that an AMPC algorithm is required to the plasma variable control. The RLS algorithm with Kalman filter interpretation is used for the online model parameter estimation method. The algorithm has an advantage in time-delay consideration which frequently occurred in the plasma etching reactor. The initial value of the parameter covariance matrix and process noise covariance matrix were inserted as the prerequisites of the recursive model parameter estimation. Subsequently, the adaptive model predictive controller was constructed by combining the recursive model parameter estimator with the model predictive controller. The performance of the adaptive model predictive controller was verified by the same control simulations and experiment that the model predictive controller conducted. The etch rate accuracy required in plasma etch processes is 99% so that the MAPE and the number of deviated sample are considered as the numerical performance indices. From the experiment results, the adaptive model predictive controller

shows 24.7% and 30.4% better performance in terms of the MAPE and n_{y_d} respectively compared to the model predictive controller. These results demonstrate that the adaptive model predictive controller using the recursive model parameter estimator can operate successfully in plasma-based systems, and is the effective controller for the plasma etching reactor. It is expected to make a significant contribution to plasma variable control processes requiring high sophistication and flexibility.

5.2. Future work

It is believed that the future work is recommended to design an adaptive model predictive controller that handles plasma from F species chemical, i.e., CF_4 or SF_6, which is the most commonly used etchant gas in plasma etching processes. If the controller design is conducted in a manner similar to that of this thesis, a more practical adaptive model predictive controller will be expected. Moreover, if the adaptive model predictive controller can deal with more complex target systems, for example, MIMO system, the controller's capabilities can be maximized. It will be a very challenging work, but if realized, the controller will be considered invaluable.

Also, it is recommended to improve the robustness of the proposed controller. Tuning of adaptive model predictive controller in this thesis has a limit in relation to the variation level of disturbances. For example, if another type of disturbance or drift introduced in this thesis affects to the target system when an adaptive control is performed, the performance might be getting worse. This is because the process noise covariance is assumed to be constant. If a design of recursive model parameter estimator considering the process noise covariance as a time dependent parameter, the robustness of the adaptive model predictive controller will surely be improved significantly.

The most valuable recommended future work, which is expected to be the most challenging work, is to develop a self-tuning adaptive model predictive controller. The recommended controller may have both advantages in accurate

model parameter estimation and accurate weight parameter. The proposed adaptive model predictive controller in this thesis modifies model parameters adaptively but does not revise the MPC weight parameters. However, if an adaptive controller can update MPC weight parameters as well as model parameters concurrently, it is expected to lead a brilliant development in all control processes including plasma variable control processes.

Nomenclature

AMPC	Adaptive model predictive control
ARX	Autoregressive exogenous
CCP	Capacitively coupled plasma
CN	Condition number
CN*	Minimized condition number
CV	Controlled variable
EEDF	Electron energy distribution
GD	Gain drift parameter
ICP	Inductively coupled plasma
ISE	Integral squared error
MAPE	Mean absolute percentage error
MIMO	Multi-input multi-output
MPC	Model predictive control
MPM	Model-plant-mismatch
MV	Manipulated variable
OD	Offset drift parameter
OES	Optical emission spectrometer
PECVD	Plasma-enhanced chemical vapor deposition

PFC	Predictive functional control
PI	Proportional integral
PID	Proportional integral derivative
PRBS	Pseudo random binary sequence
QP	Quadratic program
RF	Radio frequency
RGA	Relative gain array
RLS	Recursive least squares
SISO	Single-input single-output
SVA	Singular value analysis
SVD	Singular value decomposition
UV	Ultraviolet
VM	Virtual metrology
A	Effective area for particle loss
$A_{id}, B_{id}, C_{id}, D_{id}$	State space model parameters for input disturbance model
A_n, B_n, C_n, D_n	State space model parameters for measurement noise
$A_{od}, B_{od}, C_{od}, D_{od}$	State space model parameters for output disturbance model
$A_p, B_{pu}, B_{pv}, B_{pd}, C_p, D_{pu}, D_{pv}, D_{pd}$	State space model parameters for plant model
a.u.	Arbitrary unit
$a_i, b_i (i = 1, 2, 3, 4)$	The components of the ARX model parameter

a_1, a_2, b_3, b_4	The effective ARX system model parameter
a_3, a_4, b_1, b_2	The components of the ARX model parameter induced by time-delay
B_u	Equivalent to $[B_{pu} \ \ 0 \ \ 0 \ \ 0]^T$
C_m	Equivalent to $\left[C_p \ \ D_{pd}C_{id} \ \ C_{od} \ \ C_n\right]$
D	Offset matrix or disturbance matrix
D_{mv}	Equivalent to D_{pv}
D_v	Equivalent to D_{pv}
D_1, D_2	Diagonal scaling matrices
d	Unmeasured input disturbance signal
E	Error matrix
E_1, E_2	Energy threshold in excited state 1 and 2
e	Error
e_y	Prediction error of output variable
$e(k+i\|k)$	$k+i^{th}$ predicted error calculated at k
$f(E)$	Electron energy distribution function (EEDF)
G_p	Process transfer function
G_d	Disturbance transfer function
$G_{i,j}$	Transfer function between i^{th} MV and j^{th} CV
J	Cost function for MPC
K	Steady state gain

K_c	Controller gain
K_{iz}	Electron-neutral ionization rate constant
K_p	Plant model gain
K_{wall}	Particle loss rate to the reactor wall
k	Boltzmann constant
m_e	Electron mass
m	Control horizon
$\mathcal{M}_n$	Noise disturbance model
$\mathcal{M}_{od}$	Output disturbance model
N	Number of samples
n_a	Number of previous output terms in ARX model structure
n_b	Number of previous input terms in ARX model structure
n_e	Electron density
n_{F}	F species plasma density
n_g	Neutral gas density
n_0	Number density of ground state atoms
n_{y_d}	Number density of deviated output
$P(t)$	Parameter covariance matrix
$P(0)_{max}, P(0)_{min}$	Upper and lower limit of the parameter covariance matrix
$P(0)^*$	Optimal parameter covariance matrix

p	Prediction horizon
$p(t)$	Controller output
$\bar{p}(t)$	Bias value of controller output
$p'(t)$	Deviation variable of the controller output (Equivalent to $p(t) - \bar{p}(t)$)
Q, R	Weight matrices for MPC (MPC tuning parameters)
$[Q \;\; R]^*$	Optimal MPC weight parameters
R_1	Process noise covariance matrix
$R_{1_{max}}, R_{1_{min}}$	Upper and lower limit of the process noise covariance matrix
R_1^*	Optimal process noise covariance matrix
${s_i}^u, {s_i}^y$	Slack variables for input and output constraints
T_1, T_2	Decoupler controllers
T_e	Electron temperature
t_d	Time-delay
U	MV matrix
U_s	Orthonormal matrix of output singular vector
$\Delta u(k+i\|k)$	$k + i^{th}$ MV movement calculated at k
u^{act}	Actual input value
u^{opt}	Optimal input value
$\Delta u^-, \Delta u^+, y^-, y^+$	Lower and upper bounds of the adjustments of the input movement and output variables
$\bar{u}, \bar{y}$	Reference values of input and output variables

u^*, y^*	Scale factors of input and output variables
V	Discharge model volume
V_s	Orthonormal matrix of input singular vector
w_{id}	White noise for input disturbance model
w_n	White noise for measurement noise model
w_{od}	White noise for output disturbance model
x	Controller state
$x(k+i\|k)$	$k+i^{th}$ predicted state calculated at k
x_{id}	State of input disturbance model
x_n	State of measurement noise model
x_{od}	State of output disturbance model
x_p	State of plant model
x^{rev}	Revised state estimate
$y(k+i\|k)$	$k+i^{th}$ predicted output calculated at k
y_d	Deviated output
y_{id}	Input disturbance model output
y_m	Measured output
y_n	Measurement noise model output
y_{od}	Output disturbance model output
y_p	Plant model output

y_{sp}	Setpoint of output
y_u	Unmeasured output
z	QP decision
β	Weighting function
γ_{MAPE}	Performance index in terms of MAPE
γ_n	Performance index in terms of n_{y_d}
θ	Model parameter vector
$\hat{\theta}$	Estimate of the model parameter vector
Λ	Relative gain array
λ	Forgetting factor
λ_{ij}	Relative gain between i^{th} CV and j^{th} MV
Σ	Singular value matrix
σ_i	i^{th} singular value
σ_l	Largest nonzero singular value
σ_s	Smallest nonzero singular value
σ_{pk}	Excitation cross section from level *p* into level *k*
τ	Time constant of the plant model in the form of 1st order transfer function
τ_I	Integral time
τ_D	Derivative time
Φ_{pk}	Emission intensity from a particular pth state to kth state

φ	Regression vector

References

Al-Ghazzawi, A., Ali, E., Nouh, A., & Zafiriou, E. (2001). On-line tuning strategy for model predictive controllers. Journal of Process Control, 11, 265-284.

Albertos, P., & Piqueras, A. S. (2012). Iterative identification and control: Advances in theory and applications: Springer Science & Business Media.

Armaou, A., Baker, J., & Christofides, P. D. (2001). Feedback control of plasma etching reactors for improved etching uniformity. Chemical Engineering Science, 56, 1467-1475.

Armaou, A., & Christofides, P. D. (1999). Plasma enhanced chemical vapor deposition: Modeling and control. Chemical Engineering Science, 54, 3305-3314.

Baek, K. H., Han, P. K., Choi, G., Kang, H.-K., Seung Jung, E., Song, K., Han, C., & Edgar, T. F. (2013). Multiple input multiple output controller design to match chamber performance in plasma etching for semiconductor manufacturing. Journal of Vacuum Science & Technology B, Nanotechnology and Microelectronics: Materials, Processing, Measurement, and Phenomena, 31, 062201.

Boffard, J. B., Lin, C. C., & DeJosephJr, C. A. (2004). Application of excitation cross sections to optical plasma diagnostics. Journal of Physics D: Applied Physics, 37, R143-R161.

Box, G. E., Jenkins, G. M., Reinsel, G. C., & Ljung, G. M. (2015). Time series analysis: Forecasting and Control (5 ed.): John Wiley & Sons.

Bristol, E. (1966). On a new measure of interaction for multivariable process control. IEEE Transactions on Automatic Control, 11, 133-134.

Chalupa, P. (2009). Predictive control using self tuning model predictive controllers library. In Proceedings of the 17th International Conference on Process Control (Vol. 9, pp. 419-425).

Chang, C.-H., Leou, K.-C., & Lin, C. (2001). Real-time feedback control of electron density in inductively coupled plasmas. Journal of Vacuum Science & Technology A: Vacuum, Surfaces, and Films, 19, 750-756.

Chang, C.-H., Leou, K.-C., Lin, C., Lin, T.-L., Tseng, C.-W., & Tsai, C.-H. (2003). Real-time control of ion density and ion energy in chlorine inductively coupled plasma etch processing. Journal of Vacuum Science & Technology A: Vacuum, Surfaces, and Films, 21, 1183-1187.

Chung, C. W. (2013). Plasma Electronic Engineering: Cheongmungak.

Cunge, G., Pelissier, B., Joubert, O., Ramos, R., & Maurice, C. (2005). New chamber walls conditioning and cleaning strategies to improve the stability of plasma processes. Plasma Sources Science and Technology, 14, 599-609.

Donnelly, V. M., & Kornblit, A. (2013). Plasma etching: Yesterday, today, and tomorrow. Journal of Vacuum Science & Technology A: Vacuum, Surfaces, and Films, 31.

Fukasawa, M., Kawashima, A., Kuboi, N., Takagi, H., Tanaka, Y., Sakayori, H., Oshima, K., Nagahata, K., & Tatsumi, T. (2009). Prediction of Fluctuations

in Plasma–Wall Interactions Using an Equipment Engineering System. Japanese Journal of Applied Physics, 48, 08HC01.

Fukushima, H., Kim, T.-H., & Sugie, T. (2007). Adaptive model predictive control for a class of constrained linear systems based on the comparison model. Automatica, 43, 301-308.

Ha, D., Park, D., Koo, J., Baek, K. H., & Han, C. (2016). Improvement of principal component analysis modeling for plasma etch processes through discrete wavelet transform and automatic variable selection. Computers & Chemical Engineering, 94, 362-369.

Hamaoka, F., Yagisawa, T., & Makabe, T. (2009). Numerical investigation of relationship between micro-scale pattern, interfacial plasma structure and feature profile during deep-Si etching in two-frequency capacitively coupled plasmas in SF6/O2. Journal of Physics D: Applied Physics, 42.

Keville, B., Zhang, Y., Gaman, C., Holohan, A. M., Daniels, S., & Turner, M. M. (2013). Real-time control of electron density in a capacitively coupled plasma. Journal of Vacuum Science & Technology A: Vacuum, Surfaces, and Films, 31.

Kim, T. W., & Aydil, E. S. (2003). Effects of chamber wall conditions on Cl concentration and Si etch rate uniformity in plasma etching reactors. Journal of The Electrochemical Society, 150, G418-G427.

Kokkoris, G., Panagiotopoulos, A., Goodyear, A., Cooke, M., & Gogolides, E. (2009). A global model for SF_6 plasmas coupling reaction kinetics in the gas

phase and on the surface of the reactor walls. Journal of Physics D: Applied Physics, 42.

Koo, J., Ha, D., Park, D., Roh, H.-J., Ryu, S., Kim, G.-H., Baek, K. H., & Han, C. (2017). Design of optical emission spectroscopy based plasma parameter controller for real-time advanced equipment control. Computers & Chemical Engineering, 100, 38-47.

Kothare, M. V., Mettler, B., Morari, M., Bendotti, P., & Falinower, C.-M. (1997). Linear parameter varying model predictive contr for steam generator level control. Computers & Chemical Engineering, 21, S861-S866.

Lakshmanan, N. M., & Arkun, Y. (2010). Estimation and model predictive control of non-linear batch processes using linear parameter varying models. International Journal of Control, 72, 659-675.

Lieberman, M. A., & Lichtenberg, A. J. (2005). Principles of plasma discharges and materials processing (2 ed.): John Wiley & Sons.

Lin, C., Leou, K.-C., Huang, H.-M., & Hsieh, C.-H. (2009). Feedback control of plasma electron density and ion energy in an inductively coupled plasma etcher. Journal of Vacuum Science & Technology A: Vacuum, Surfaces, and Films, 27, 157-164.

Ljung, L. (1999). System Identification: Theory for the User (2 ed.): Prentice-hall.

Lynn, S. A., MacGearailt, N., & Ringwood, J. V. (2012). Real-time virtual metrology and control for plasma etch. Journal of Process Control, 22, 666-676.

Manos, D. M., & Flamm, D. L. (1989). Plasma etching: An Introduction: Elsevier.

May, G. S., & Spanos, C. J. (2006). Fundamentals of semiconductor manufacturing and process control: Wiley-Interscience.

McLaughlin, K. J., Edgar, T. F., & Trachtenberg, I. (1991). Real-time monitoring and control in plasma etching. IEEE Control Systems, 11, 3-10.

Miwa, K., Takada, N., & Sasaki, K. (2009). Fluorination mechanisms of Al_2O_3 and Y_2O_3 surfaces irradiated by high-density CF_4/O_2 and SF_6/O_2 plasmas. Journal of Vacuum Science & Technology A: Vacuum, Surfaces, and Films, 27, 831-835.

Mockus, J. (2012). Bayesian approach to global optimization: Theory and applications (Vol. 37): Springer Science & Business Media.

Močkus, J. (1975). On Bayesian methods for seeking the extremum. In Optimization Techniques IFIP Technical Conference (pp. 400-404): Springer.

Moyne, J., Del Castillo, E., & Hurwitz, A. M. (2000). Run-to-run control in semiconductor manufacturing: CRC press.

Ogunnaike, B. A., & Ray, W. H. (1994). Process dynamics, modeling, and control. New York, USA: Oxford University Press

Park, S., Choe, J.-M., Roh, H.-J., & Kim, G.-H. (2014). Characteristics of a non-Maxwellian electron energy distribution in a low-pressure argon plasma. Journal of the Korean Physical Society, 64, 1819-1827.

Pizzi, A., & Mittal, K. L. (2003). Handbook of adhesive technology, revised and expanded: CRC Press.

Qin, S. J., & Badgwell, T. A. (2003). A survey of industrial model predictive control technology. Control engineering practice, 11, 733-764.

Rauf, S., & Kushner, M. J. (1998). Virtual plasma equipment model: A tool for investigating feedback control in plasma processing equipment. IEEE transactions on semiconductor manufacturing, 11, 486-494.

Seborg, D. E., Edgar, T. F., & Mellichamp, D. A. (2008). Process Dynamics and Control (2 ed.): Wiley.

Shahriari, B., Swersky, K., Wang, Z., Adams, R. P., & De Freitas, N. (2016). Taking the human out of the loop: A review of bayesian optimization. Proceedings of the IEEE, 104, 148-175.

Shun'ko, E. V., & Belkin, V. (2007). Cleaning properties of atomic oxygen excited to metastable state $2s^22p^4(^1S_0)$. Journal of Applied Physics, 102, 083304.

Skogestad, S., & Postlethwaite, I. (2007). Multivariable feedback control: analysis and design (2 ed.): Wiley.

Söderström, T., & Stoica, P. (1989). System Identification. London, UK: Prentice-hall.

Stephanopoulos, G. (1984). Chemical process control: An introduction to theory and practice (Vol. 3): PTR Prentice Hall, Inc.

Tsai, C. C., Teng, F. J., & Lin, S. C. (2003). Direct self-tuning model following predictive control of a variable-frequency oil-cooling machine. In American Control Conference (Vol. 1, pp. 603-608): IEEE.

Waschl, H., Alberer, D., & del Re, L. (2011). Automatic tuning methods for MPC environments. In International Conference on Computer Aided Systems Theory (pp. 41-48): Springer.

Yeom, G. Y. (2006). Plasma Etching Technology: Miraecome.

Young, P. C. (2011). Recursive estimation and time-series analysis: An introduction for the student and practitioner (2 ed.): Springer Science & Business Media.

Zhu, X.-M., & Pu, Y.-K. (2010). Optical emission spectroscopy in low-temperature plasmas containing argon and nitrogen: determination of the electron temperature and density by the line-ratio method. Journal of Physics D: Applied Physics, 43.

Abstract in Korean (국문초록)

수 많은 공정으로 이루어진 반도체 제조 공정 내에서 가장 큰 비중을 차지하고 있는 반도체 식각 공정은 최근 10 nm 급 반도체의 양산이 이뤄짐에 따라 식각의 높은 정교성이 요구되고 있다. 반도체 식각 공정은 현재 산업계에선 플라즈마를 이용하여 물리적, 화학적 식각을 일으키는 방법을 통해 이루어지고 있으며, 공정이 10 nm 급 이하 스케일로 미세화된 후로 이 방법이 더욱 각광 받고 있다. 공정의 결과는 식각 프로필을 기준으로 결정되는 데 이 식각 프로필이 플라즈마 변수들에 크게 의존함이 입증됨에 따라 이 변수들을 실시간으로 측정하고 제어하는 것이 공정의 핵심이 되었다. 그동안 플라즈마 변수 제어에 관한 연구들이 활발히 진행되어 왔으나 아직까지 산업계에선 그 이론들을 바로 활용하지 못하고 경험 많은 엔지니어의 감에 의존하고 있다. 그 이유는 근본적으로 시스템이 매우 복잡하고 예민할 뿐 아니라 시간에 따라 변하는 특성을 갖고 있기 때문이다. 그러나 이전의 연구들은 훌륭한 결과를 보였음에도 불구하고, 플라즈마 시스템에 직접적으로 영향을 미치는 침투성 센서를 이용했거나, 플라즈마 변수들과 장치 변수들이 서로 복잡하게 얽혀 있어 야기되는 상호작용을 간과할 수밖에 없는 단변수 제어를 수행한 데에 그치고 있다. 게다가 외란

때문에 발생되는 시간에 따라 변하는 특성을 고려하지 못하고 있다. 따라서, 본 학위논문에서는 변수간 상호작용을 최소화하는 다변수 제어 전략과 시스템이 시간에 따라 변하는 상황에서도 성능이 악화되지 않는 적응모델예측제어기의 설계를 제안한다.

먼저, 전자 밀도와 전자 온도가 제어 대상이 되는 플라즈마 변수로 선정되었다. 이는 식각 프로필, 특히 식각률이 이 변수들에 대한 함수로 표현될 수 있으며, 이 변수들은 침투성 센서인 광학적 발광 분광법을 통해 측정될 수 있기 때문이다. 그 다음에, 최적의 다변수 시스템 정의를 위해 특이치 분석과 상대이득배열을 이용하여 가장 효과적으로 제어를 수행할 수 있는 장치 변수 선정이 이루어졌다. 이를 바탕으로 두 개의 병렬로 연결된 비례적분미분제어기를 설계, 아르곤 플라즈마 전자 밀도와 전자 온도의 제어 시뮬레이션을 수행하였다. 해당 시뮬레이션에서 변수들간 상호 작용이 확연함을 입증하였으며 이를 효과적으로 해결하기 위해 디커플러 제어기가 비례적분미분제어기에 결합되었다. 이 제어기는 아르곤 플라즈마의 전자 밀도와 전자 온도 제어를 훌륭하게 수행함으로써 다변수 플라즈마 시스템의 제어 가능성을 분명하게 입증하였다.

다변수 플라즈마 시스템의 제어 가능성이 입증 됐음에도 불구하고, 이 제어 전략은 비례적분미분제어기의 정교성 측면에서의 한계와 디커플러 제어기의 시스템 모델에 대한 높은 의존도 특성으로 인한 한계가 존재한다. 시스템이 변하는 상황에서도 성능을 유지하기 위해선 더욱 수준 높은 제어 전략이 요구되며, 모델예측제어가 그 대안이 될 수 있다. 모델예측제어기의 설계는 제어의 정교성을 극대화 시키기 위해 베이시안 최적화 기법을 통해 이루어졌다. 이 모델예측제어기는 인위적인 외란이 적용되지 않은 순수 아르곤 플라즈마 시스템에서의 전자 밀도 제어를 훌륭하게 수행함으로써 그 성능을 입증하였다. 하지만, 시스템이 시간에 따라 변하는 상황을 모사한 시뮬레이션과 산소 플라즈마가 아르곤 플라즈마 시스템에 주입되어 시스템 변화를 야기시키는 상황에서 수행된 제어 실험에서 제어기의 성능이 확연히 악화됨을 확인할 수 있었다. 따라서 이를 극복할 수 있는 더욱 발전된 제어 전략이 요구되었다.

적응 제어 기법은 시스템에서 얻어진 정보를 조절 메커니즘 부분으로 보내 실시간으로 제어기의 수정 사항을 결정하여 이를 바탕으로 제어를 수행하는 기법이다. 본 학위논문에서는 대표적인 적응 제어 알고리즘인 순환형 최소자승법 알고리즘을 활용하였다. 이 알고리즘에 칼만 필터 해석을 접목시킴에 따라, 플라즈마 식각

장치로부터 비롯되는 시간 지연의 효과를 고려할 수 있게 하였다. 이 알고리즘이 탑재된 순환형 모델 파라미터 추정기는 베이시안 최적화 기법을 통해 튜닝되었다. 순환형 모델 파라미터 추정기가 실시간으로 감지하는 모델 파라미터의 변화를 모델예측제어기에 전달하면 수정된 모델을 기반으로 제어기는 최적의 조절 변수를 계산한다. 이렇게 설계된 적응모델예측제어기는 앞서 모델예측제어기가 수행한 것과 동일한 시뮬레이션과 실험을 수행하였다. 모델예측제어기와 달리 적응모델예측제어기는 시간에 따라 시스템이 변하는 상황에서도 훌륭한 제어를 수행하였으며, 평균절대오차율을 기준으로 했을 때 기존의 모델예측제어기보다 24.7%의 향상된 제어 성능을 보여주었다. 이 결과는 본 학위논문에서 제안하고 있는 적응모델예측제어기가 시스템의 변화가 빈번한 플라즈마 시스템에서의 제어에 매우 가치 있음과 더불어 플라즈마 식각 장치에 유효한 제어기라는 것을 반증한다. 이 결과가 플라즈마 기반 시스템을 대상으로 하는 모든 제어 공정의 발전에 크게 이바지할 것을 기대하는 바이다.

주요어: 플라즈마 변수 제어; 실시간 제어; 다변수 PID 제어; 외란제거제어; 적응모델예측제어; 순환형 모델 파라미터 추정

학 번: 2014-21587